ABSTRACT

Reconstructing Land Surface Processes of the
1930s Dust Bowl Drought, U.S. Great Plains

Kasey C. Bolles, Ph.D.

Advisor: Steven L. Forman, Ph.D.

Mineral dust aerosols are a key component of the Earth system and a growing public health concern under climate change as levels of dustiness increase. The U.S. Great Plains is particularly vulnerable to dust episodes, but land-atmosphere feedbacks contributing large-scale dust particle transport are poorly constrained, introducing uncertainty in future dust-borne risks to air quality and drought persistence. The 1930s Dust Bowl drought (DBD) is a well-studied, historical example of extreme climate variability. A leading hypothesis to explain the intensity of the DBD is landscape denudation associated with agriculture. However, historical reanalysis indicates that ~30% of the Great Plains was cultivated in the 1930s, thus human agency as the ultimate cause of degradation has been questioned. This work explores the surface processes and meteorological conditions influencing dust particle emission and eolian transport from historical aerial photographs and archival records of the Soil Conservation Service, combined with contemporary field surveys using a Portable In-Situ Wind Erosion Laboratory (PI-SWERL).

Over 40% of the variance in DBD dust storms is explained by air temperature at the surface and 850 hPa and relative humidity at 850 hPa, highlighting the impact of elevated temperatures and spring precipitation deficits associated with 1930s heatwaves. The dominant sources of degradation found for sites east of the 100th meridian are cultivated fields and fluvial deposits. For sites to the west, denuded surfaces are predominantly eolian sandsheets and dunes, correlated with intensity of drought conditions and reduced plant diversity. Discrete spatial signatures of the drought are observed not only within the classically recognized southern Dust Bowl area, but also in the northern and central plains. The $PM_{2.5}$ and PM_{10} emissivity estimates for a single dust event with winds over 6 m s^{-1} in the study area were 510-4,514 μg m^{-3} d^{-1} and 4,700-41,607 μg m^{-3} d^{-1} respectively, similar in magnitude to current dust storm events from North Africa and East Asia. Drought frequency is forecast to increase in late 21st century, potentially with greater severity than the DBD, and may be associated with magnitude increase in atmospheric dust loads.

Reconstructing Land Surface Processes of the
1930s Dust Bowl Drought, U.S. Great Plains

by

Kasey C. Bolles, B.A., M.Sc.

A Dissertation

Approved by the Department of Geosciences

_____

Stacy Atchley, Ph.D., Chairperson

Submitted to the Graduate Faculty of
Baylor University in Partial Fulfillment of the
Requirements for the Degree
of

Doctor of Philosophy

Approved by the Dissertation Committee

_____

Steven L. Forman, Ph.D., Chairperson

_____

Peter Allen, Ph.D.

_____

Steven Driese, Ph.D.

_____

Julie Hoggarth, Ph.D.

_____

Daniel Peppe, Ph.D.

_____

Mark Sweeney, Ph.D.

Accepted by the Graduate School

December 2018

_____

J. Larry Lyon, Ph.D., Dean

Page bearing signatures is kept on file in the Graduate School.

TABLE OF CONTENTS

LIST OF FIGURES

LIST OF TABLES

ACKNOWLEDGMENTS

I would like to recognize and thank the main proponents of this re-evaluation of the Dust Bowl, Steven Forman and Mark Sweeney, whose curiosity and willingness to cross disciplines enabled the fruition of this dissertation. I am thankful for the opportunity to forge a non-traditional pathway through the geosciences.

I am deeply grateful to my parents for their life-long support and encouragement. And thank you to my parents and other loved ones for celebrating the milestones along the way and sharing their enduring optimism. Your faith in me throughout this process is something I will cherish far beyond the Ph.D.

DEDICATION

To the Todd

CHAPTER ONE

Introduction

The climate of the United States Great Plains (USGP), like many semi-arid areas, is characterized by large mode shifts in water availability on decadal to millennial timescales (Woodhouse and Overpeck, 1998; Forman et al., 2001; Holliday, 2001; Miao et al., 2007; Boulter et al., 2010; Hanson et al., 2010; Woodhouse et al., 2010). Specifically, eolian landscapes on the Southern High Plains (SHP), within the influence of the North American Monsoon (NAM), are highly sensitive to moisture variability and record a history of episodic aridity (e.g. Forman et al., 2001; Holliday, 2001; Muhs and Holliday, 2001). A large body of research on the Great Plains points to a well-established precedent for drought as a regular feature of USGP climate (e.g. Seager and Hoerling, 2014). Recent climate modeling and empirical studies indicate that sea surface temperature variability in the Equatorial Pacific and North Atlantic are driving processes for initiation and/or modulation of drought over the SHP (Schubert et al., 2004; Cook E. et al., 2007; Feng et al., 2010); what remains poorly known is the magnitude of land surface interactions with the climatic system and subsequent feedbacks that may amplify and extend drought conditions. Furthermore, it is unclear what the full effect of greenhouse-induced global and regional warming in the 20th and 21st century is on the magnitude, duration and footprint of drought conditions on the SHP (cf. Cook, B. et al., 2014; Seager and Hoerling, 2014).

Drought-stress in the SHP reverberates globally, affecting those who live in the region and who utilize USGP agricultural outputs (Basara et al., 2013). The economic damage induced by drought cost the United States $144 billion between 1980 and 2003,

and drought accounted for over 17% of all weather-related disasters that cost over $1 billion during the same period (Cook, E. et al., 2007; Cook, B. et al., 2014). The estimated cost of the 1930s Dust Bowl Drought is ~$17 billion (in 2015 dollars; inflation calculated using Consumer Price Index Data), which does not account for the social impact on those who had to abandon the Great Plains (Cook, E. et al., 2007). More recently, the 2011 drought cost ~$12 billion and caused a documented 95 deaths (Cook, B. et al., 2013). Given the population growth the SHP region – including several Texas metropolitan areas – continues to experience, the human cost (and impact) of drought variability is likely to increase. The southwestern US, including Texas, is predicted to become more vulnerable in the future to drought stress, with increasing agricultural and urban demands on water resources – particularly greater withdrawals from, and less recharge to, the Ogallala Aquifer (Woodhouse and Overpeck, 1998; Ferguson and Maxwell, 2010; Woodhouse et al., 2010; Basara et al., 2013; Cook et al., 2015). Understanding the landscape expression of drought on the SHP will better guide adaptable land management, sustainable strategies, and risk communication (Basara et al., 2013).

The 1930s Dust Bowl drought (DBD) is a well-studied, historical example of extreme climate variability. A leading hypothesis to explain the severity and spatial extent of the Dust Bowl related to human activity—mainly agriculture—and associated landscape denudation (cf. Bennett and Fowler, 1936; Worster, 1979; Schubert et al., 2004; Basara et al., 2013; Cook, B. et al., 2008; 2009; 2011; 2014; Lee and Gill, 2015). However, historical reanalysis indicates that just 30% of the Great Plains was cultivated in the 1930s, mainly concentrated on the eastern fringe, thus human agency as the ultimate cause of landscape denudation has been questioned (Cunfer, 2005). Global models of modern dust flux

identify relatively small contributions of dust aerosols from agricultural lands, even with drought conditions (Belnap et al., 2011; Ginoux et al., 2012). Furthermore, aerosol feedbacks sourced from drought-disturbed land surfaces are inferred during extreme megadroughts, like the Medieval Climate Anomaly (MCA; Cook, E. et al., 2007; Cook B., et al., 2013). Regional conditions—such as the extent of evapotranspiration, soil moisture, and dust emission—can extend and deepen the spatial and the temporal footprint of drought (Hong and Kalnay, 2002; Mo et al., 2009; Ogelsby et al., 2012; Cook, B. et al, 2015). These land surface-atmosphere feedbacks can intensify surface temperatures (e.g. Meyers, 2001), influence groundwater recharge (e.g. Ferguson and Maxwell, 2010; Kuss and Gurdak, 2014), modulate the degree of recycling in regional water-mass budgets (e.g. Dirmeyer and Brubaker, 1999), and suppress atmospheric convection associated with precipitation events (Su et al., 2014).

There is limited knowledge on the response of varying grassland ecosystems within USGP, particularly with drought. This project aims to evaluate drivers of landscape degradation, and consequent sources of eolian particles to better capture the role of agricultural and natural dust sources in propagating aridification. Analyses of first-generation aerial photography from the 1930s, field-based measurements, archival, and computational research focus on understanding the meteorological and surficial dynamics of eolian activity on the Southern High Plains, where there is currently a dearth of knowledge (cf. Hanson et al., 2010; Halfen and Johnson, 2013). This work attempts to characterize variability in Dust Bowl dust storms and quantify surficial characteristics of dust-emissive surfaces (cf. Bullard et al., 2011; Bryant, 2013), to identify the most potentially potent soil surfaces for dust particle emission under later 21st century aridity.

Climatic Variability on the U.S. Great Plains

The gathering of historic climate data for the continents and oceans spanning the past 100 years has provided insights into global climate conditions for initiating and sustaining decadal-scale drought in North America (cf. Cook, E. et al., 2007; Seager and Hoerling, 2014; Cook, B. et al, 2015). Climate model-based studies have underscored the importance of equatorial sea surface temperature (SST) variability in modulating moisture flux into the Great Plains (Schubert et al., 2004; Fye et al., 2006; Seager et al., 2008; Ruiz-Barradas and Nigam, 2010; Cook, B. et al., 2011; Nigam et al., 2011; Seager and Hoerling, 2014). Specifically, La Niña-like conditions in the equatorial Pacific Ocean and/or a warm phase of the Atlantic Multi-decadal Oscillation is associated with a significant reduction of winter-to-spring precipitation over the Great Plains (Schubert et al. 2004; Fye et al., 2006; Seager et al., 2008; Bronniman et al., 2009; Mo et al., 2009; Feng et al., 2011; Seager and Hoerling, 2014; Wang et al., 2014). Inferred teleconnections in central North America with La Niña conditions in the Equatorial Pacific, combined with a weakened Pacific Jet Stream and Rossby Wave trains enhancing a mid-troposphere ridge (high pressure) over the Great Plains, explains partially the known intensity and footprint of the 1930s drought (e.g. Shubert et al., 2004; Cook, B. et al., 2011). Other factors, such as changes in surface albedo, transient eddy flux, decrease in soil moisture (Kraukauer et al., 2010; Meng and Quiring, 2010), and dust aerosol loading of the lower troposphere appear to have extended and exacerbated past droughts (Cook, B. et al., 2008; 2009).

On inter-annual to decadal scales, the El Niño/Southern Oscillation (ENSO) is the major control on tropical Pacific SSTs, driving the occurrence of El Niño and La Niña events. La Niña-type events exhibit increasing sea level pressure (SLP), concomitant with

a decrease in SSTs in the eastern equatorial Pacific (Fig. 1.1; Wolter and Timlin, 2011). Often during La Niña events the Pacific Jet Stream weakens and shifts northward in response to cooler equatorial SSTs, reduced evaporative loss, and decreased atmospheric vertical momentum (Cook E., et al, 2007). The geostrophic response to diminished vertical

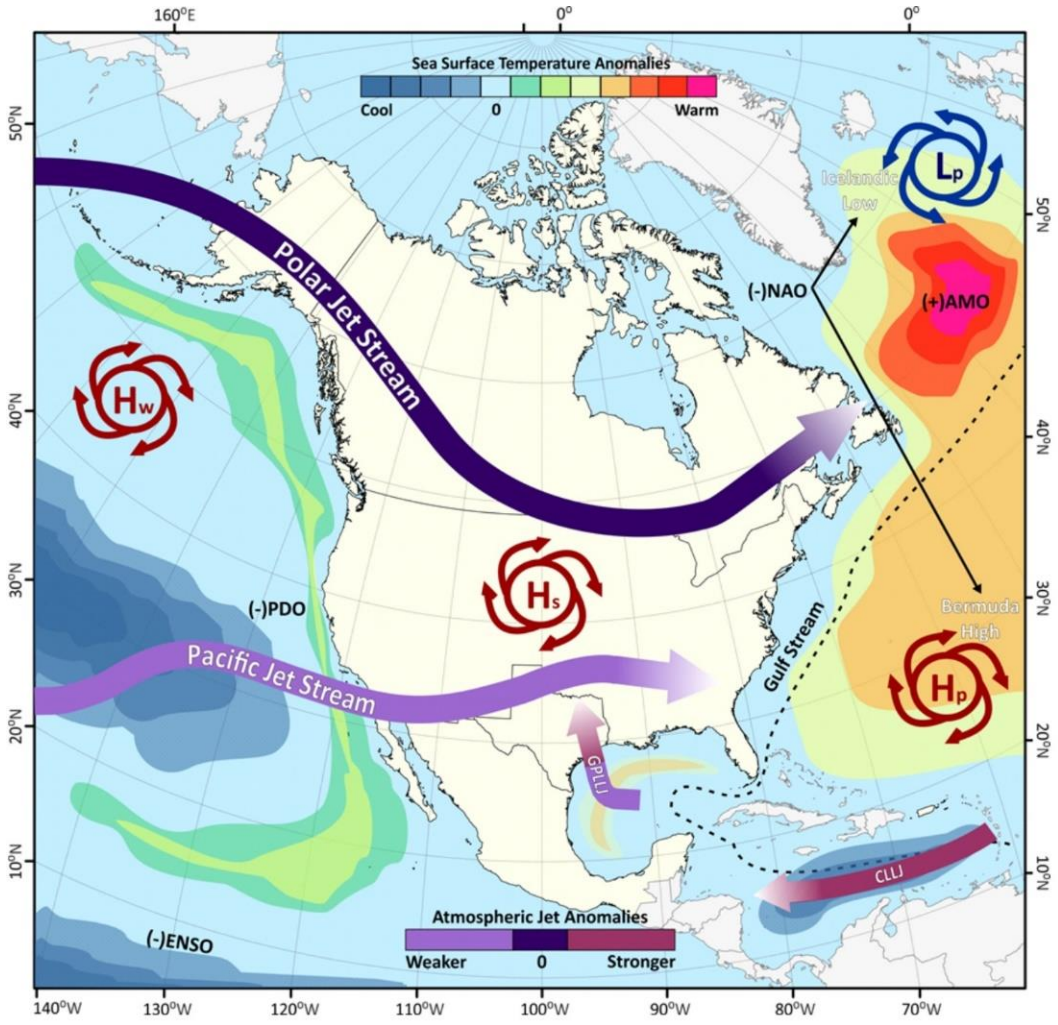

Figure 1.1 Atmospheric and oceanic conditions commonly associated with drought on the U.S. Great Plains. Persistent drought conditions occur most frequently with: anomalously cool sea surface temperatures (SSTs) in the eastern equatorial Pacific Ocean (i.e. a La Niña event, a negative phase of the El Niño/Southern Oscillation [(-)ENSO]), and also in the northern Pacific above 20°N (negative phase of the Pacific Decadal Oscillation [(-)PDO]); anomalously warm SSTs in the northern Atlantic Ocean (positive phase of the Atlantic Multi-Decadal Oscillation [(+)AMO]); a weakened Icelandic Low and weakened, eastward Bermuda High semi-permanent pressure systems (negative phase of the North Atlantic Oscillation [(-)NAO]); and a variable Great Plains Lower Level Jet (GPLLJ) and strengthened Caribbean Low Level Jet (CLLJ). Typic summer jet stream configuration is shown. High pressure systems (H) are in red, and low pressure systems (L) are in blue. Pressure systems can be semi-permanent (p notation) or form seasonally in the summer (s) or winter (w) in associated with climatic oscillations (with Figure 1.2).

atmospheric flux in the tropics and sub-tropics may be an induced dynamic high pressure over the southwestern US in summer–suppressing precipitation and warming temperatures (Fig. 1.1; Cook E., et al, 2007). During winter La Niña states, precipitation decreases in the southwestern United States (Wolter and Timlin, 2011), due to the impact of ENSO on mid-tropospheric Rossby waves, which alter the Pacific winter storm track and in turn create a precipitation deficit that can propagate into later seasons (Schubert et al., 2008). ENSO intensity can be heightened when northern Pacific SSTs (indexed by the Pacific Decadal Oscillation; PDO) are in phase with equatorial waters, possibly forming a cold season anticyclone over the N. Pacific (Fig. 1.1; Mantua and Hare, 2002; Ogelsby et al, 2012; Dai, 2013). Model results indicate that ENSO-related decrease in SSTs can account for the intensity of MCA droughts on the Great Plains, but not fully the footprint of the drought (Feng et al., 2008). Drought conditions and the spatial extent during the MCA and 1930s are more skillfully modelled when including concomitant SST variability in the North Atlantic (Schubert et al, 2008; Feng et al., 2011).

Climate models suggest that observed fluctuations in wet/dry conditions in the Great Plains are closely related to the Atlantic Multi-decadal Oscillation (AMO), specifically the warm phase (Feng et al., 2011). When the N. Atlantic is anomalously warm, there is an observed decrease in precipitation over the SHP (Fig. 1.1; Feng et al., 2011). The major AMO-like warm SST periods in the last 7,000 kyr BP correspond to dry conditions on the GP, while cold periods align with wet conditions (Feng et al., 2011). Model outputs from the CLImate VARiability and Predictability drought experiments (CLIVAR) demonstrate only a small direct effect of AMO on drought over the United States, but a large indirect effect via impacts on ENSO, particularly when the two are

opposite in phase, i.e. (-)ENSO and (+)AMO (Mo et al., 2009). Conversely, analysis of natural variability demonstrates a key role for AMO in initiating multi-year droughts over North America, as the warm phase of AMO is associated with precipitation deficits in spring, summer and fall (Nigam et al., 2011). Warm AMO states alter the strength and location of the semi-permanent Bermuda High, impacting the north/south geostrophic dipole between the Bermuda High and the Icelandic Low and dampening westerly flow (Fig. 1.1; Hurrell, 1995; Fye, 2006; Seager and Hoerling, 2014).

An important synoptic element associated with extreme precipitation events in the 20th and 21st century within the mid-continental US is the strength and trajectory Great Plains Low Level Jet (GPLLJ). This "jet" is a directional flow of moisture northward in the lower atmosphere sourced from the Caribbean Sea (Fig. 1.1; Krishnamurthy et al., 2015). The GPLLJ displays strong inter-annual variability related to Pacific and Atlantic SST anomalies (Krishnamurthy et al., 2015) and is influenced by the strength of the Pacific Jet Stream and/or the Bermuda High (Woodhouse and Overpeck, 1998). Since 1979, the GPLLJ has expanded and strengthened northward, directing more moisture to the northern plains and reducing precipitation over the southern plains by 50% (Barandiarian et al., 2013). Generally, moisture is transported northward in steps, with the source maximum for any region at the upstream boundary of that region (Dirmeyer and Brubaker, 1999). A stronger GPLLJ increases the probability of drought conditions at the entrance region and flood conditions at the exit region, further reducing precipitation over the SHP (Krishnamurthy et al., 2015). Stronger GPLLJ events are typically associated with spring La Niña conditions (the high SLP leads to stronger easterlies, creating a stronger Caribbean Low Level Jet (CLLJ) and thus stronger GPLLJ), positive SST anomalies in the Gulf of

Mexico, and negative SSTs in the Caribbean Sea (Fig. 1.1; Dirmeyer and Brubaker, 1999; Krishnamurthy et al., 2015).

On the SHP only about one third of short term (6-year) rainfall variability is SST-forced; the remaining variance is attributable to internal system variability (Basara et al., 2013). Land-atmosphere interactions impact climatic conditions on the SHP through changes in surface albedo, vegetation cover, soil moisture, and particle emission (Fig. 1.2). Land-surface moisture levels can affect local and regional climate via changes in precipitation circulation, intensity of rainfall anomalies, and regional water-mass budgets (Dirmeyer and Brubaker, 1999). Hydroclimatic variability over North America is thusly

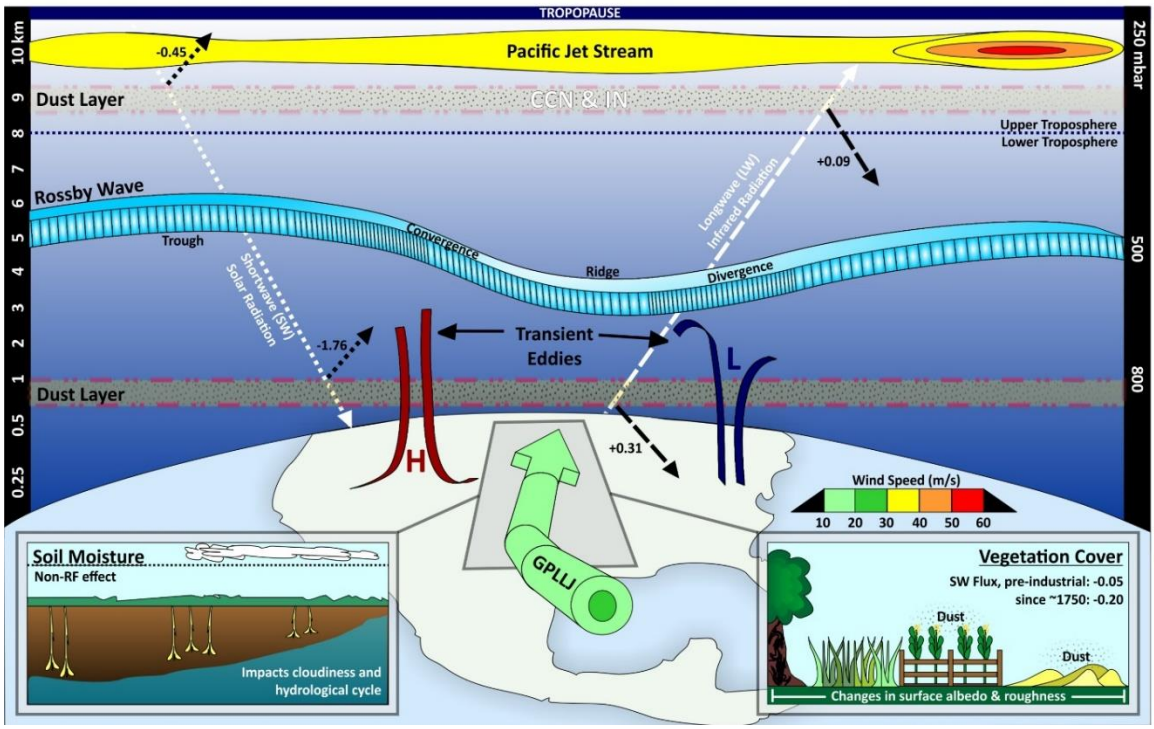

Figure 1.2 Idealized vertical configuration of atmospheric dynamics over the U.S. Great Plains and relative radiative forcings of land-atmosphere interactions. Radiative forcings (RF) are in W m^{-2}l dust RF measurements are taken from Yu et al. (2010) and land surface RF feedbacks (gray boxes) are taken from Myhre et al. (2013). Air warms locally around dust particles (red boxes) as the absorb passing shortwave (SW, dotted line) and/or longwave (LW, dashed line) radiation. Mineral dust aerosols suspended in the upper troposphere can also act as cloud condensation nuclei (CCN) and ice nuclei (IN).

dependent on how land surface-atmosphere interactions modulate climatic conditions (Cook, B., et al., 2013). Soil moisture interactions are a major pathway for surface heat flux to influence the atmospheric boundary layer (Hong and Kalnay, 2000; 2002; Mo et al., 2009; Ferguson and Maxwell, 2010; Ogelsby et al., 2012; Su et al., 2014; Wang et al., 2014). A strong coupling between soil moisture and precipitation exists on the Great Plains, where soil moisture conditions can lead to drought persistence (Hong and Kalney 2000; 2002; Koster et al., 2004; Cook, E., et al, 2007; Mo et al., 2009; Ogelsby et al., 2012; Wang et al, 2014). A comparison of conditions on the SHP during the drought year of 1988 and the pluvial year of 1993 suggests moisture sources are more terrestrial—and recycling more dominant—during drought periods, and marine moisture sources more dominant during wet periods (Dirmeyer and Brubaker, 1999). During pluvials, synoptic eddies related to large-scale atmospheric conditions heighten the efficiency of moisture advection from low-level humidity, provided by wetter soil, thereby increasing precipitation (Su et al., 2014). Drier soil tends to exhibit higher sensible heat flux, which warms surface temperatures, reducing vegetation cover and evapotranspiration (ET), thereby effectively decreasing precipitation (Basara et al., 2013).

Changes in radiative forcing of dust can also induce changes in the hydrological cycle and in regional circulation patterns that feedback to changes in dust sources and sinks (Tegen et al., 1996). Dust is unique in that particles can both absorb and scatter radiation, unlike other types of aerosols (Fig. 1.2; Volland, 2010). Dust radiative forcing in the atmosphere reduces downward mixing of momentum within the planetary boundary layer, changing the surface wind speed and, subsequently, rates of dust emission (Boucher et al., 2013). Dust is key for ice nuclei when it reaches the upper troposphere, and conversely,

causes a greenhouse effect when suspended in the lower troposphere (Boucher et al., 2013). The dust production process is controlled by levels of: rainfall, wind, surface roughness, temperature, topography and vegetation cover – interdependent factors that respond to climate nonlinearly (Hugenholtz and Wolfe, 2005; Jickells et al., 2005; Werner et al., 2011; Houser et al., 2013). A global study of remotely sensed data indicates that 75% of dust emissions are derived from natural sources (Ginoux et al., 2012). Anthropic emissions account for 25% of all dust, and 85% of this is associated with ephemeral water bodies linked to croplands, grazing and urban use (Ginoux et al., 2012). Global estimates of anthropogenic land use activities find human activity impacted 42 to 68% of the land surface between 1700 and 2000 (Hurtt et al., 2006).

On the USGP however, it is estimated only ~30% of the landscape has ever been plowed, though the rest likely experienced grazing (Cunfer, 2005). One hypothesis of the intensity of the 1930s drought holds that large-scale changes to the land surface during this time period amplified the drought (see Cook, B. et al., 2013). In this scenario, the large-scale crop failure of drought-sensitive wheat —which replaced drought-resistant prairie grass— at the beginning of the drought left devegetated fields barren and easily eroded soil exposed to winds, and subsequent dust aerosol forcing exacerbated the drought (Cook, B. et al., 2013). However, it is unknown if that areal extent of crop failure is sufficient to explain the intensity of the 1930s megadrought. More investigations into the source of Dust Bowl drought dust particles are needed in order to determine this.

Attribution

The following chapters have been published and/or submitted to peer-reviewed journals with contributions from this author (KCB) and co-authors Steven L. Forman (SLF)

and Mark Sweeney (MRS). For CHAPTER TWO, KCB and SLF conceived of the project and both performed archival research of historical documentation. KCB spearheaded image processing and analysis and manuscript preparation. SLF provided guidance throughout the study and assisted in manuscript preparation.

For CHAPTER THREE, KCB, SLF, and MRS conceived of the project and carried out field surveys. MRS operated the PI-SWERL for data collection and post-processing. KCB and SLF reviewed the Soil Conservation Service records used in this study. KCB performed analyses of the dust storm inventory and PI-SWERL data regressions, and spear-headed manuscript preparation. SLF and MRS contributed to manuscript preparation and provided guidance throughout the study.

Finally, for CHAPTER FOUR, KCB and SLF conceived of the project and both performed archival research of historical documentation. KCB spearheaded image processing and analysis, dust estimation modeling, and manuscript preparation. SLF directed stratigraphic and OSL analyses and provided guidance throughout the study. MRS provided interpretation of PI-SWERL data, and both MRS and SLF assisted in manuscript preparation.

CHAPTER TWO

Evaluating Landscape Degradation Along Climatic Gradients During the 1930s Dust Bowl Drought from Panchromatic Historical Aerial Photographs

This chapter is published as: Bolles, K.C. & Forman, S.L. (2018) Evaluating Landscape Degradation Along Climatic Gradients During the 1930s Dust Bowl Drought from Panchromatic Historical Aerial Photographs, U.S. Great Plains. *Frontiers in Earth Science* 6, Article 153.

Abstract

The U.S. Great Plains (USGP) are some of the most productive rangelands globally and a significant carbon sink for the atmosphere, but grassland response to precipitation is highly variable and poorly constrained over time and space. There is a rich historical aerial photographic record of the USGP which provides an unparalleled view of past landscapes and allows for evaluation of surficial response to drought beyond the satellite record, such as during the 1930s Dust Bowl Drought (DBD). This study classified the extent and loci of surficial denudation from seamless mosaics of radiometrically-corrected and georectified digitized aerial negatives acquired in the late 1930s from six counties distributed across USGP ecoregions. The dominant sources of degradation found for sites east of the 100th meridian are cultivated fields and fluvial deposits, associated with woody vegetation response to water availability in uncultivated areas. For sites to the west, denuded surfaces are predominantly eolian sandsheets and dunes, correlated with intensity of drought conditions and reduced plant diversity. Discrete spatial signatures of the drought are observed not only within the classically recognized southern Dust Bowl area, but also in the northern and central plains. Statistical analyses of site variability suggest landscape response to the DBD is most strongly influenced by the arid–humid divide and severity of

precipitation and temperature anomalies. With a projected increase 21st century aridity, eolian processes cascading across western grasslands, like during the Dust Bowl, may significantly impact future dust particle emission and land and carbon storage management.

Introduction

Grasslands of the U.S. Great Plains (USGP; Fig. 2.1) are globally one of the most productive rangelands. These prairies and soils contribute to carbon storage via above- and below-ground net primary productivity (ANPP, BNPP) and the decadal-to-century residence time of soil organic matter (SOM; Sims and Bradford 2001; Lei et al., 2016; Petrie et al., 2016). However, grassland response to extreme drought is highly variable over space and time and remains a significant factor for adapTable 2.land and carbon management during forecasted 21st century aridity (Basara et al., 2013; Cook et al., 2015; Ruppert et al., 2015; Lei et al., 2016; Petrie et al., 2016; Byrne et al., 2017; Seager et al., 2018). Carbon flux is sensitive to precipitation on daily-to-seasonal timescales because shifting water availability, with associated plant physiological response and biomass changes, impact the fixation of carbon (Sims and Bradford, 2001; Petrie et al., 2016; Konings et al., 2017). Disturbance-induced plant loss can amplify aridity (Cook et al., 2008; 2009; 2013; Hu et al., 2018), causing potentially irreversible ecotone transitions (Schlesinger et al., 1990; Bestelmeyer et al., 2006), with vulnerability partially controlled by soil type (Tongway and Ludwig, 1994) and temperature impacts on ecosystem functioning (Petrie et al., 2016). The Dust Bowl of the 1930s is a vivid example of such cascading landscape degradation and offers insight into potential land surface response, and dust sources during severe droughts, projected for the future across the Great Plains.

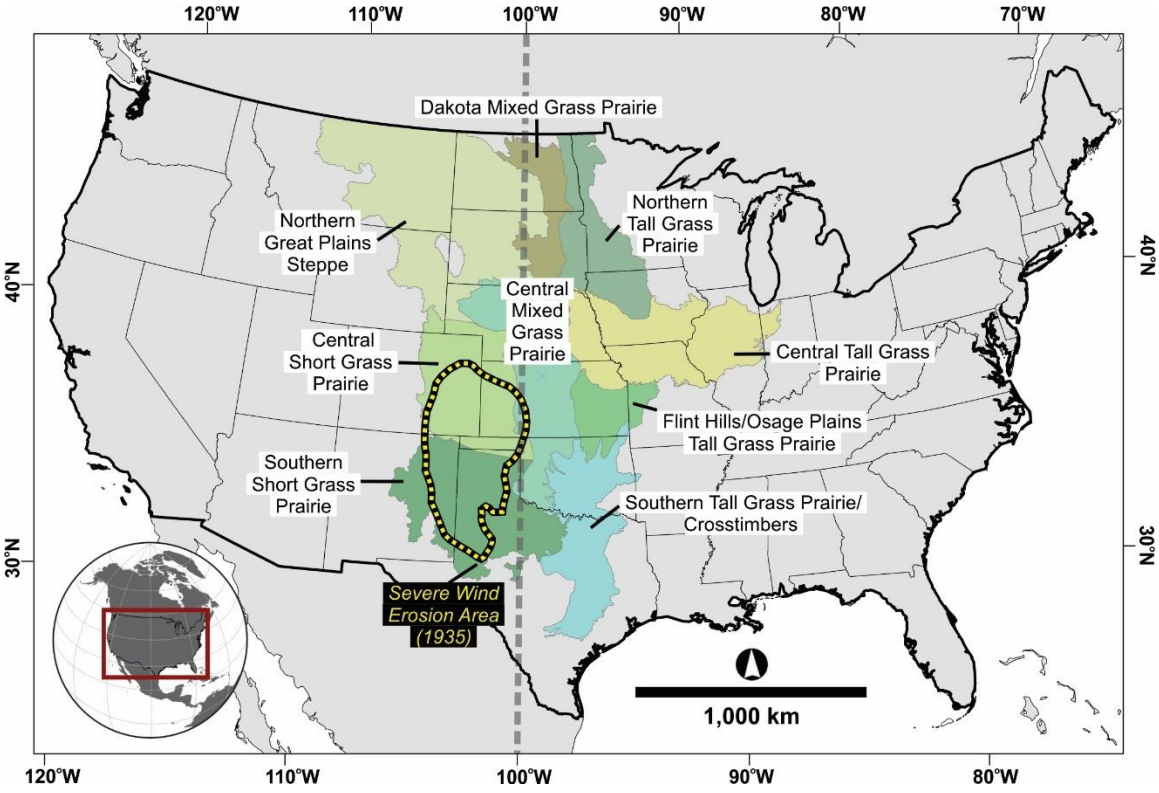

Figure 2.1 Location of the U.S. Great Plains delineated by terrestrial ecoregion (TNC-modified Bailey, 1995), with the 100th meridian demarcated by a dashed line and the classically recognized area of severe wind erosion at its maximum extent in 1935 (Worster 1979; Cunfer 2005).

There exists a large archive of pre-satellite panchromatic aerial photography for the conterminous U.S. that provides an unparalleled network of images for historical landscapes coincident with large-scale human modification characteristic of the 20th century (Redweik et al., 2009; Morgan et al., 2010; Nagarajan and Schenk, 2016). The U.S. Great Plains (USGP) has a particularly rich photographic record beginning in the 1930s, when the U.S. Department of Agriculture was tasked with reducing acreage under cultivation to stabilize crop prices during the Great Depression (Leedy, 1948; Rango et al., 2008; 2011; NARA, 2017). The resulting record, completed from 1935 to 1954, covers approximately 7,627,515 km^2, or 99.5% percent, of the contiguous US (Leedy, 1948; NARA, 2017) and is comparable in resolution to QuickBird and IKONOS satellite imagery

(Laliberte et al., 2004; Rango et al., 2008; Browning et al., 2009). Recently a new historical image product was created from this record by applying advances in remote sensing and geospatial techniques to digital reproductions of original reel film (Bolles et al., 2017).

Previous studies using early aerial photographs are typically focused on changes in the distribution and cover of vegetation (cf. Carmel and Kadmon, 1998; Laliberte et al., 2004; Rango et al., 2008; Browning et al., 2009; Williamson et al., 2011; Morgan and Gergel, 2013; Murray et al., 2013; Lishawa et al., 2013). Bare surfaces are often filtered from analyses to increase accuracy of vegetation studies given the noise introduced to image classification schemes by soil spatial heterogeneity (Escadafal and Huete, 1992; Browning et al., 2009; O'Brien et al., 2010; Murray et al., 2013). However, heterogeneity is a significant concept in landscape ecology linked to ecosystem functioning, defined as the degree of spatial variability of a particular property within a scale-dependent system (Turner, 1989; Wiens, 1989; Li and Reynolds, 1995; Pickett and Cadenasso, 1995; Morgan and Gergel, 2010). Heterogeneity of bare soil surfaces is an indicator of landscape sensitivity to aridity, with increased patchiness frequently correlated with degradation (Schlesinger et al., 1990; Tongway and Ludwig, 1994; Bastin et al., 2002; Bestelmeyer et al., 2006; Ravi et al., 2010). Patch size, condition, and landscape context are significant factors in determining ecosystem resistance and resilience to climatic perturbations (Samson et al., 2004; Collins et al., 2014; Moran et al., 2014; Ruppert et al., 2015; Svejcar et al., 2015; Byrne et al., 2017). A framework for assessment of grassland degradation is defined by an index of the spatial distribution of land cover, coupled with an index of soil stability largely related to sediment texture and/or surface crusts (Tongway and Ludwig, 1994; Maestre et al., 2003). Utilizing semi-automated image analysis techniques, these

metrics can be quantified for historic landscapes to examine biotic and abiotic controls on land cover changes (Browning et al., 2009; Morgan and Gergel, 2010; Morgan et al., 2010; Morgan and Gergel, 2013; Vogels et al., 2017). The resultant image products offer extended spatial scales to paleoarchives such as lake cores, stratigraphic sections, and tree-rings, and elucidate the interplay between climate, geomorphology, vegetation, and land use (e.g. Lishawa et al 2013; Bolles et al 2017; Schook et al., 2017).

There are well developed standards for manual interpretation of individual or stereoscopic pairs of aerial photographs with traditional photogrammetry. However, methods are emerging for semi-automated radiometric and spatial homogenization and structure-from-motion (SfM) photogrammetry for large numbers of archival black and white photographs (e.g. Morgan et al 2010; Morgan and Gergel, 2013; Nebiker et al., 2014; Bakker and Lane, 2016; Gonçalvez, 2016; Giordano et al., 2017; Mertes et al., 2017; Mölg and Bolch, 2017; Pacina and Popelka, 2017; Sevara et al., 2017; Vogels et al., 2017). Raw panchromatic aerial photographs are produced via black and white emulsions, where color is related to relative brightness of the visible light spectrum reflected from the surface (Caylor, 2000). When digitized, photographs are displayed as a single-band, gray-scale image, wherein each pixel is assigned a digital number (DN) that is proportional to the brightness of that pixel. Surface brightness is potentially altered by several parameters, not limited to viewing angle, azimuth and intensity of radiation source, sample geometry (i.e. particle size, aggregate size, roughness), vegetation cover, surface crusts, soil moisture and organic matter content (Escadafal and Huete, 1992; Ben-Dor, 2002; Mather and Koch, 2011). Particle size specifically can alter the shape of bare surface spectra by 5% of the absolute surface reflectance (Hunt and Salisbury, 1970; Ben-Dor, 2002). In field conditions

aggregate size can be more significant than particle size and may change over sub-daily to monthly timeframes due to tillage, soil erosion, eolian accumulation, and/or crust formation. Therefore, surface roughness is an important determinant of the range of spectra expressed in aerial imagery (Ben-Dor, 2002; Zhang et al., 2003). These local factors are a challenge for analysis of aerial imagery, as manual interpretation of features can be subjective and labor-intensive to undertake over large areas and/or fine-scales (Morgan et al., 2010; Morgan and Gergel, 2013).

The principal characteristics available for feature identification in panchromatic imagery are variation and relative differences in tone (Morgan et al., 2010). Classification of tonal variation assigns individual pixels a label based on a specific property (Gennaretti et al., 2011), in this case the DN of each pixel. Relative differences in tone, also referred to as image texture, are determined by the spatial relationships between pixels within a defined area and directionality (Morgan et al., 2010; Morgan and Gergel, 2010; Morgan and Gergel, 2013; Vogels et al., 2017). Quantification of image texture can account for tonal heterogeneity and thereby, surface roughness (Morgan and Gergel, 2010), and is particularly useful for landform and land use classification where radiometric properties are being classified (Morgan et al., 2010). A significant assumption of this approach is that separate classes are represented by discrete differences between gray scale values and that these classes are spectrally independent (Anderson and Cobb, 2004). Where vegetation cover is only partial, a mixed signal from soil and vegetation occurs, making extrication of overlapping soil–vegetation signals complex (Ben-Dor, 2002), but this can be addressed via geographic object-based image analysis (GEOBIA; Morgan and Gergel, 2010; Morgan and Gergel, 2013; Blaschke et al., 2014; Vogels et al., 2017).

Herein we present methods to analyze pre-1945 panchromatic aerial photographs along climatic gradients of USGP grasslands and evaluate landscape response to the 1930s Dust Bowl Drought (DBD). Specifically, we (1) identify representative study sites across various ecoregions of the USGP, (2) incorporate spectral, texture and object-based parameters to classify photo-mosaics and verify surface types of historic landscapes, and (3) quantify surficial heterogeneity and evaluate potential drivers of landscape response to drought. This research will examine the indicators and extent of landscape sensitivity to precipitation variability prior to widespread irrigation of the USGP and address controls on ecosystem degradation during severe drought years in the DBD.

Ecological and Geomorphic Factors for the U.S. Great Plains Landscape

Mean annual temperature (MAT) on the USGP is typically 15^0 to 18^0C and mean annual precipitation (MAP) ranges from <250 mm in the west to >1500 mm in the east, spanning the transition between semi-arid to sub-humid climates. The latitudinal zonation of northern to southern ecoregions generally follows temperature trends (Fig. 2.2a); the short-to-tall grass prairie transition parallels the strong west-to-east MAP gradient (Fig. 2.2b, c). Grassland ANPP is highly correlated to precipitation, with peak values of >700 g m^{-2} along the eastern margin of the Plains and decreasing to 80 g m^{-2} in the fore of the Rocky Mountains (Sala et al., 1988). On the USGP, terrestrial carbon storage may range from ~0.3 to 0.9 kg C m^{-2} (Derner et al 2006; Petrie et al., 2016), but can be a net atmosphere carbon source through diminished evapotranspiration and/or increased soil erosion (Meyers, 2001).

The USGP arid–humid divide roughly coincides with the 100^{th} meridian, where precipitation levels decrease from ~600 mm in the east to ~400 mm in the west (Fig. 2.2b;

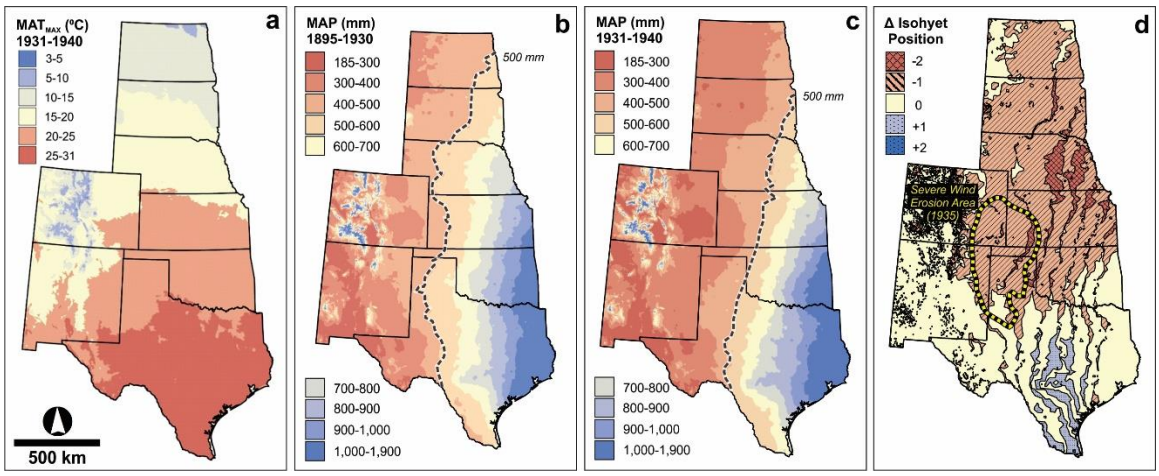

Figure 2.2 (a) The latitudinal gradient of northern to southern grasslands generally follows mean annual maximum temperature (MATMAX). (b) From 1895 to 1930 the position of the longitudinal mean annual precipitation (MAP) gradient generally corresponds to the short-to-tallgrass transition, but (c) during 1931 to 1940 MAP over the plains was significantly drier, and (d) this gradient was shifted eastward ~250 km compared to MAP in the previous 35-year period, encompassing the largest extent of recognized severe wind erosion during the Dust Bowl (Worster, 1982; Cunfer, 2005). Temperature and precipitation data is derived from PRISM Historical Past time series datasets (PRISM Climate Group, Oregon State University, http://prism.oregonstate.edu, created October 3, 2017).

Nielsen, 2018; Seager et al., 2018). This gradient shifted about 250 km eastward between 1931 to 1940 compared the prior MAP between 1895 and 1930, encompassing the largest extent of previously recognized severe wind erosion during the DBD (Fig. 2.2d). Drought and land use directly impact grassland functioning via an increased risk of degradation, desertification, and subsequent reduction in stability and productivity, such as that observed during the DBD (Cook et al 2009; Koerner et al 2014; Ruppert et al., 2015; Lei et al., 2016; Byrne et al., 2017; Hu et al., 2018). However, the DBD was not a homogeneous event in time or space but consisted of several droughts and relative wet phases affecting different regions at different times (Fig. 2.3; Laird et al., 1998). Drought conditions were exacerbated by above-average temperatures exceeding 40^0C and land-atmosphere interactions that increased the threshold for precipitable water (Cook et al., 2011a; b; 2014; Su et al., 2014; Donat et al., 2016). Climate modelling studies of the DBD have found that

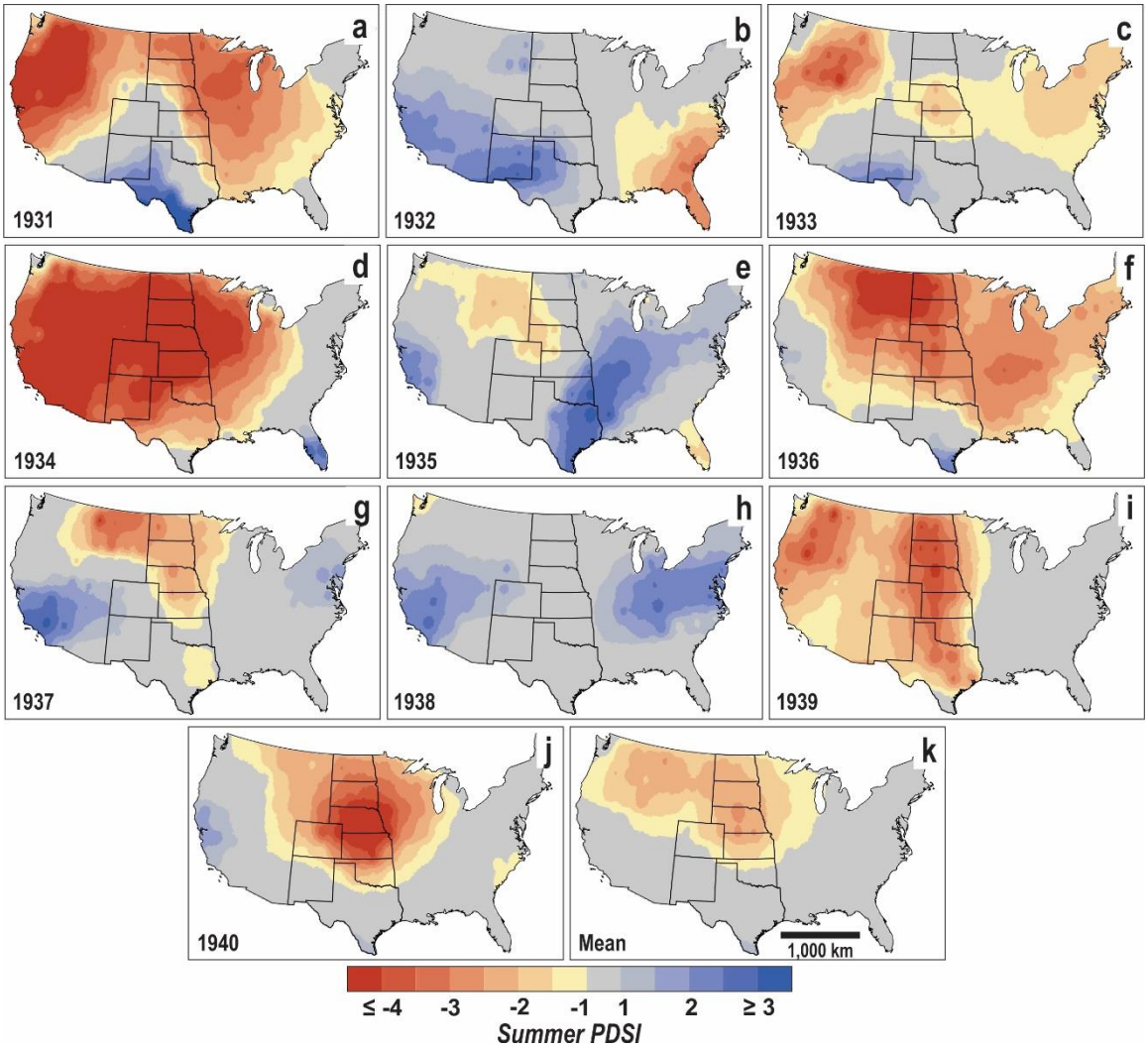

Figure 2.3 Summer (June-August) Palmer Drought Severity Index (PDSI) for the years 1931 to 1940 and the decadal mean calculated from the North American Drought Atlas (Cook E et al., 2010).

land cover changes increased the intensity and altered the spatial footprint of drought across the USGP (cf. Cook et al., 2008; 2009; Hu et al., 2018).

Reduced vegetation cover allows for enhanced wind erosion of soils, burying of adjacent grasses by the accumulation of eolian sediment and an increase in overland flow and riling from episodic and extreme rainfall events (Schlesinger et al., 1990). The subsequent recovery of plant communities may be delayed a decade or more, even with five years of precipitation above the historical average, as observed after the DBD (Weaver

and Albertson, 1956, p. 128-162). Ecological studies in the 20th century indicated that the diversity of grassland species decreased with drought, excessive grazing, and range fire (Weaver and Albertson, 1944; Tilman and Downing, 1994; Collins et al., 1998). The climax grassland species, such as Blue Grama (*Boutelousa gracilisi*) and Buffalo Grass (*Buchloe dactyloides*), have decreased vitality with drought because of a shallow root system (<1 m). As drought persists for grasslands, the surficial heterogeneity increases with the dominance of bare surfaces with biomass and nutrients focused by deeply-rooted (2 to 5 m) woody vegetation, forming "islands of fertility" (Weaver and Albertson, 1943; Weaver and Albertson, 1956, p. 86-116; Schlesinger et al., 1990; Jurena and Archer, 2003). In semi-arid regions such as the USGP, there are also apparent responses in eolian and fluvial geomorphic systems to extreme precipitation variability (Ewing et al., 2006; Derickson et al., 2008; Ewing and Kocurek, 2010; Ravi et al., 2010; Turnbull et al., 2010; Belnap et al., 2011; Liu and Coulthard, 2015). The pattern of stabilized dunes is often linked to bioclimatic variations. Wetter spring and summer conditions and heavy winter snowfall provide excess moisture for eolian systems to stabilize more effectively, with colonization by climax vegetation assemblages (Cordova et al., 2005; Ravi et al., 2010; Turnbull et al., 2010). Drier conditions are often correlated with decreased vegetation coverage and increased eolian activity, such as during the Medieval Climate Anomaly (MCA) when multiple, multi-decadal droughts propagated across the Americas with numerous presently-stabilized eolian sand systems apparently reactivated, but to an unknown spatial extent (e.g. Mason et al., 2004; Forman et al., 2005; 2008; Lepper and Scott, 2005; Siefert et al., 2009; Halfen and Johnson, 2013). Many periods of eolian reactivation exhibit discontinuous blow-outs, parabolic dunes and sandsheet accretion,

often leaving a spatially heterogeneous landform assemblage (Schlesinger et al., 1990; Hugenholtz and Wolfe, 2005; 2006). Questions remain if such degradation is in response to landscape-scale drier conditions, or if soil erosion is a stochastic process reflecting randomness or localized surficial disturbance of vegetation with drought, grazing, fire and/or pestilence (e.g. Schlesinger et al., 1990; Bel and Ashkenazy, 2014).

Methods

A standardized workflow (Fig. 2.4) was developed to select, process, analyze, and archive aerial photographs captured between AD 1936 and 1941 from counties across the USGP based on previously defined iterative analyses (Okeke and Karniele, 2006; Redweik et al., 2009; Morgan et al., 2010; Morgan and Gergel, 2013; Doneus et al., 2016; Gonçalvez, 2016; Bolles et al., 2017; Vogels et al., 2017). In brief, photogrammetric scans of original reel film are corrected for interior and exterior distortions of position and light exposure. Processed frames are spatially referenced to the North American Datum 1983, Universal Transverse Mercator, Zone 14N (NAD83 UTM 14N), with a residual root mean square error (RMSE) ≤5 m. Frames are then resampled to a standard resolution (1 pixel = 0.25 m^2) and blended into a mosaic based on county and date of negative acquisition.

Surface properties are retrospectively verified using historical primary documentation, contemporary field surveys, and digital surface models (DSMs) derived with SfM photogrammetry, allowing for assessment of uncertainty of manual and automated classifications. Spectral analysis of individual pixels, texture analysis of multiple pixels within a sliding window (i.e. a texel), and subsequent segmentation of groups of pixels into objects are applied to mosaics. Image and verified data are combined

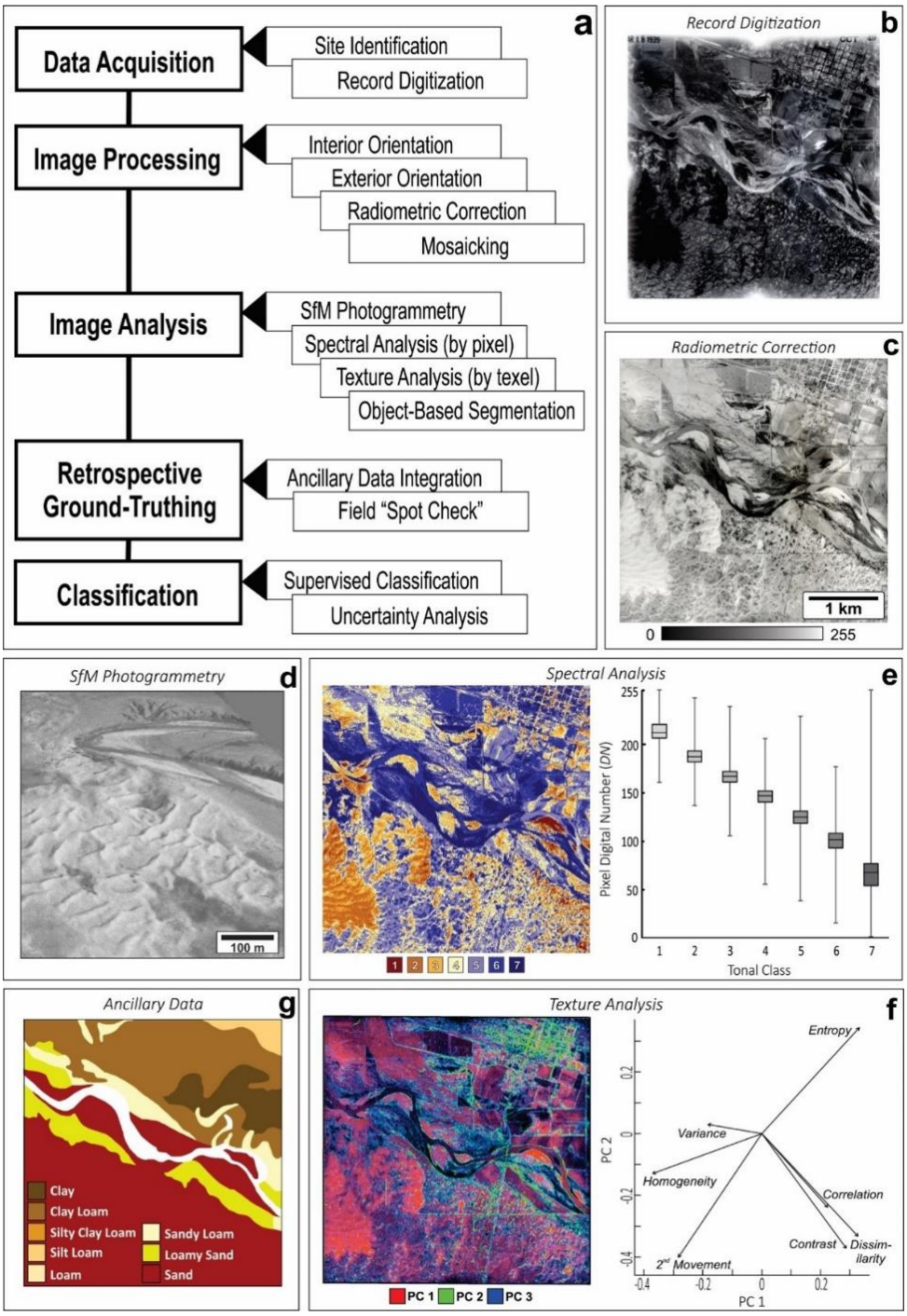

Figure 2.4 Outline of semi-automated analysis of historical panchromatic aerial photographs used in this study with illustrative example: (a) diagrammatic workflow of methods used, (b) raw scan of original negative reel film of frame 145-CCT-049-155 from Syracuse, Hamilton County, Kansas taken March 22,1939, (c) oriented, radiometrically-corrected, and resampled image, (d) digital surface model (DSM) generated from multi-view stereoscopy, (e) results of unsupervised spectral classification of pixel digital numbers (DN) with box and whisker plot of cluster distribution, where the gray-scale color of the box in the plot corresponds to the mean DN of the cluster; refer to Table 2.2 for legend description, (f) results of principal component analysis of image texture layers to delineate image objects, (g) soil surface texture gathered from the Web Soil Survey (Soil Survey Staff, 2017).

to classify objects based on surficial properties, including soil texture, land cover, land use, and geomorphic form, and classification results are statistically analyzed. The number of surface types accounting for ≥ 50% and ≥ 90% of a respective study area are used to define thresholds in surficial diversity. ‘

Study Site Identification and Photograph Reproduction

A multi-criterion, spatially-explicit weighted overlay is employed to identify USGP counties that are representative of the broader landscape for the time and place of negative acquisition and to minimize subjectivity in site selection (Table 2.1). We include three climatic parameters to estimate the magnitude of anomalies in each county between 1931 and 1940, with larger deficits given greater weight: percent change in maximum MAT and MAP relative to the preceding 35-year period (1895 to 1930), and the central tendency of

Table 2.1. Criteria included in the weighted overlay for site identification (with Figure 2.5).

Type	Notation	Description	Data Source
Climatic	Δ MAT_{MAX}	Percent change in maximum mean annual temperature between the DBD (1931-1940) and the preceding 35-year period (1895-1930)	Calculated from: Historical Past time series data (PRISM, 2017)
	Δ MAP	Percent change in mean annual precip-itation between the DBD and the preceding 35-year period	Calculated from: Historical Past time series data (PRISM, 2017)
	$PDSI_{MR}$	Mid-range Palmer Drought Severity Index during the DBD (1931-1940)	Calculated from: North American Drought Atlas PDSI Reconstructions (Cook E et al., 2010)
Landscape	CLAY	Average percent clay content of top 20 cm of soil countywide	Calculated from NRCS soil survey (Wieczorek, 2014; Soil Survey Staff, 2017)
	SILT	Average percent silt content of in county top 20 cm of soil countywide	Calculated from NRCS soil survey (Wieczorek, 2014; Soil Survey Staff, 2017)
	SAND	Average percent sand content of top 20 cm of soil countywide	Calculated from NRCS soil survey (Wieczorek, 2014; Soil Survey Staff, 2017)
	DD	Drainage density (ratio of length of linear water features within the county to county area, m m^{-2})	Calculated from Small-Scale Streams and Waterbodies dataset (USGS, 2005)
	CULT	Percentage of county area` under cult-ivation by AD 1935	Calculated from the USDA Agricultural Census of 1935 (Gutmann et al, 2005)

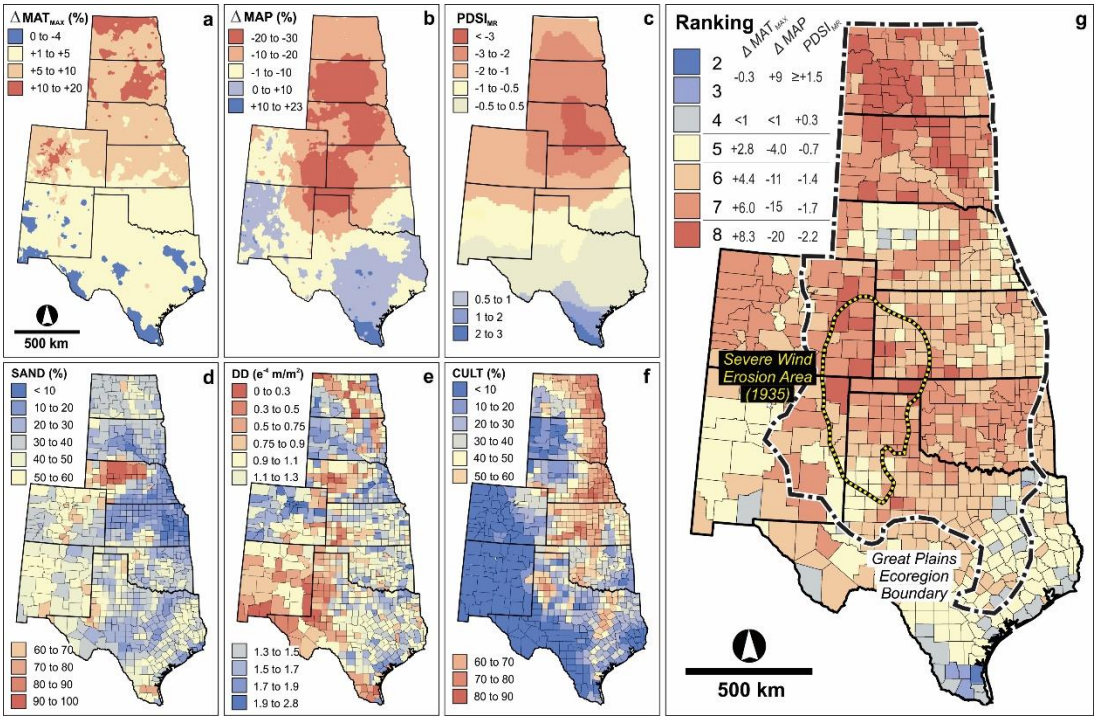

Figure 2.5 Layers included in the multi-criterion site selection scheme: (a) percent change in mean annual maximum temperature (MAT_{MAX}) during 1931 to 1940 in comparison to preceding 35-year period (1895 to 1930), (b) percent change in mean annual precipitation (MAP) during 1931 to 1940 in comparison to preceding 35-year period, (c) mid-range Palmer Drought Severity Index ($PDSI_{MR}$) during 1931 to 1940, (d) average percent sand, silt, and clay content of soil, (e) average drainage density (DD) expressed as a ratio of total length of linear water features to county area, and (f) the percent of acreage under cultivation at the peak of agricultural expansion in 1935. (g) Criteria were standardized to a scale of 1 to 9 and given equal influence in a weighted overlay to assign each county a rating based on its respective properties. For data sources, refer to Table 2.2.1.

evapotranspiration as expressed by the mid-range Palmer Drought Severity Index ($PDSI_{MR}$; Fig. 2.5a-c). Three physical surficial parameters averaged at the county level were included to evaluate the similarity of landscape setting amongst counties within the same ecoregion, with values closest to the regional mean weighted highest: sediment texture (% sand, silt, and clay in upper 20 cm of soil), density of fluvial drainages expressed as a ratio of total channel length to county area, and percent area under cultivation per the Agricultural Census of 1935, identified in historical analyses as the year of maximal cropland extent on the USGP (Cunfer, 2005; Fig. 2.5d-f). These criteria are standardized to a scale of 1 to 9 and given equal influence in an overlay to assign each county a final

rating that reflects the intensity of drought conditions and similitude of surficial properties to the broader ecoregion (Fig. 2.5g). A fishnet of 1,000 km^2 cells is created across counties within USGP ecoregions, and a random sample of cells distributed across the precipitation and temperature gradients is selected for acquisition of aerial photographs.

Access to the primary photo archive is through the National Archives and Record Administration (NARA) II facility in College Park, MD, where much of early aerial imagery has been centralized, with limited holdings at smaller archives (Rango et al., 2008; Sylvester and Rupley, 2012). At the facility, photograph reproductions are available as hardcopy photomosaics of the original flight lines, organized by record group, state, county and year. Once the appropriate survey symbol, flight line and photo number associated with an area of interest are identified, the specific canister of original reel film, typically held at off-site cold storage, is ordered to NARA for digitization by a vendor with approved scanning equipment. The original scans used in this study are archived by county and available from the Historical Air Photo Dataverse at the Texas Data Repository (Bolles, 2018a-i). A subset of 657 high resolution (≥ 1200 dpi) photogrammetric scans of overlapping negatives from six counties is utilized in this study (Table 2.2; Fig. 2.6). These images were taken at 1:20,000 scale between November 1936 and November 1940, with 35% lateral overlap between images and forward overlap from ~35 to 67%.

Processing and Analysis of Digitized Historical Imagery

In lieu of coeval camera calibration reports, which are largely unavailable, the interior orientation of digitized images is corrected to pseudo-calibrated fiducial coordinates from a template image frame via an affine transformation in MATLAB (Leedy, 1948; Redweik et al., 2009; Gonçalvez, 2016; Nagarajan and Schenk, 2016; Giordano et

al., 2017). Images are then cropped to standard dimensions to remove outlying pixels from the frame, such as those obscured by the photograph collar and identification numbers (Heipke, 1997; Redweik et al., 2009; Doneus et al., 2016). Ground controls points (GCPs) are identified to correct for exterior orientation between image and coordinate space. Absent detailed flight logs containing roll, pitch, yaw, and position coordinates, GCPs are obtained by matching time-invariant features (TIF) within the image to features in contemporary imagery with a known location (Narajaran and Schenk, 2016). The base map within ERSI ArcGIS and vector data of roads from state GIS data repositories are used to derive 5 to 20 GCPs per frame to attain an RMSE ≤5 m.

Color correction is concentrated on contrast enhancement to distinguish the intergrades in brightness from bare to fully vegetated surfaces, and between the textural properties of those surfaces (Kadmon and Harari-Kremer, 1999; Murray et al., 2013; Liu and Mason, 2016). The open-source, python-based GNU Image Manipulation Program is

Table 2.2 Survey details and spatial extent of photos reproduced for this study from U.S. Department of Agriculture contracted surveys (with Figure 2.6).

ID	Location	# of Photos	Acquisition Date(s)	Survey Company	# of GCPs	Extent (km^2)
a	Ward County, ND	85	August 4 & 5, 1938 September 22, 1938 October 19, 1938	Edgar Tobin Aerial Surveys	634	927
b	McPherson County, NE	95	June 22 & 23, 1939 July 9 & 17, 1939 August 12 & 21, 1939 October 31, 1939	Kargl Aerial Surveys, Inc.	496	926
c	Hamilton County, KS	198	March 18 & 19, 1939 April 1 & 19, 1939	Aero Service Corporation	1,384	1,662
d	Quay County, NM	104	November 17 & 20, 1936 January 26, 1937	Fairchild Aerial Surveys	556	1,018
e	Tillman County, OK	83	March 20 & 22, 1937	Kargl Aerial Surveys, Inc.	435	888
f	Lamar County, TX	92	November 15, 1940	Aero Exploration Co.	540	588

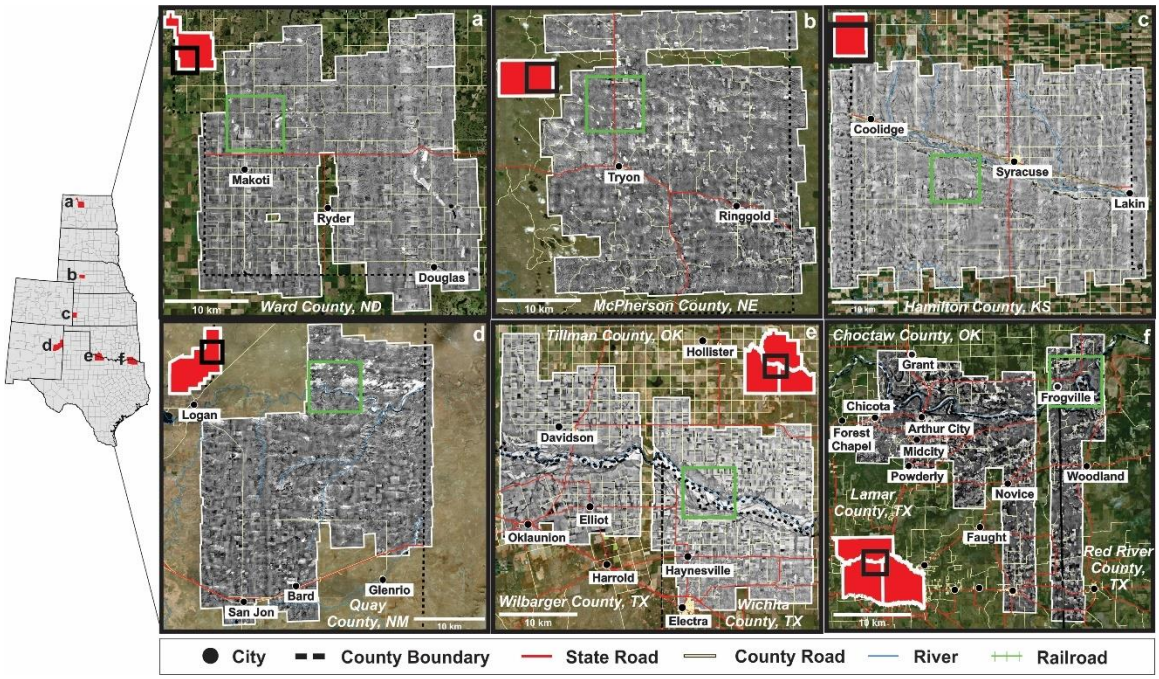

Figure 2.6 Location map of selected areas showing county position on the Great Plains and extent of aerial photographic coverage reproduced for this study in: (a) Ward County, ND, (b) McPherson County, NE, (c) Hamilton County, KS, (d) Quay County, NM, (e) Tillman County, OK, Wilbarger & Wichita Counties, TX, and (f) Choctaw County, OK, Lamar & Red River Counties, TX\. Survey details for the mosaics are presented in Table 2. The green box denotes location of imagery shown in Figure 2.7. Where coverage crosses county boundaries, the county with the largest portion of aerial coverage is denoted as the location. All reproductions used in this study are available from the Historical Air Photo Dataverse archived in the Texas Data Repository (Bolles, 2018a-i).

utilized to normalize the histogram of each frame individually, then to gamma-balance across frames so overlapping features are displayed along the same radiometric range (Kadmon and Harari-Kremer, 1999; Murray et al., 2013). Images are monochromatically balanced to correct for light fall-off introduced by lens distortion, spatially variable characteristics of the original film, and/or improper exposure of the photograph (Fig. 2.4b, c; Redecker, 2008; Morgan et al., 2010). Frames are then further color balanced in an ESRI ArcGIS mosaic dataset using a first-order smoothing algorithm to minimize merging of pixels that do not match. Frames are blended together along seamlines generated from spectral patterns of overlapping features; the frames with greatest spatial accuracy (i.e. lowest RMSE) are weighted forward in seamline delineation and blending.

Multi-view stereoscopy of overlapping aerial photography is a rapidly developing method for landscape-level analyses of historical surfaces (Gomez et al., 2012; Nebiker et al., 2014; Doneus et al., 2016; Mertes et al., 2017; Mölg and Bolch, 2017; Pacina and Popelka, 2017; Sevara et al., 2017). The Agisoft Photoscan (APS) software package is used for automated three-dimensional reconstruction of the surface; the APS algorithm generates dense point clouds on par with airborne LiDAR data to derive a triangulated surface representing a DSM (Fig. 2.4d; Nebiker et al., 2016; Pacina and Popelka, 2017). Subsequently the DSM is used to calculate slope and elevation as covariate parameters for image classification. The centroid coordinates of each frame footprint created in the mosaic dataset is utilized to approximate the camera position at the time of acquisition to increase accuracy in photogrammetric alignment within APS.

The Iterative Self-Organizing Data Analysis (ISODATA) classification in ESRI ArcGIS is a robust clustering algorithm for areas with sparse ground-truth data and is used initially to understand the distribution of pixels DNs within a mosaic (Ball and Hall, 1967; Liu and Mason, 2016). An exaggerated number of clusters (≥15) is established across the range of spectral values, and neighboring clusters are merged until the overlap between cluster quartiles is ≤1% (Fig. 2.4e; Anderson and Cobb, 2004; Skirvin et al., 2004; Okeke and Karniele, 2006; Bolles et al., 2017). A majority filter is applied to reclassify pixels where it can be reasonably assumed the pixel belongs to the surrounding cluster, producing a smoothing effect (Mather and Koch, 2011; Liu & Mason, 2016). Whereas this is a powerful tool to assess vegetation cover and soil texture, distinctions in land use and geomorphic form are often obscured. For example, an unpaved road, eroding field, and migrating dune are clustered together given similarities in surficial brightness. Thus, more

information about patterns between adjacent pixels is needed to classify surficial processes and land use.

Using a MATLAB script, we calculate gray-level co-occurrence matrices for several textural properties within a 3 x 3 moving window (Haralick et al., 1973; Laliberte et al., 2004; Morgan et al., 2010; Morgan and Gergel, 2010; Mather and Koch, 2011; Schowengerdt, 2012; Morgan and Gergel, 2013; Vogels et al., 2017). This returns the probabilities of occurrence of a specific pixel pairing in eight directions, the average of which is taken to define the final texture parameter for each texel (i.e. the block of pixels within the moving window). The resulting texture rasters are used as inputs for principal component analysis to identify statistically significant relationships between texture parameters and group pixels for object-based image segmentation (Fig. 2.4f). Segmented objects are overlaid with the DSM to categorize landform and land use, then combined with surficial soil texture and tonal class to obtain the final classification of unique surface types (cf. Morgan and Gergel, 2010; Morgan and Gergel, 2013; Blaschke et al., 2014; Parajuli et al., 2014; Baddock et al., 2016; Parajuli and Zender, 2017; Vogels et al., 2017).

Retrospective Land Surface Verification

There is a wealth of observations on land surface conditions during the 1930s that has previously provided the basis for environmental interpretations (Browning et al., 2009; Skaggs et al., 2011; Williamson et al., 2011). Data sources are from contemporaneous peer-reviewed publications, government records from the Soil Conservation Service (SCS), ancillary experiment stations, and ground-based photographs held at National Archives and Record Administration (NARA) II facility in College Park, MD. Items reviewed and digitized include: handwritten field notes, field photographs, planimetric maps,

documentation of tillage operations, and correspondence between land owners, scientists and government officials. A complementary data source is the study of near-surface eolian deposits and landforms that are associated with landscape degradation during the DBD (e.g. Forman et al., 2008; Bolles et al., 2017). Specifically, the dry Munsell Color of bare sand and buried soils is a useful corollary to connect image grayscale and soil texture. This index designates the hue, chroma, and value of a given material, where value (or brightness) is the first parameter established and ranges in equal intervals from black to white. The Web Soil Survey from the National Resource Conservation Service (NRCS; Soil Survey Staff, 2017) is also used to delineate the lateral variability in soil texture. Finally, an Abrams stereoscope is used with hardcopy image stereo-pairs to randomly "spot check" the sense of slope and elevation measurements taken from the DSMs.

Statistical Analyses

Bivariate and multivariate statistical approaches are applied to parse the potential relationships between a matrix of 52 variables measured from the six study sites. Variables include criteria from the site selection scheme, classified land surface parameters, and summer PDSI from 1931 to 1940 interpolated from the North American Drought Atlas (Fig. 2.3; Cook et al., 2010). Data are standardized, and a comparison of skewness and standard error values indicates about half of variables measured are not normally distributed. Therefore, Spearman's rank correlation coefficient (R_S) is calculated to explore the strength and direction of dependence between the rank order of variable pairs (Borradaile, 2003). Pairs with an R_S over ± 0.8 and a *p*-value ≤ 0.05 are considered as significant variables with a strong monotonic relation. A principal component analysis (PCA) reveals linear combinations of variables with the maximum amount of covariance,

and the subsequent principal components (PCs) are mutually uncorrelated (Wilks, 2011). A threshold is applied to extract coefficients in the upper or lower quintile of PC eigenvalues and identify the dominant variables contributing to intra- and inter-site variance. Finally, two pairwise distance metrics are computed between sites to create hierarchical cluster trees (Wilks, 2011): cosine (one minus the cosine of the angle between points) and hamming (percentage of coordinates that differ).

Results

Great Plains counties during the 1930s exhibit a range of inferred drought conditions and degree of similarity in antecedent landscape setting to the broader region, from a ranking of 4, associated with moderately mesic conditions, to a score of 8 indicating severe drought areas (Fig. 2.5g). The counties rated ≤4 display relatively neutral conditions over the decade and are largely located near the Texas coast. Whereas those counties rated five or higher are associated with increasing intensity of drought conditions on the USGP. Counties rated five or six are largely evenly distributed across the short- to tallgrass transition but show a slight increase in frequency east of the 100th meridian. The majority of counties ranked seven contain shortgrass species (52%), most frequently located in the central shortgrass prairie ecoregion. Forty-six counties (6%) receive the highest rank of eight, characterized by $PDSI_{MR}$ of less than -2, maximum temperatures 5 to 10% higher than normal, and ≥20% deficit in precipitation. Of these counties, >70% are west of the 100th meridian in shortgrass ecoregions, most frequently Northern Great Plains Steppe.

The surface processes are discussed for six cells from across the USGP fishnet; note that if a cell crosses county boundaries, the county with the largest portion of aerial coverage is denoted as the location. The subset of counties selected for this study are: Ward,

ND, McPherson, NE, Hamilton, KS, Quay, NM, Tillman, OK and Lamar, TX. These counties reflect mild-to-severe DBD conditions and generally contain surficial properties typical of the respective ecoregion (Table 2.3). Across these six counties, seven clusters are derived from the spectral classification, and these tonal classes are indicative of plant cover and/or soil texture and moisture. This treatment includes the relative density of plant cover and general species assemblage from historical documentation, a scheme modified from Bolles et al. (2017). Broadly, 34% of the 652 unique surface types are classified as denuded, with the remaining 66% covered by natural vegetation or crops, though this ratio, type of vegetative cover, and loci of degradation fluctuate across ecoregions (Table 2.4, 2.5).

Ward County, North Dakota

Ward County, ND (Fig. 2.7a) occurs at the transition from northern mixed-grass prairie to steppe vegetation and by 1935 was ~60% cultivated. This county ranked seven, experiencing maximum temperatures 11% higher in the 1930s than in the prior three decades, and with a 13% precipitation deficit. At the time of negative acquisition in the fall of 1938, most of the study area (~70%) is an uncultivated mix of grasslands over alluvial floodplains and lacustrine basins, with 71% vegetation cover irrespective of land use or landform. Nearly 40% of uncultivated areas with plant cover are classified as patchy weeds and grasses, 25% as denser grasses and forbs, and ~5% as woody vegetation. Cultivated fields appear mostly vegetated (73%) with severe cover loss when bare. Of the most extreme denudation, 80% is associated with natural landforms, at least half of which are identified as dried-out lake beds exposing silty clay loam. Nearly all lacustrine basins lack

Table 2.3. Climatic conditions and landscape setting for the six study areas during the 1930s Dust Bowl Drought with county ranking and criteria from the site selection scheme (Table 2.1; Figure 2.5).

Figure Letter	County	Ranking	Terrestrial Ecoregion	MAT_{MAX} (^{0}C)		MAP (mm)		$PDSI_{MEAN}$	Cultivated (%)	Avg. Soil Texture (%)			Drainages (1×10^{-4} m m^{-2})
				1931-1940	% Δ 1896-1930	1931-1940	% Δ 1896-1930	1931-1940		Sand	Silt	Clay	
a	Ward, ND	7	Northern Shortgrass Dakota Mixed Grass	11.7	+11	343	-13	-2.1	59	37	35	27	0.6
b	McPherson, NE	5	Central Mixed Grass	18.1	+7	429	-19	-2.5	23	95	2	3	0.1
c	Hamilton, KS	8	Central Short Grass	22.1	+5	316	-25	-1.5	35	27	50	23	0.8
d	Quay, NM	6	Southern Short Grass	23.4	+1	345	-18	-0.6	15	49	27	23	0.9
e	Tillman, OK	7	Southern Short Grass Central Mixed Grass Southern Tall Grass	25.3	+2	632	-11	-0.6	65	36	31	31	1.3
f	Lamar, TX	4	Southern Tall Grass Crosstimbers	24.7	+2	1,112	< 1	-0.7	29	29	29	41	1.6

Table 2.4. Distribution of quantified landscape variables across the six study counties, number of unique surface types classified, and number of surface types accounting for at least 50% and 90% of the study area.

Feature	Code	Percentage of Study Area					
		WND	**MNE**	**HKS**	**QNM**	**TOK**	**LTX**
Bare: Extreme	C1	3.8	2.6	28.5	5.0	28.0	7.6
Bare: Severe	C2	12.9	12.0	15.1	14.4	8.2	6.0
Bare: Moderate	C3	7.0	6.6	6.6	16.4	7.3	6.0
Bare: Slight Vegetation: Sparse	C4	6.5	6.1	6.0	15.0	6.8	6.8
Vegetation: Dense	C5	38.3	51.5	20.2	12.4	15.2	22.0
Vegetation: Denser	C6	25.7	19.5	19.2	28.0	19.1	37.7
Vegetation: Densest	C7	5.7	1.8	4.6	8.9	15.4	13.9
Structure	L1	0.9	0.3	0	0	0.3	0.6
Road	L2	2.0	2.2	0.4	0	0.7	2.4
Cultivated Field	L3	30.5	22.0	5.3	0	33.8	45.2
Pasture	L4	1.0	0	0	0	0.3	0.6
Grassland	L5	55.0	35.0	29.5	47.7	9.1	30.5
Fluvial Channel	L6	0	0	2.6	2.1	0.8	4.1
Fluvial Deposit	L7	0	0	5.4	3.3	14.6	2.4
Fluvial Terrace	L8	0	0	2.6	2.3	22.5	14.4
Eolian Dune	L9	0	0.7	9.0	3.9	1.7	0
Eolian Sandsheet	L10	0	39.7	45.3	40.6	16.1	0
Lacustrine Basin	L11	10.4	0	0	0	0	0
Sand	S1	0.2	93.8	69.7	43.7	13.4	0
Loamy Sand	S2	0.4	6.2	26.8	6.2	41.3	1.5
Sandy Loam	S3	18.9	0	1.7	23.5	40.1	41.7
Loam	S4	71.7	0	0	4.9	22.7	1.1
Silty Loam	S5	0.2	0	0	0	0.3	23.1
Silty Clay Loam	S8	7.7	0	0	0	0.6	0
Clay Loam	S9	0	0	1.8	0	0	0
Clay	S12	0	0	0	0	1.0	26.2
Bedrock	S13	0	0	0	21.7	0	0
	Total	242	105	241	232	452	343
# of Surface Types	*≥ 50%*	6	3	6	9	14	16
	≥ 90%	49	21	51	54	106	124

WND: Ward County, North Dakota; MNE: McPherson County, Nebraska; HKS: Hamilton County, Kansas; QNM: Quay County, New Mexico; TOK: Tillman County, Oklahoma; LTX: Lamar County, Texas.

Table 2.5. Surface types covering at least fifty percent of the respective study area. Refer to Table 2.4 for surface type code description.

County	WND	MNE	HKS	QNM	TOK	LTX
Surface Types Accounting for ≥ 50% of Study Area (%)	C5-L5-S4 (*19.5*)	C5-L10-S1 (*23.1*)	C5-L10-S1 (*11.5*)	C6-L10-S1 (*11.5*)	C1-L7-S2 (*10.4*)	C6-L3-S12 (*6.73*)
	C6-L5-S4 (*9.67*)	C5-L5-S1 (*20.5*)	C6-L10-S1 (*9.22*)	C2-L10-S1 (*8.53*)	C1-L3-S3 (*5.75*)	C6-L5-S3 (*4.37*)
	C5-L3-S4 (*7.4*)	C6-L5-S1 (*13.2*)	C1-L9-S1 (*8.93*)	C3-L10-S1 (*5.72*)	C6-L8-S2 (*3.53*)	C5-L3-S12 (*4.16*)
	C6-L3-S4 (*6.28*)		C2-L10-S1 (*8.29*)	C6-L5-S3 (*5.67*)	C7-L8-S2 (*3.10*)	C6-L5-S12 (*3.93*)
	C2-L5-S4 (*5.79*)		C1-L10-S1 (*7.82*)	C4-L10-S1 (*4.71*)	C6-L10-S1 (*2.81*)	C6-L5-S5 (*3.79*)
	C3-L5-S4 (*3.56*)		C6-L5-S2 (*4.69*)	C6-L5-S13 (*4.06*)	C5-L3-S3 (*2.80*)	C5-L3-S5 (*3.65*)
				C5-L10-S1 (*4.05*)	C5-L8-S2 (*2.71*)	C6-L3-S5 (*3.19*)
				C7-L10-S1 (*3.89*)	C7-L3-S3 (*2.58*)	C7-L5-S3 (*3.09*)
				C1-L9-S1 (*3.73*)	C6-L3-S3 (*2.40*)	C6-L3-S3 (*2.92*)
					C2-L3-S3 (*2.38*)	C7-L5-S5 (*2.81*)
					C6-L10-S2 (*2.29*)	C5-L3-S3 (*2.52*)
					C5-L10-S1 (*2.28*)	C1-L3-S3 (*2.21*)
					C6-L3-S3 (*2.13*)	C6-L3-S8 (*2.19*)
					C5-L3-S3 (*2.11*)	C5-L5-S3 (*1.95*)
						C7-L5-S12 (*1.85*)
						C6-L8-S12 (*1.75*)

standing water; by 1939 total lake surface area was about one-third of the recorded high from 1868 to 1877 (Shapley et al., 2005). In total, 242 surface types are identified, with over half the study area described by six types (Table 2.5). The most common surface type is grassland dominated by weeds and perennial grasses colonizing loamy soils developed on glacial till.

McPherson County, Nebraska

McPherson County, NE (Fig. 2.7b), ranked five, falls within the central mixed-grass prairie ecoregion, was 23% cultivated by 1935, and during the DBD experienced a 7% increase in maximum temperatures and a 19% deficit in precipitation. The soils in this county, at the margin of the Nebraska Sand Hills, are characterized by ≥90% sand content (Fig. 2.5d). The earliest available aerial photographic coverage for this county was July 1939, with 22% of the surface in cropland, ~40% uncultivated undulating sandsheets and

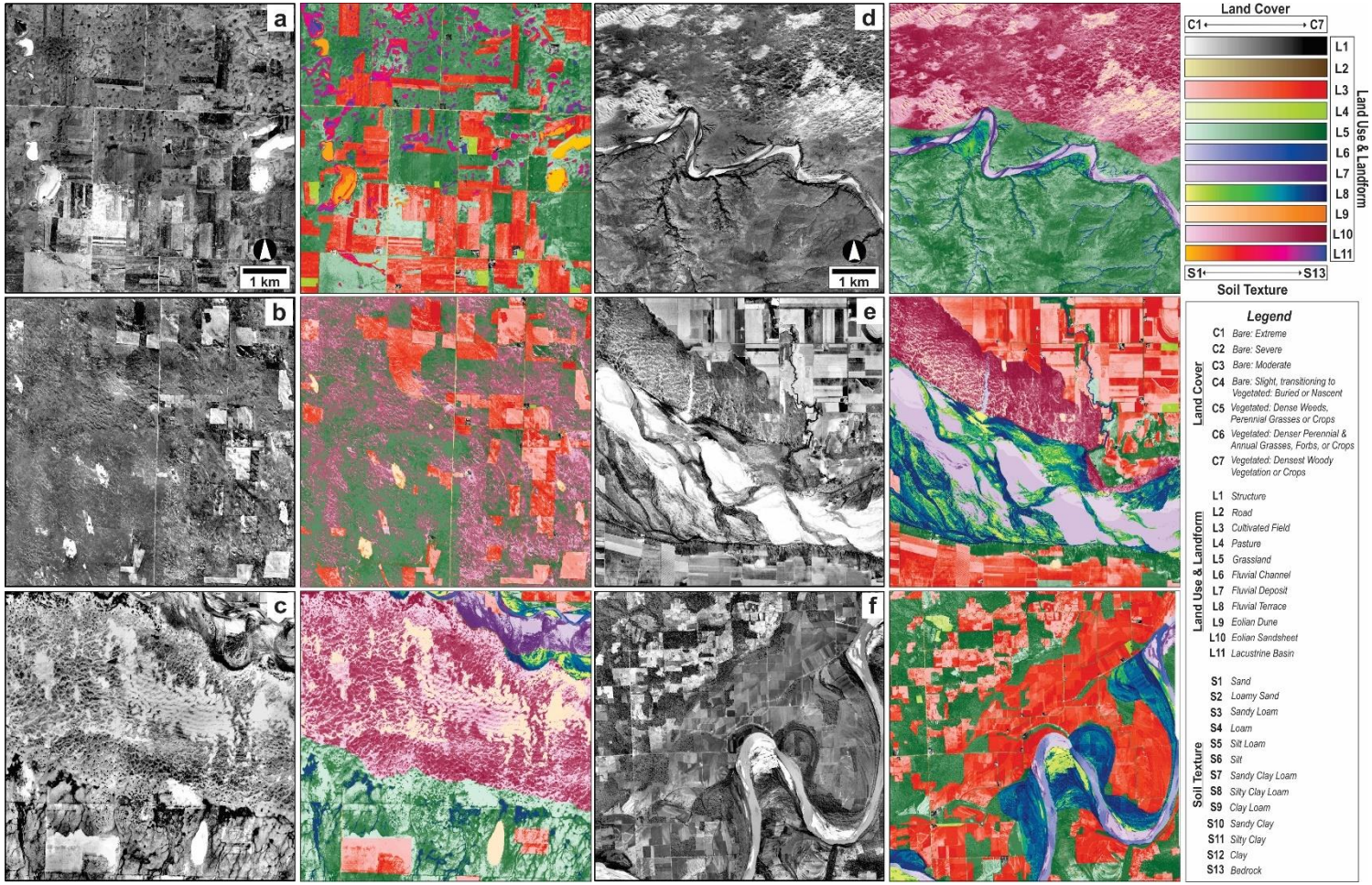

Figure 2.7 Illustrative samples from image analysis and classification from processed aerial photographs of (a) Ward County, ND, (b) McPherson County, NE, (c) Hamilton County, KS, (d) Quay County, NM, (e) Tillman County, OK, Wilbarger & Wichita Counties, TX, and (f) Choctaw County, OK, Lamar & Red River Counties, TX; refer to the corresponding letter in Figure 2.6 for location denoted by a green box. Column one is an enhanced view of ~45 km^2 from the blended mosaic, column two presents the final supervised image classification of landscape features.

35% interdunal grassland. Nearly three-quarters of the surveyed area (74%) is vegetated, though severe vegetation loss is frequently mapped in cultivated fields. Surfaces classified with the greatest degradation occur 64% on cultivated fields and 31% on blowout dunes, nascent parabolic dunes, and sandsheets. The crests of sandsheet ridges are most frequently disturbed. Blowouts are trough-shaped, sometimes reaching 0.5 km in length along the dominant axis, oriented NNW/SSE. In total, 105 surface types are identified, with >50% of the study area described by three classes (Table 2.5). This area is ~23% vegetated sandsheet, and nearly equally common are patchy-to-dense weeds, grasses, and forbs in interdunal grasslands.

Hamilton County, Kansas

Hamilton County, KS (Fig. 2.7c) yielded a ranking of 8, and experienced significant drought conditions during the DBD, with 5% higher maximum temperatures and an extreme precipitation deficit (-25%). Shortgrass prairie dominates this county, with largely sandy soils and smaller areas of clay loam soils. In 1935, agricultural census data indicates that 35% of the county was under cultivation, though only ~5% is observed as actively tilled in the 1939 imagery used for this study, suggestive of farmland abandonment. Much of the vegetation present are grasses on alluvial surfaces and sparse cover on sandsheets, with the densest vegetation along fluvial channels. However, nearly half of the study area is devoid of vegetation at the time of negative acquisition. Almost 33% of bare areas are severely denuded with the presence of barchanoid-type ridges palimpsest with sand sheet deposits and occasional large blowouts (~1 km). Slight-to-severe degradation is typically associated with sandsheets, nascent barchan dunes, and devegetated alluvial floodplains. Approximately 25% of cultivated surfaces are eroded, with sand apparently saltating across

the landscape from the northern edges of fields. Cultivated fields and pastures exhibiting degradation are most often associated with loamy sand or clay loam soils, whereas nearly all bare uncultivated landforms are composed of sand or silty sand. In total, 241 surface types are identified, with over half the study area described by six classes (Table 2.5). Most common in this study area is vegetated sandsheet on sandy soil, followed by active sand dunes, and severely-to-extremely denuded sandsheet surfaces.

Quay County New Mexico

The southern shortgrass prairie of Quay County, NM (Fig. 2.7d) experienced slightly warmer maximum temperatures than previous decades but a large precipitation deficit during the DBD and is ranked a six in the site selection scheme (Table 2.3). A maximum of 15% of the county was under cultivation in 1935, and few cultivated surfaces are observed in the 1936 photographs analyzed in this study. Forty-five percent of the study area is bare; where vegetation is present, it is typically grasses and shrubs. Extreme degradation is largely associated with sand dunes (>75%) which most frequently are parabolic or partially-reactivated barchanoid ridges, oriented NE-SW. Severe degradation is also observed for some fluvial surfaces, such as point bars and tributaries of the Canadian River, and sheet and rill erosion above incised channels. In total, 232 surface types are identified, with over half the study area described by nine classes (Table 2.5). The largest proportion of the study area is mapped as vegetated sandsheets developed on antecedent eolian sands, followed by severely degraded sandsheets.

Tillman County, Oklahoma

Tillman County, OK (Fig. 2.7e) falls at the confluence of the three dominant ecoregions of the Great Plains: short-, mixed-, and tallgrass prairie. This county, rated seven, experienced an 2% increase in maximum temperatures and 11% precipitation deficit during the DBD, and in spring of 1937 exhibited ~40% bare surfaces. Vegetated surfaces are evenly distributed across grasses, woody vegetation, and cropland. Cultivated surfaces are frequent; over half of fields are bare, with 25-30% classified as severely denuded. However, of the unvegetated areas ~60% is associated with fluvial deposits in the main channel and tributaries of the Red River, with dunes superimposed on terraces and partially active, reflecting a complex interaction between eolian and fluvial geomorphology and potentially influencing the evolution of both features (Liu and Coulthard, 2017). The majority of moderate-to-severe degradation occurs on cultivated fields, with the remainder common to older, topographically higher fluvial terraces with active sandsheets. This county exhibits a marked increase in diversity of soil type, land use and landforms than those counties west of the 500 mm precipitation isohyet. In total, 452 surface types are identified, with over half the study area described by fourteen classes (Table 2.5). The greatest portion of denuded area is mapped as bare fluvial deposits of loamy sand, followed by cultivated fields with sandy loam soils.

Lamar County, Texas

Lamar County, TX (Fig. 2.7f) covers the transition between southern tallgrass prairie to crosstimbers ecoregion and experienced largely neutral conditions during the DBD, receiving a rating of four. Approximately 45% of the study area is classified as cultivated fields and ~50% associated with the fluvial landforms and floodplain of the Red

River. Less than 30% of the surveyed area is bare, and a robust population of woody vegetation colonizes uncultivated surfaces. Generally dense vegetation is absent where land was cleared for cultivation. The majority (50-60%) of bare surfaces occurs in cultivated fields, and many fields relict show nebkha dunes, ~10 to 25 m in diameter and up to 2 m in relief (cf. Seifert et al., 2009). Among natural surfaces, deposits within the active channel of the Red River lack plant cover. Much of the moderate-to-severe degradation is associated with gullies on older fluvial terraces, whereas incipient vegetation loss is most frequently observed across the active floodplain. In total, 343 surface types are identified, with over half the study area described by sixteen classes (Table 2.5). The largest percentage of the study area is mapped as vegetated cultivated fields on clay soils, and dense vegetation on uncultivated loamy sand, silt loam, and clay soils.

Correlations, Components and Clusters of Ecoregion Variance

A statistical analysis was undertaken to evaluate the relation amongst land cover classes, landscape attributes and climatic variables. The extent of extremely denuded surfaces is positively correlated to loamy sand soils and fluvial deposits (e.g. point bars, alluvial islands; Fig. 2.8a). Areas of severely denuded surfaces are negatively monotonic with silty loam soils, cultivated fields, and MAP (Fig. 2.8b). Patchy cover of weeds and grasses increases where the summer PDSI of 1932, 1937, and the mean PDSI from 1931 to 1940 are lower (Fig. 2.8c). Dense, woody vegetation coverage increases with area of sandy loam soils, the density of fluvial drainages, the mid-range PDSI value during the DBD, and the number of surface types explaining at least 50% of site surficial diversity (Fig. 2.8d). The association between woody vegetation and greater diversity of surface types is further reinforced by shared monotonic trends with the summer PDSI for 1934 and

1935 (R_S = 0.943, p = 0.017), the change in maximum MAT (R_S = -0.841, p = 0.044), the average percentage of clay in county soils (R_S = 0.886, p = 0.033), and dominant ecoregion (R_S = 0.882, p = 0.033). The total count of surface types classified is positively correlated with area of silty loam soils (R_S = 0.88, p = 0.05) and the proportion of area under cultivation by 1935 (R_S = 0.886, p = 0.033). There is a positive correlation between areas of silty loam soils and cultivated fields (R_S = 0.941, p = 0.017). Cultivated fields are negatively correlated with sandsheets (R_S = -0.841, p = 0.044), though sandsheets trend positively with active dunes (R_S = 0.941, p = 0.022).

Principal component analysis (PCA) reduces the 52 variables included to three PCs that explain >80% of the variance, and >90% of the variance is accounted for by including the fourth PC (Fig. 2.9a, b). In component space, Ward County, ND plots in the lower

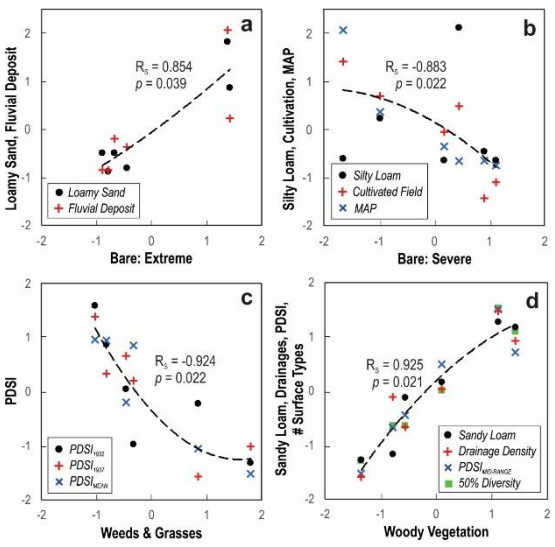

Figure 2.8 Scatter plots of selected variable pairs receiving a Spearman's rank correlation coefficient (R_S) equal to or over ± 0.8 and where $p \leq 0.05$ exhibit monotonic relationships between land cover, sediment texture, land use, and/or climatic factors: (a) area of extremely bare surfaces increases with area of loamy sand soils and fluvial deposits; (b) extent of severely bare surfaces increases where areas of silty loam soils and mapped cultivated fields decrease, and where mean annual precipitation (MAP) is lower; (c) cover of patchy weeds and grasses increases in counties where the Palmer Drought Severity Index (PDSI) is lower in 1932, 1937, and in the overall mean from 1931 to 1940; and (d) the densest, woody vegetation increases in coverage with areas of sandy loam soils, greater density of fluvial drainages, a higher mid-range PDSI from 1931 to 1940, and the number of surface types explaining at least half of the total surface area (50% Diversity).

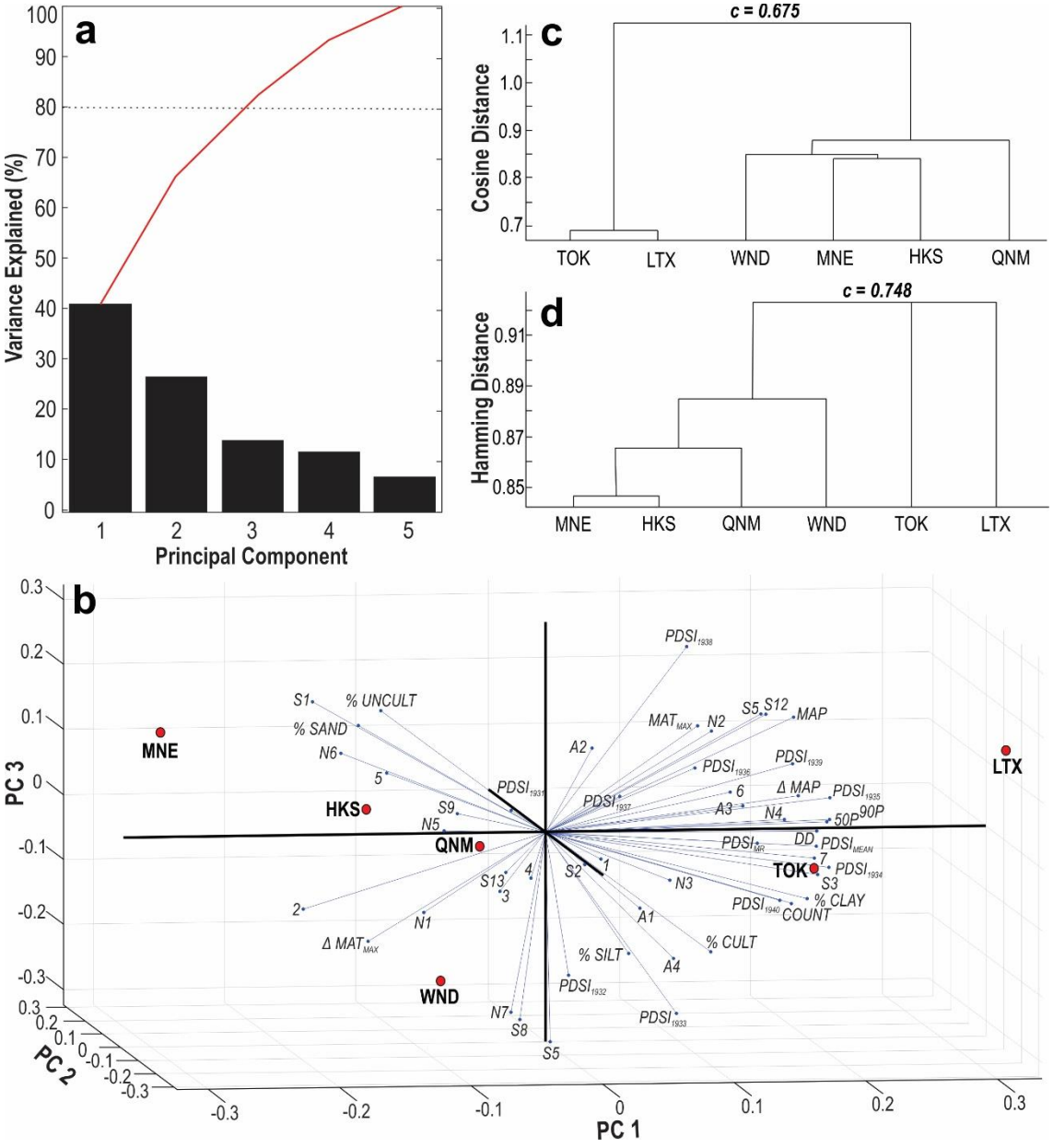

Figure 2.9 Multivariate statistical analyses of surface types by location in Ward County, ND (WND), McPherson County, NE (MNE), Hamilton County, KS (HKS), Quay County, NM (QNM), Tillman County, OK (TOK) and Lamar County, TX (LTX): (a) Scree plot of principal components, (b) Triplot of the first three principal components, (c) dendrogram of hierarchical clusters measured by cosine distance and (d) hamming distance, with cophenetic correlation coefficient, *c*.

quintile of the first three PCs, most closely associated with silty loam and silty clay loam soils, grassland, lacustrine basins, and change in maximum MAT. McPherson County, NE ranks in the lower quintile of PC1 and the upper quintile of PC3, with weed and grass cover and the average percentage of sand in county soils. Hamilton County, KS falls in the lower quintile of PC1 and the upper quintile of PC2, most closely associated with areas of mapped sand, clay loam soils, sandsheets, and the percentage of area uncultivated by 1935. Quay County, NM is in the upper quintile of PC2, generally correlated with areas of exposed bedrock, dunes, and moderately-to-extremely denuded surfaces. Tillman County, OK is in the upper quintile of PC1, most closely associated with: the total count of surface types classified, summer PDSI of 1934, 1935, and mid-range during the DBD, drainage density, and occurrence of sandy loam soils and woody vegetation. Lamar County, TX plots in the upper quintiles of PC1 and PC3, and in addition to the variables associated with Tillman County, is also correlated with 50% and 90% diversity thresholds in surface type, clay soils, percentage of land cultivated by 1935, and MAP.

As the PCA indicates four components explain > 90% of the variance between sites, four hierarchical clusters elucidate the covariance in surficial response across sites. Cosine distance of site linkages provides a relatively reliable cluster tree, with a cophenetic correlation coefficient (*c*) of 0.676 (Fig. 2.9c), though hamming distance determines a somewhat stronger correlation ($c = 0.748$, Fig. 2.9d). The former measure demarcates four clusters as: (1) Tillman County, OK and Lamar County, TX, (2) Quay County, NM, (3) Ward County, ND, and (4) McPherson County, NE and Hamilton County, KS. For both distance measures, the largest break occurs between cluster 1 and clusters 2-4; however, cosine distance closely links Tillman and Lamar counties where hamming distance creates

a discrete separation. Likewise, cosine distance calculates close linkages amongst clusters 2, 3, and 4 where hamming distance estimates more distinct, gradational steps between sites.

Discussion

Ecoregional Response to the Dust Bowl

The DBD is a vivid example for an annual record of drought on the USGP, though is modest in intensity and duration compared to droughts in the past 1,000 years (Cook et al., 2007; 2010; Woodhouse et al., 2010) and forecasted droughts for the 21st and 22nd centuries (Cook et al., 2015). Spatial analysis of countywide anomalies in maximum MAT, MAP, and PDSI from 1931 to 1940, concomitant with average soil texture, density of linear water features, and extent cultivated by 1935, illuminates the magnitude of DBD aridity in USGP counties and surficial coherence within ecoregions. The distribution of the highest ranked counties (8) reveals a cluster of impacted counties on the northern USGP in the Dakotas (Fig. 2.5g). The greater clastic influx between 1930 and 1950 observed in lake cores from the Dakotas and Minnesota underscores this regional aridity (Dean, 1997; Shapley et al., 2005; Wigdahl et al., 2014). Dust storms, like that observed November 12, 1933, moved progressively over Bismarck, ND and Omaha, NE, with suspended particles eventually raining out across southern and eastern states (Miller, 1934; Hovde, 1934). A less continuous cluster of southern counties occurs within the classically defined DBD area of severe wind erosion, constrained by a maximum MAT range of 20 to 25^{0}C, MAP of >500 mm, and the ~250 km eastward shift of this isohyet compared to the previous 35-year period (Fig. 2.2). Interestingly, the highest ranked counties within this region are also

where private hospitals were at capacity and Red Cross emergency hospitals were set-up to deal with a conspicuous increase in "dust pneumonia" (Chicago Tribune, 1935).

The apparent exception to this ranking system are the counties comprising the Nebraska Sand Hills, which ranked 4 and 5 despite persistent drought conditions. This suggests grassland response observed in this area may not be correlaTable 2.to other counties with respect to the surficial criteria included in the site selection overlay. The high infiltration capacity of sandy soils in tandem with the high levels of regional groundwater tables contribute to the dominance of baseflow control on local response, and baseflow is generally resistant to interannual climate variability (Wang et al., 2009). On annual time-scales the Sand Hills generate higher rates of mean runoff and recharge, correlated with lower actual evapotranspiration, than in adjacent areas with siltier soils and relative to the amount of precipitation received (Gosselin et al., 2006; Harvey et al., 2007; Wang et al., 2009). The consistency of groundwater levels since AD 1700 appears to buffer the impact of the DBD in this region of Nebraska. However, multi-decadal droughts during the MCA (~AD 800 to 1200) were sufficiently severe for a regional decline in the water table, with concomitant landscape denudation and increase of eolian transport and deposition (e.g. Harvey et al., 2007; Miao et al., 2007; Halfen and Johnson, 2013).

Influence of Surficial Properties and Climate on Great Plains Landscape Degradation

The spread of landscape degradation identified reflects ephemeral and cumulative effects of multiple controls that vary with antecedent landscape conditions and persistence of climatic anomalies (Turner, 1989; Schlesinger et al., 1990; Peters et al., 2007; He, 2014; Petrie et al., 2016). Principal component analysis indicates that site variance largely parallels location east or west of the 100th meridian, coupled with the severity of the

precipitation deficit during the 1930s. The secondary component is related to the latitudinal temperature gradient and predominant land use and geomorphology, with a tertiary influence from soil texture and/or the annual PDSI during the DBD. Similar studies of USGP grasslands find that many ecosystem processes are primarily driven by precipitation and modified by temperature (Petrie et al., 2016; Nielson et al., 2018; Seager et al., 2018). This analysis is also consistent with a linear relationship between drought intensity and ecosystem resistance observed in a global analysis of grassland response to ~500 drought events (Ruppert et al., 2015).

Clustering analysis illustrates the differences in landscape stability across the arid-to-humid divide. Biotic controls tend to drive ecosystem stability east of the 100th meridian, with increased plant functional diversity and greater below-ground biomass of woody species (He, 2014; Lei et al., 2016). Both Tillman County, OK and Lamar County, TX, are characterized by mostly continuous dense or woody vegetation increasing with areas of greater soil clay content, near-river landforms, and reduced temperature anomalies, likely reflecting water availability. Tallgrass prairie is generally resistant to inter-annual precipitation variability and resilient to daily or weekly extremes (Jones et al., 2016), and more sensitive to monthly and seasonal precipitation distribution (Petrie et al., 2016). The distribution of the densest vegetation cover in this region is most strongly correlated with the summer PDSI of 1934 and 1935. This association would suggest ecosystem degradation in the eastern USGP was largely driven by plant response to the magnitude shift in seasonal conditions from 1934, recognized as the most severe drought year of the last millennium (Cook et al., 2014), to 1935, a wet period for the southeastern USGP (Fig. 2.3e). Noteworthy in Lamar County, TX are the relict nebkha dunes revealed at the surface in

areas cleared for cultivation. These features are similar to sites dated to 700 to 1,000 yr BP on the Ozark Plateau and underscore the spatial extent and intensity of MCA droughts in the late Holocene (e.g. Seifert et al., 2009).

Abiotic controls appear to more strongly influence grassland degradation west of the 100th meridian and are associated with latitudinal temperature effects (Nielsen, 2018). The northern ecoregion of Ward County, ND experienced some of the most pronounced increases in maximum temperature during the DBD but is largely detached from other western sites in component space related to the overall lower MAT and dominance of siltier soils. Quay County, NM is likewise clustered individually but is near in component space to Tillman County, OK, as both are southern ecoregions with milder DBD conditions, and shows a greater diversity of surface types than other western counties. Nonetheless, this area of eastern New Mexico is statistically linked to Hamilton County, KS and McPherson County, NE, and correlated with the distribution of increasingly sandy soils and large patches of eolian landforms indicative of soil erosion. These latter two counties are both central ecoregions with a similar distribution of land use, high soil sand content, and exhibit less surficial diversity than eastern sites as sandsheets and dunes cascade across the landscape. McPherson County is influenced by groundwater levels at the margins of the Sand Hills and classified as mostly vegetated sandsheet and interdunal grassland with little change to extent of cultivation. Whereas Hamilton County shows ~50% vegetation loss of shortgrass prairie, associated with active eolian landforms and a sharp increase in apparently fallow fields.

Broadly, the distribution of denuded surfaces during the DBD exhibits stronger nonparametric correlations with surficial properties than climatic factors. Land use

interacts with degradation regardless of setting but is more significant to explain site variance in eastern counties, whereas uncultivated landforms dominate the drier, western areas. Sand-dominated soil textures on landscapes with maximum relief are correlated with more frequent denudation for western counties. The areal extent of blow-outs, parabolic dunes, sinuous ridges, and sandsheets positively covary, and this heterogenous landform assemblage correlates to intensity and persistence of 1930s aridity (Hugenholtz and Wolfe, 2005; 2006). Particle sources for the DBD have been attributed solely to areas of agricultural disturbance in the south-central Great Plains (cf. Bennett and Fowler, 1936; Johnson, 1947; Worster, 1979; Hansen and Libecap, 2004; Schubert et al., 2004; Cook et al., 2008, 2009; Lee and Gill, 2015). This analysis identifies large uncultivated areas that were equally or more a source of dust during the DBD than plowed agricultural fields. On the Northern Great Plains (North Dakota), one significant source of dust is with the drop of lake level and the exposure of lake sediments and adjacent eolian deposits. In the classic DBD area, the many stabilized, high-relief sand-rich dune systems adjacent to major rivers were partially to wholly denuded and were significant sources of dust.

Implications for Future Great Plains Grassland Response to Drought

A similar shift in the arid-to-humid transition as observed during the 1930s is projected for the future, which can strongly influence settlement sustainability and agricultural development (Nielsen 2018; Seager et al., 2018). The overuse of groundwater coupled with rising costs of irrigation could cause groundwater tables to lower and increase susceptibility of previously-stable systems (Parton et al., 2007). Future warming may reduce vegetation cover and soil moisture over large areas of USGP grasslands, exacerbating soil erosion, degradation feedbacks, and decline of terrestrial carbon sinks

(Schlesinger et al., 1990; Lei et al., 2016; Hu et al., 2018). Regional hydroclimatic variability and carbon sequestration is therefore dependent on how land surface changes modulate climatic conditions (Cook et al., 2013; Petrie et al., 2016; Hu et al., 2018). Given the potential speed and irreversibility of such changes (Breshears and Barnes, 1999; Collins et al., 2014; Moran et al., 2014; Svejcar et al., 2015), characterizing USGP grassland response during severe drought is significant to constrain the large variability in landscape degradation (Petrie et al., 2016), and to better guide adapTable 2.land and carbon management (Basara et al., 2013; Ruppert et al., 2015; Lei et al., 2016; Petrie et al., 2016; Byrne et al., 2017).

Conclusion

The wealth of images and associated documentation for the 1930s Dust Bowl enables quantitative evaluation of land surface processes and inferred vegetation changes on a regional- to sub-meter scale. The extent of landscape degradation during this historic drought was assessed across a latitudinal temperature and longitudinal precipitation gradient for the USGP from historical aerial negatives acquired from six representative counties to better understand biotic and abiotic processes during the nearly decade-long drought. During the DBD, the 500 mm isohyet shifted several hundred kilometers to the east. The surficial response on the USGP during the DBD is found to most strongly correlate with this redistributed arid–humid divide, the magnitude of precipitation and temperature anomalies, and soil texture. Similar surficial response to the DBD was observed from sites within the same ecoregion, highlighting the role of dominant species and functional diversity of plants (Lei et al., 2016) and a nearly linear relationship with

intensity of aridity (Schlesinger et al., 1990; Tongway and Ludwig, 1994; Bestelmeyer et al., 2006; Ravi et al., 2010; Ruppert et al., 2015).

The dominant sources of degradation found for study sites east of the 100th meridian were cultivated fields and fluvial deposits, associated with woody vegetation response to water availability in uncultivated areas. For sites to the west, denuded surfaces are predominantly eolian sandsheets and dunes, correlated with intensity of drought conditions and reduced plant diversity. Discrete spatial signatures of the drought are observed not only within the classically recognized southern Dust Bowl area, but also in the northern and central plains, suggesting a much larger regional response to the drought than previously recognized. The source of the namesake dust storms of the DBD has hitherto been attributed solely to areas of agricultural disturbance in the south-central Great Plains (cf. Bennett and Fowler, 1936; Johnson, 1947; Worster, 1979; Hansen and Libecap, 2004; Schubert et al., 2004; Cook et al., 2008, 2009; Lee and Gill, 2015). This analysis demonstrates the potential of locally denuded, uncultivated, sand-rich areas across the USGP as equivalent or greater sources for particle emission during intense drought than plowed agricultural fields. The USGP is forecast to become more vulnerable to drought stress in the 21st century, with increasing demands on water resources and concomitant increase in dominance of abiotic drivers, which could precipitate a landscape response similar to the DBD (Ravi et al., 2010; Woodhouse et al., 2010; Basara et al., 2013; Cook et al., 2015).

Acknowledgments

This research is supported by the National Geographic Society (#9990-16), the National Science Foundation Award GSS-1660230, and the Glasscock Endowed Fund for

Excellence in Environmental Science (032MBCU31). We are grateful to National Archives staff for research assistance and material access and to Dirk Burgdorf of AAA Research for aerial photograph reproduction.

CHAPTER THREE

Meteorological Conditions and Particle Source Dynamics for Dust Storms During the 1930s Dust Bowl Drought, Southern High Plains, USA

Abstract

Mineral dust aerosols are a key component of the Earth system and a growing public health concern under climate change as levels of dustiness increase. The U.S. Great Plains is particularly vulnerable to dust episodes, but land-atmosphere feedbacks contributing large-scale dust particle transport (i.e. a dust storm) are poorly constrained, introducing uncertainty in predicting future dust-borne risks to air quality and drought persistence. This study utilizes dust storm records and experiment station reports from the Soil Conservation Service (SCS) gathered between April 1938 and May 1940, Global Historical Climate Network and 20th Century Reanalysis data products, combined with contemporary field surveys using a Portable *In-Situ* Wind Erosion Laboratory (PI-SWERL), to examine surficial dynamics of particle emission and identify meteorological catalysts for storm frequency and intensity on the Southern High Plains, the heart of the 1930s "Dust Bowl." The SCS experiment sites reported 1,360 storms during these 25 months, lasting a total of ~9,603 hours – nearly 50% of the elapsed time. Multivariate statistical analyses of dust storm variance yield 6 principal components, individually explaining >5%, and together capturing ~60%, of the variance of all dust-storm days, related to surface and lower-level atmospheric air temperatures, low-level relative humidity, storm start time and total duration, and the extent of eolian deposits in the county of storm origin. Four dominant modes of dust storms are identified related to the season of

occurrence and dominant meteorological controls. A broader assessment of the potential emissivity of SHP soils reveals that disturbed surfaces begin to emit at a magnitude-higher rate than undisturbed surfaces as soon as the threshold wind velocity (8 to 10 m s^{-1}) is reached, and this rate increases linearly with windspeed. Conversely crusted, undisturbed soil surfaces do not begin to reach the same flux rate until much higher wind speeds, at which point crusts are broken and emissivity rates increase exponentially. Significantly, the particle emissivity of undisturbed, loose sandy soils mirrors that of disturbed surfaces in relation to windspeed and potential magnitude of dust emission. This suggests that the prevalent sandier, rangeland soils of the SHP could be equal or greater dust sources than cultivated fields during periods of sustained, severe aridity.

Introduction

A persistent feature of 21st century climate models is the increased frequency of droughts on the U.S. Great Plains (USGP), often with a severity and duration exceeding conditions of the 1930s Dust Bowl Drought (DBD; e.g. Woodhouse et al., 2010; Cook et al., 2014; 2015; Pu and Ginoux, 2017). Past and future megadroughts on the USGP are associated with ecotone changes, an increase in dust generation from denuded surfaces, and particle transport to nearby urban centers resulting in significant public health risks (Morman and Plumlee, 2013; Takaro et al., 2013; Goudie, 2014; Takaro and Henderson, 2015; Sprigg, 2016). The Southern High Plains (SHP) is a particularly potent source for atmospheric dust loading, likely to be exacerbated by competing agricultural and urban interests in water resources as drought intensifies (Basara et al., 2013; Cook et al., 2015). Historic records of drought in the past ca. 200 years document common large-scale dust storms, with the dense entrainment of mineral dust and other aerosols (Peters et al., 2007;

Cook et al., 2009; 2013; Ravi et al., 2010), affecting air quality for a day to weeks at a time (Hand, 1934; Raman et al., 2014; Eagar et al., 2017). A deeper understanding of dust sources related to landscape denudation during the DBD, the last continental-scale drought for North America, offers necessary context to better inform the extent, the severity, and the possible societal impacts of forecast severe dustiness on the SHP in the late 21st century (e.g. Pu and Ginoux, 2017).

The DBD was a time of elevated summer temperatures and pronounced deficits in evapotranspiration (ET). Record-setting negative precipitation anomalies and agricultural practices across the SHP, a broad area inclusive of the Texas and Oklahoma panhandles, northeastern New Mexico, eastern Colorado and western Kansas (Fig. 3.1a), led to surficial degradation and 1,000s of dust storms, particularly post-1933 (Joel, 1937; Cronin and Beers, 1937; Johnson, 1947; Chepli, 1957; Chepli et al., 1963; Borchert, 1971; Worster, 1979; Cunfer, 2005; Egan, 2006; Burnette et al., 2010; Burnette and Stahle, 2013; Lee and Gill, 2015; Donat et al., 2016). Climate modeling studies and reanalysis of climate data places the DBD in a global context and underscores the complex land-ocean-atmospheric interactions during extreme droughts (Schubert et al., 2004; Fye et al., 2006; Cook, E. et al., 2007; Seagar et al., 2008; Cook, B. et al., 2011; Nigam et al., 2011; Seagar and Hoerling, 2014; Donat et al., 2016; Hu et al., 2018). However, there is insufficient knowledge of land surface processes, ecosystem changes, atmospheric feedbacks, and concomitant physical controls on dust emissivity across the classic Dust Bowl region (Fig. 1b; Cordova and Porter, 2015; Lee and Gill, 2015; Bolles et al., 2017; Bolles and Forman, 2018), which can limit climate model performance.

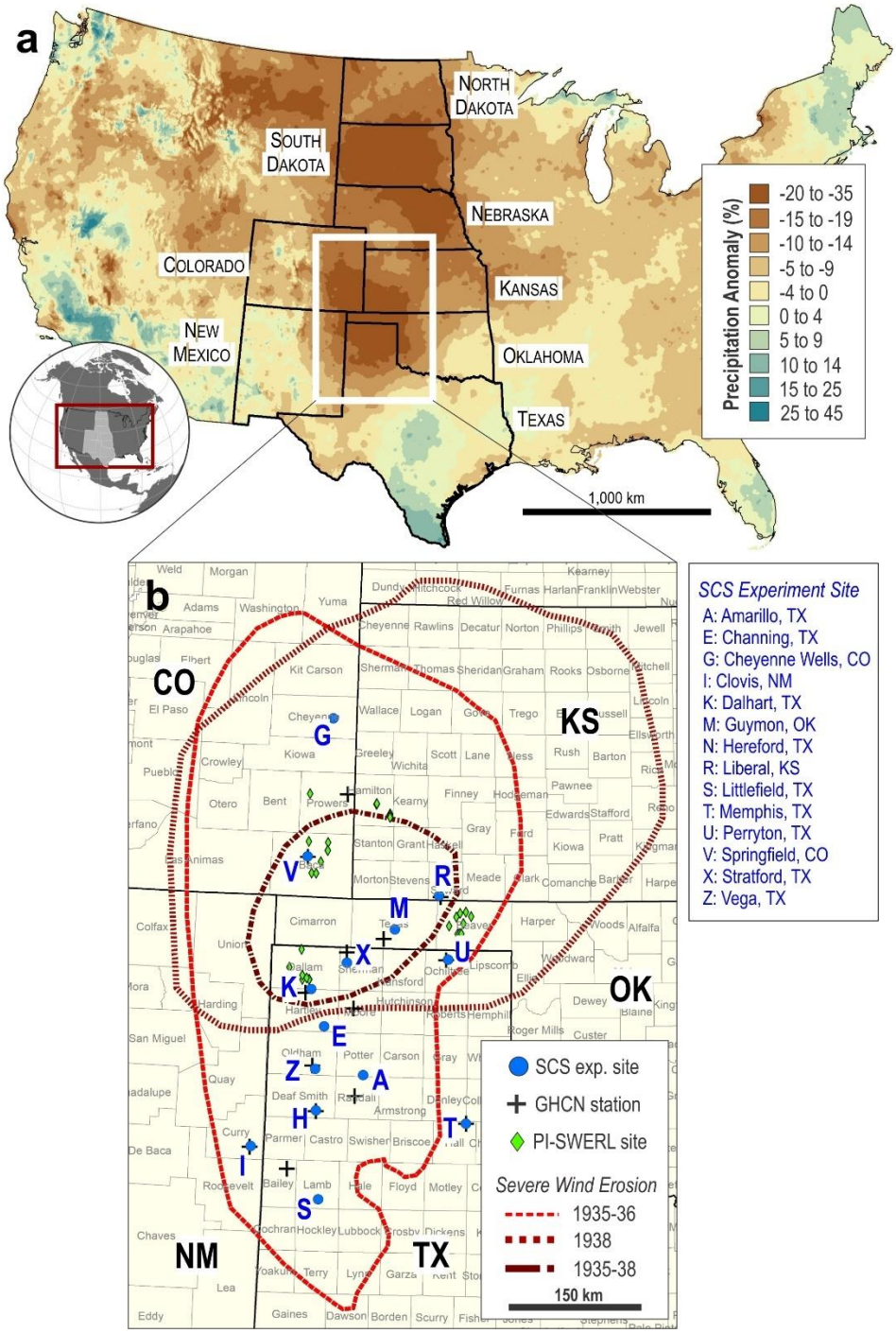

Figure 3.1. Location of the Southern High Plains (SHP) and spatial distribution of observations incorporated in this study: (a) For the SHP (white box) precipitation anomalies during the Dust Bowl, 1931-1940, indicate significantly drier conditions than during the previous 36-year period, 1895-1930 (calculated from PRISM Historical Past data series, http://prism.oregonstate.edu, created August 30, 2018), and (b) The locations of former Soil Conservation Service (SCS) experiment sites recording dust storms, weather stations used from the Global Historical Climate Network (GHCN), and emissivity measurements recorded in the field with the PI-SWERL, in relation to the classically-defined severe wind erosion area (erosion boundaries redrawn from SCS map, dated March 1954, National Archives, Record Group 114, Entry 5).

This study attempts to unite meteorological and land surface observations from the 1930s with contemporary field surveys and measurements to better define the variance in SHP dust activity during the DBD. We seek to address three over-arching questions: (1) What is the role of meteorology in controlling the variability of dust storms during this prolonged period of aridity? (2) Is there an observational basis to characterize dust storm events within the classically-recognized Dust Bowl? (3) How does the surficial emissivity of potential dust sources across the SHP differ by soil texture, and by what magnitude does anthropogenic disturbance impact particle flux from soils of varying particle size distributions? To explore these questions a daily record of dust storm occurrence between April 1938 and May 1940 was compiled from archival records of SCS experiment stations (National Archives, Record Group 114), and coeval meteorological conditions retrieved from the Global Historical Climate Network (GHCN; Menne et al., 2012), and the 20th Century Reanalysis Project (2RAP; Compo et al., 2011). Principal component analysis (PCA) of the resultant dust storm inventory reveals potential causative factors for event generation and persistence. Further, hierarchical clustering analysis distinguishes groups of dust storms based on parallel covariance, illuminating common modes of dust storms. Finally, the relative contribution of available particle sources for SHP dust storms is assessed based on the magnitude of surficial particulate matter (PM_{10}) flux as a function of windspeed, measured in the field for different soil textures and land uses.

Mechanisms of Dust Particle Generation and Transport on the Southern High Plains

Dust emissions from mesic to semi-arid environments often reflect an interaction between extreme climate variability and human-induced landscape degradation, particularly since at least the early 20th century (Ginoux et al., 2012). Previous studies have

examined individual dust storms (e.g., Lee et al., 2012; Eagar et al., 2017), scrutinized synoptic climatology of dust events (e.g., Novlan et al., 2007; Knippertz, 2014), meteorological controls on atmospheric dust levels (e.g., Hahnenberger and Nicoll, 2012; Lei and Wang, 2014; Achakulwisut et al., 2017), and surface dust source extent and emissivity (e.g., Lee et al., 2009; Rivera Rivera et al., 2010; Sweeney et al., 2011; Flagg et al., 2014; Parajuli et al., 2014). Locally, dust emission is controlled by soil texture and moisture, surface roughness, the presence of soil crusts, wind speed, topography and vegetation cover: interdependent factors that respond nonlinearly to climate (Hugenholtz and Wolfe, 2005; Jickells et al., 2005; Werner et al., 2011; Houser et al., 2015). Changes to vegetation cover, soil moisture, and surface albedo may alter the atmospheric boundary layer, amplifying regional ET and precipitation deficits and, most significantly for dust emission, mesoscale cyclonic disturbances sufficient to generate strong winds (Hahnenberger and Nicoll, 2012; Knippertz, 2014). Once entrained, the radiative effects of dust particles can modify the temperature gradient, pressure differential and local wind field, which then can alter cyclogenesis and rates of dust emission, transport and deposition across North America (Tegen et al., 1996; Boucher et al., 2013).

Poor agricultural stewardship has been designated as the major cause for widespread landscape denudation during the DBD, which purportedly left cultivated areas barren and exposed to eolian erosion (e.g. Bennett and Fowler, 1936; Johnson, 1947; Worster, 2004; Hurt, 1981; Hansen and Libecap, 2004). The still photographic record captured during the 1930s under the auspices of the Farm Security Administration (Ohm, 1980; Lange, 1981; Packer, 2011), showed desolate fields covered by wind-rippled sands, and dunes that engulfed homes, out buildings, fields and fence-lines (Fig. 2).

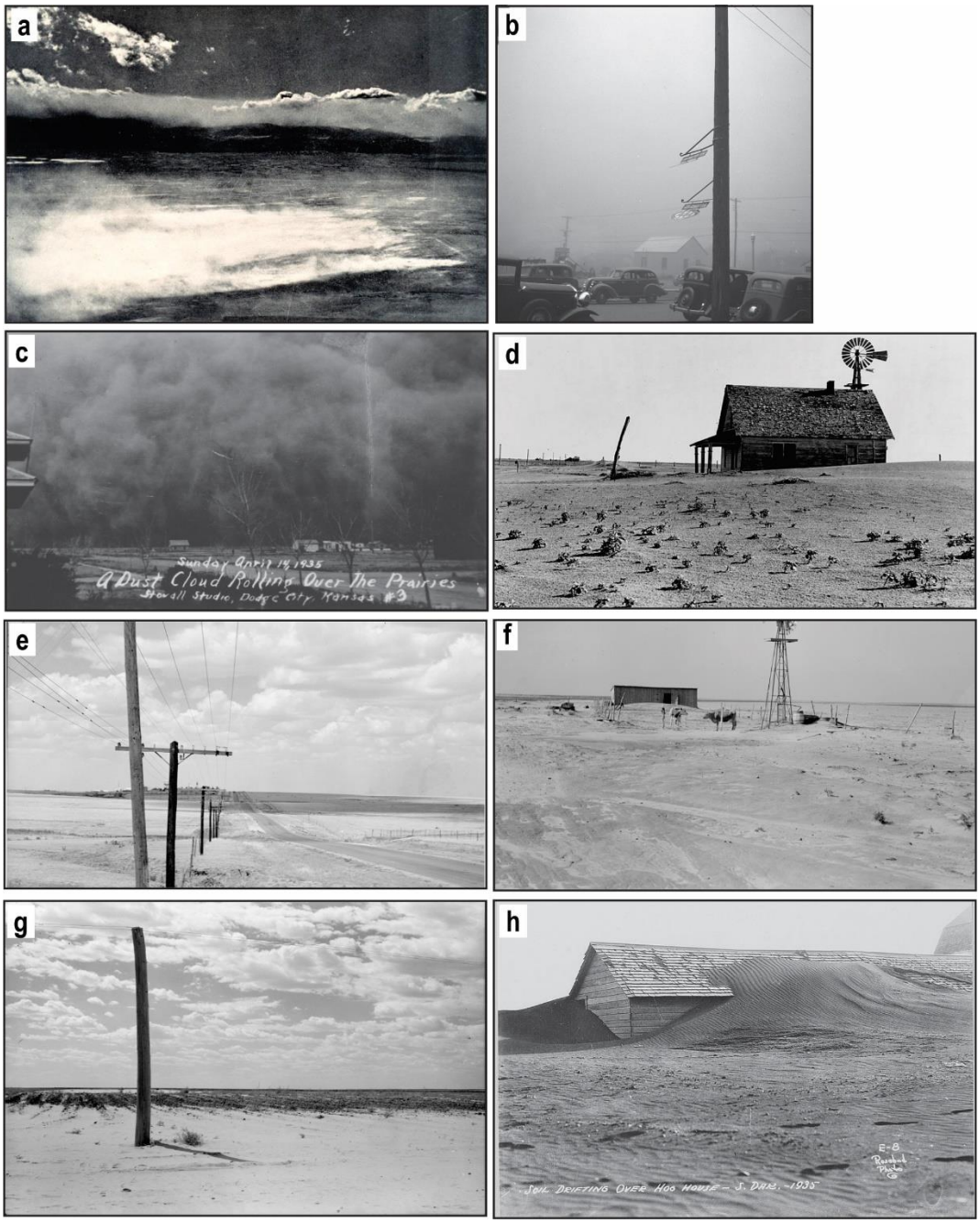

Figure 3.2. Dust Bowl Drought still photographic record; (a) Aerial view of the beginning of a dust storm over the Piedmont west of Denver (from Choun 1936, p. 197). (b) Dust storm in Amarillo, TX, April 1936, photographed by Arthur Rothstein (Farm Security Administration [FSA], National Archives, Digital I.D. 8b27557). (c) The dust storm on Black Sunday April 14, 1935, near Hugoton, KS (accessed from: http://www.kansasmemory.org/item/323). (d) Dust Bowl farm in the Coldwater District, north of Dalhart on June 1938, taken by Dorothea Lange (FSA, National Archives, Digital I.D. 8b32396). (e) Great Plains and highway north of Amarillo, TX, August 1938 taken by Dorothea Lange (FSA, National Archives, Digital I.D. 8b34910). (f) Barn and shed of farm in the Texas Panhandle near Boise City, TX on 1938 June taken by Dorothea Lange (FSA, National Archives, Digital I.D. 8b38680). (g) View near Dalhart, TX of plants and sand on July 1936, taken by Arthur Rothstein (FSA, National Archives, Digital I.D. 8b28143). (h) Soil drifting over hog house, South Dakota (FSA, National Archives, Digital I.D. 8e03187).

This photographic record documented in some areas the severity of land surface responses to intense drought and was evoked to characterize the geomorphic consequence of the DBD (cf. Lockeretz, 1978; Riebsame 1986; Lookingbill, 2001; Porter and Finchum, 2009; Porter, 2012; Duncan and Burns, 2012). However, analyses of historical agricultural census data underscores that just one-third of the Dust Bowl area was under cultivation in the 1930s and questioned if poor agricultural practices were the only cause for soil loss (Cunfer, 2005; Hornbeck, 2012). Closer scrutiny of agricultural treatments in an analysis of mosaicked aerial photographs from the 1930s across Kansas concluded that the misuse of land unsuitable for cultivation was relatively rare (Sylvester and Ripley, 2012). Additionally, stratigraphic studies documented partial re-activation of stabilized dune fields during the 1930s in western Kansas (Forman et al., 2008; Bolles et al., 2017). Aerial photographs acquired during the 1930s have revealed many areas of active-eolian sand transport, indicating natural and anthropogenic dust sources during the DBD (Bolles et al., 2017; Bolles and Forman, 2018).

Dust storms with fine particulate transport ($PM_{2.5}$) of >500 $\mu g\ m^{-3}\ d^{-1}$ are common occurrences in the Northern Hemisphere and often originate from arid and semi-arid land surfaces (e.g. Goudie, 1983; 1994; 2001; 2009; Goudie and Middleton, 1992; Péwé, 1981; Engelstaedter et al., 2006; Mahowald et al., 2014). Natural mineral dust sources such as semi-arid sandy lands of the USGP are not typically considered global dust sources. However, sandy areas are frequently identified as a major contributor to regional dust aerosol loads (e.g. Bullard and White, 2005; Lee et al., 2009; 2012; Goossens and Buck, 2011a, b; Sweeney et al., 2011; 2016). The landforms most prone to dust emission contain abundant sand sources, and such surfaces begin to emit dust at lower friction velocities

compared to crusted soils with higher silt content (Gillette et al., 1980; Sweeney et al., 2011; Flagg et al., 2014). Sandy soils, such as those that predominate the SHP, commonly emit dust via sustained and high magnitude events through mechanisms that include chipping of sand grains during ballistic impact, removal of grain coatings, and saltation bombardment (Shao et al., 1993; Bullard and White, 2005; Crouvi et al., 2012; Sweeney et al., 2016). These micro-scale mechanisms, when combined with severe drought conditions, have the potential to cause magnitude increases in the production of mineral dust aerosols. Though dust emissions can be short-lived and occur in isolation, often it is part of a succession of events leading to large-scale dust episodes spanning days to weeks, with continental-scale impacts (Donarummo et al., 2004; Peters et al. 2004; 2007; Knippertz, 2014).

Meteorological conditions (Lei and Wang, 2014; Raman et al. 2014; Achakulwisut et al., 2017; Tong et al., 2017), synoptic pressure gradients (Knippertz, 2014), and land-atmosphere feedbacks (Cook et al., 2009; Hu et al., 2018) contribute to the scale and intensity of dust emission. The most vigorous dust storm, or haboob, (Sutton, 1931; Idso et al., 1972; Williams et al., 2009) generally forms with the passage of a steep front and a sustained, deep low-pressure system that induces intense atmospheric convection over a sparsely vegetated terrain (Sidwell, 1938; Smith et al., 1970; Idso et al., 1972; Chen and Fryrear, 2002; Novlan et al., 2007). Haboobs in the western U.S. are often characterized by a dense dust-cloud associated with Mesoscale Convective Complexes (MCCs), particularly during the summer monsoon season (Idso et al., 1972; Patterson and Gillette, 1977; Maddox, 1983; Lee and Tchakerian, 1995; Novlan et al., 2007; Camino et al., 2015; Baddock et al., 2016; Eagar et al., 2017). Eastward shifts of atmospheric dust

concentrations and zones of light dust air-fall across the Midwest during the DBD extended nearly to the eastern seaboard, reflecting the passage of such dust-laden low-pressure systems (Handy et al., 1960; Brown et al., 1968; Namias, 1982; Mo et al., 1997).

Methods

Archived Records of the Soil Conservation Service

The SCS established a series of soil experiment stations focused on developing new methods to prevent eolian erosion, runoff, and stabilize blowing soils to mitigate the environmental devastation of the DBD. The archived records from these experiment stations span from 1929 to 1942 and yield detailed accounts of land surface conditions at the township scale. In particular, these records reveal for the 1930s annual changes in soil and water conservation practices, observations on vegetation type, cover, and distribution, tillage operations, documentation of erosion and revegetation of abandoned fields, still photographs, and field-level erosion maps. This study utilized records from four experiment stations in Fort Hays, KS, Elkhart, KS, Amarillo, TX, and Dalhart, TX. Records from the Dalhart SCS substation, where data was centralized from dozens of smaller experimental sites, offer a particularly comprehensive record of dust storms from 1937 to 1941. The datasheets from these sites report the dust storm days per month, providing an inventory of dust storms at the center of the traditionally-drawn Dust Bowl boundaries (Fig. 1b). This study focused on data from April 1938 to May 1940 because at least 80% of experimental sites submitted monthly data series during this period, and thus minimizes the error introduced by inconsistent reporting.

Statistical Analyses of Dust Storm Variability

Statistical analyses were utilized to decompose dust storm variance during the study period, which were computed on a matrix of 31 variables for 1,018 dust events. Dust storms with missing values were excluded from this portion of analysis to ensure data standardization without undue skewing. A pairwise correlation using Spearman's Rho (R_S) was calculated to explore the strength and direction of dependence between the rank order of variable pairs, with an R_S over ± 0.8 and a p-value ≤0.05, indicative of a strong monotonic relation (Borradaile, 2003). A principal component analysis (PCA) of the same matrix reveals the strength and direction of variable covariance, and the subsequent principal components (PCs) are mutually uncorrelated (Wilks, 2011). We consider individual PCs explaining at least 5% of the variance to have a substantial correlation to the distribution of dust storms. The specific eigenvectors most closely associated with each PC above this 5% threshold are identified within the 90th percentile of absolute variable coefficients. Finally, seven distance metrics are computed between storm observations to determine the hierarchical cluster tree(s) with the strongest cophenetic correlation (Wilks, 2011), as evaluated by Euclidean, squared Euclidean, correlation, cosine, city block, hamming, and Spearman's linkages. The number of PCs needed to explain 90% of the variance is set as the maximum number of clusters, with linked cluster tree nodes aggregated to the number of PCs needed to explain 50% of the variance, to characterize common dust storm modes.

Assessment of Potential Emissivity from Modern Analogous Surfaces

The Portable *In-Situ* Wind Erosion Lab (PI-SWERL; Etyemezian et al., 2007) measures the potential of soil surfaces to emit dust. Dust emissions from the PI-SWERL

are equitable to large field wind tunnels (Sweeney et al., 2008) and it has been tested on a variety of geomorphic surfaces (Bacon et al., 2011; Goossens and Buck, 2009; King et al., 2011; Sweeney et al., 2011; 2016a, 2016b; Sweeney and Mason, 2013). In the field, 139 sites were measured from a spectrum of soil textures ranging from silt-loam to sand, derived from Late Pleistocene and/or Holocene eolian and fluvial deposits. Sites were distributed across land use and landforms on: 1) active dune sand, 2) stabilized dune sand, 3) buried soils developed in eolian sand, 4) sandsheet areas, 5) cultivated areas, both fallow and actively used. A hand cultivator was used to pulverize soil crusts and aggregates for "disturbed" surface tests to simulate the effect of tillage on dust emission, particularly "listing," a documented practice in the 1930s that enhanced particle flux (Lee and Gill, 2015). At each site a bulk soil sample was collected for particle size analysis by a Malvern Mastersizer 2000.

The PI-SWERL contains an annular blade in an enclosed 0.5 m diameter cylindrical chamber, open to the ground surface, that rotates at prespecified speeds that are equated to friction velocities (u*, m s^{-1}). The rotation speed can be increased in a step-wise fashion to measure the response of the surface to different friction velocities. A DustTrak II aerosol monitor (TSI, model 8530) measures the concentration of PM_{10} dust emitted during testing in mg m^{-3}. Dust concentrations are converted to a dust emission rate (mg m^{-2} s^{-1}) using the area under the annular blade, duration of the test, air flow rate, and dust concentration (Sweeney et al., 2008). The friction velocities exerted by the PI-SWERL assume a smooth surface, so a surface roughness correction must be applied (Etyemezian et al., 2014). The surface roughness correction, alpha (α), is chosen from a look-up table based on grain size

of the soil surface, the presence of a smooth or rough crust, stones, or soil clods. Values range from 0.84 to 0.98, with 1.0 equaling a perfectly smooth surface (Table 3.1).

To equate PI-SWERL friction velocities to 2-m wind speeds, we applied the "law of the wall" and estimated landscape-scale surface roughness values. Surface roughness lengths for sand dunes was estimated at 0.00023 m (Oke, 1978; Gillette et al., 1982; Lancaster, 2004), and bare to sparsely vegetated agricultural fields were estimated at 0.0005 m (Gillette, 1988). Flux curves for a particular surface type are derived from goodness-of-fit tests for exponential and quadratic polynomial functions, with and without robust bisquare fitting enabled. Iterative experimentation demonstrated these models provide more accurate fits than linear polynomial and power law functions. Initial coefficients are estimated from the fit tests and used in model runs to determine the regression with the lowest root mean squared error (RMSE) and functional simultaneous 95% confidence intervals. Where the RMSE between models is equal or nearly equal, the regression returning the lowest mode value of residuals is selected.

Table 3.1. Alpha (α) coefficients and corrected shear velocities for particulate matter (PM_{10}) flux measured by the PI-SWERL for each soil condition.

α	**Soil Condition**	**Shear velocity (m s^{-1}) of PI-SWERL RPM**			
		2000	*3000*	*4000*	*5000*
1.0	—	0.38	0.53	0.68	0.82
0.98	Smooth crust, Very fine sand	0.40	0.56	0.72	0.87
0.96	Loose fine-medium sand	0.42	0.60	0.77	0.93
0.94	,Rough Crust, Medium-coarse sand	0.45	0.64	0.82	1.00
0.92	Crust with small clods	0.47	0.68	0.89	1.08
0.9	Sand with small clods	0.50	0.73	0.96	1.18
0.86	Stones or Clods, 1-4 cm	0.58	0.86	1.14	1.42
0.84	Clods, 4-5 cm	0.63	0.95	1.26	1.57

Results

Data Constraining the Distribution and Character of the 1930s Dust Storms on the Great Plains

There are few localities with continuous records of dust storms for the 20th century on the Great Plains. Records for Dodge City and Garden City, KS show peak occurrence at 100 to 120 dust storms per year from 1936 to 1939 (Fig. 3.3a), a ten-fold increase compared to the wettest periods of the 1920s and 1940s, with an average of <10 storms per year (Orgill and Sehmel, 1976). A similar "background" dust storm frequency was documented for Lubbock, TX between 1942 and 1965, with the threshold for dust storm

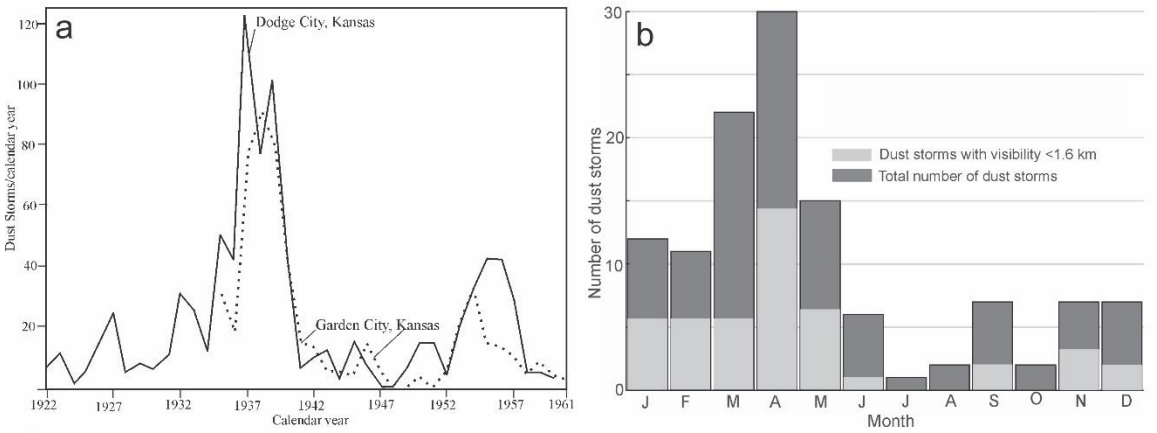

Figure 3.3 (a) Dust storm occurrence for Dodge City and Garden City, KS between 1922 and 1961 (from Chepli et al., 1963); and (b) Monthly Dust Storm frequency for 1933 and 1934 for Amarillo, TX (from Choun, 1936).

identification a visibility of ≤10 km (Orgill and Sehmel, 1976), a somewhat higher threshold than many DBD metrics. The highest frequency of dust storms in the 1930s occurred preferentially in the spring, usually during April and May (Fig. 3.3b), with the increased west to east passage of cyclonic disturbances (cf. Schubert et al., 2004; Novlan et al., 2007) and similar to dust storm frequency between 1942 and 1970 for the conterminous U.S. (Orgill and Sehmel, 1976). A secondary peak in dust storm activity occurred in January with a preponderance of severe dust storms (>30%) when visibility

was <1.6 km (Fig. 3.3b), which mirrors broader trends for dust storm occurrence post-DBD across the U.S. (Orgill and Sehmel, 1976).

There is limited data on dust deposition rates, concentrations, and TSP for the Great Plains during the 1930s, though there are multiple sources of dust recognized across the DBD landscape (Lee and Gill, 2015). The most common dust deposition measurements were completed post passage of a dust storm as deposited thicknesses of sediment for a known area over a period of time, usually within 24 hours (Table 3.2). These measurements included sediment thicknesses for deposits on agricultural fields, within flat "Texas" cake-baking pans placed on elevated areas (usually roof tops) prior to passage of a storm, and particulates accumulated in rain gauges. A few pioneering scientific studies in the 1930s used the available dust sampling technology to quantify atmospheric particulate flux, such as an Owens Dust Counter (Hand, 1934) or an Impinger Tube (Langham et al., 1938). The study by Langham et al. (1938) is of significance because of the continuous measurement of dust flux, wind speeds, and visibility for twenty-nine dust storms from April 1935 through April 1937 at the core of the DBD in Goodwell, OK (Table 3.2). TSP values for individual dust storms vary from 0.1 to 4.0 g m^{-3} (Langham et al., 1938) and were similar in magnitude to contemporary dust storms sourced from North Africa and the southwestern U.S., with visibility often below 0.5 km and advancing "wall" of dust rising 2 to 4 km in height (Langham et al., 1938; Englestaedter et al., 2006; Flagg et al., 2014; Camino et al., 2015; Eagar et al., 2017).

Monthly maps showing the spatial distribution of dust-storm days and/or "dense dust" atmospheric conditions of the conterminous U.S. provide insight on the cross-continent impact of suspended dust loads prior to the study period (Fig. 3.4). These maps

Table 3.2. Estimated wind speed, visibility, dust deposition rate and total suspended sediment for dust storms during the 1930s.

Date	Location	Measurement method	Wind speed ($m\ s^{-1}$)	Visibility (km)	Estimated dust deposition rate ($g\ m^{-2}\ hr^{-1}$)	Sample duration (hr)	Estimated TSP ($g\ m^{-3}$)	Data Source
05/11/1934	Washington, D.C.	Owens dust counter			3.6	9.75		Hand, I., 1934
03/15/1935	Jewell CO, KS	Wet bake pan			~19.4	~24		Brown et al., 1935
03/26/1935	Jewell CO, KS	Wet bake pan			~10.4	~24		Brown et al., 1935
03/26/1935	Jewell CO, KS	Rain gauge			~9.3	~24		Brown et al., 1935
04/26/1935	Jewell CO, KS	Wet small pan			~4.2	~24		Brown et al., 1935
04/22/1935	Jewell CO, KS	Wet small pan			~1.2	~24		Brown et al., 1935
04/04/1936	Goodwell, OK	Impinger tube	10 ± 2	0.1	2.5 ± 0.6	0.75	2 ± 0.4	Langham et al., 1938
04/05/1936	Goodwell, OK	Impinger tube	12 ± 1	0.1	1.4 ± 0.2	1	1.4 ± 0.2	Langham et al., 1938
04/08/1936	Goodwell, OK	Impinger tube	11 ± 1	0.6 ± 0.2	0.3 ± 0.1	1.5	0.3 ± 0.1	Langham et al., 1938
04/09/1936	Goodwell, OK	Impinger tube	14 ± 1	0.1 ± 0.1	2.8 ± 0.8	0.75	2.2 ± 0.6	Langham et al., 1938
04/20/1936	Goodwell, OK	Impinger tube	13 ± 1	0.1	6.0 ±2.8	0.6	3.6 ± 1.7	Langham et al., 1938
04/23/1936	Goodwell, OK	Impinger tube	11 ± 8	0.6 ± 0.3	0.06 ± 0.01	5.2	0.3 ± 0.1	Langham et al., 1938
04/29/1936	Goodwell, OK	Impinger tube	9 ± 2	0.5 ± 0.2	0.15 ± 0.08	1.3	0.2 ± 0.1	Langham et al., 1938
05/05/1936	Goodwell, OK	Impinger tube	10 ± 1	0.2 ± 0.2	0.42 ± 0.21	2.4	1 ± 0.5	Langham et al., 1938
05/08/1936	Goodwell, OK	Impinger tube	10 ± 1	0.1	2.0 ± 0.7	1.2	2.4 ± 0.8	Langham et al., 1938
02/1937	Page CO, Iowa	Observation			~1.3	~24		Martin, 1937a
02/1937	Sault. Ste. Marie, MI	Observation			~0.2	~24		Martin, 1937a
02/1937	Marquette, MI	Observation			~0.07	~24		Martin, 1937a
02/07/1937	Goodwell, OK	Impinger tube	13 ± 1	0.1 ± 0.1	0.24 ± 0.02	8.3	2 ± 0	Langham et al., 1938
02/11/1937	Goodwell, OK	Impinger tube	10 ± 1	0.4	0.05 ± 0.01	3.75	0.2 ± 0	Langham et al., 1938
02/14/1937	Goodwell, OK	Impinger tube	11 ± 1	0.1 ± 0	0.20 ± 0.12	6.75	1.3 ± 0.8	Langham et al., 1938
02/15/1937	Goodwell, OK	Impinger tube	8 ± 0.4	0.3 ± 0.1	0.03 ± 0.02	6.3	0.2 ± 0.1	Langham et al., 1938
02/16/1937	Goodwell, OK	Impinger tube	11 ± 1	0.3 ± 0.4	0.24 ± 0.19	7.2	1.7 ± 1.4	Langham et al., 1938
02/17/1937	Goodwell, OK	Impinger tube	10 ± 1	0.1 ± 0.1	0.05 ± 0.03	6.2	0.3 ± 0.2	Langham et al., 1938
02/18/1937	Goodwell, OK	Impinger tube	14 ± 0	0.1 ± 0.1	0.82 ± 0.73	2.2	1.8 ± 1.6	Langham et al., 1938
03/03/1937	Goodwell, OK	Impinger tube	9 ± 3	0.2 ± 0.1	0.03 ± 0.01	10.3	0.3 ± 0.1	Langham et al., 1938
03/09/1937	Goodwell, OK	Impinger tube	10 ± 1	0.4 ± 0.3	0.20 ± 0.1	4	0.7 ± 0.4	Langham et al., 1938
03/17/1937	Goodwell, OK	Impinger tube	8 ± 1	0.4 ± 0	0.10 ± 0.01	1.75	0.2 ± 0	Langham et al., 1938
03/19/1937	Goodwell, OK	Impinger tube	10 ± 1	0.1 ± 0.1	1.4 ± 0.5	6	1.4 ± 0.5	Langham et al., 1938
03/23/1937	Goodwell, OK	Impinger tube	13 ± 1	0.1 ± 0	0.30 ± 0.01	13.7	4 ± 1.1	Langham et al., 1938
03/24/1937	Goodwell, OK	Impinger tube	9 ± 1	0.1 ± 0.1	0.01 ± 0.01	11.3	1.5 ± 0.9	Langham et al., 1938
04/02/1937	Goodwell, OK	Impinger tube	8 ± 2	0.5 ± 0.3	0.05 ± 0.01	8.4	0.4 ± 0.2	Langham et al., 1938
04/03/1937	Goodwell, OK	Impinger tube	6 ± 1	0.4 ± 0.1	0.04 ± 0.01	5	0.2 ± 0.1	Langham et al., 1938
04/06/1937	Goodwell, OK	Impinger tube	11 ± 1	0.1 ± 0.1	0.2 ± 0.1	5	1 ± 0.6	Langham et al., 1938
04/16/1937	Goodwell, OK	Impinger tube	9 ± 1	0.2 ± 0.1	0.05 ± 0.01	8	0.4 ± 0.2	Langham et al., 1938
04/22/1937	Goodwell, OK	Impinger tube	9 ± 1	0.1 ± 0.1	0.2 ± 0.1	5	1.1 ± 0.5	Langham et al., 1938
04/23/1937	Goodwell, OK	Impinger tube	9 ± 2	0.3 ± 0.3	0.2 ± 0.1	5.6	1.2 ± 0.7	Langham et al., 1938
4/27/1937	Fort Collins, CO	Observation			~6.1	~24		Martin, 1937a
05/03/1937	Goodwell, OK	Impinger tube	10 ± 1	0.4 ± 0.2	0.05 ± 0.02	11	0.5 ± 0.2	Langham et al., 1938

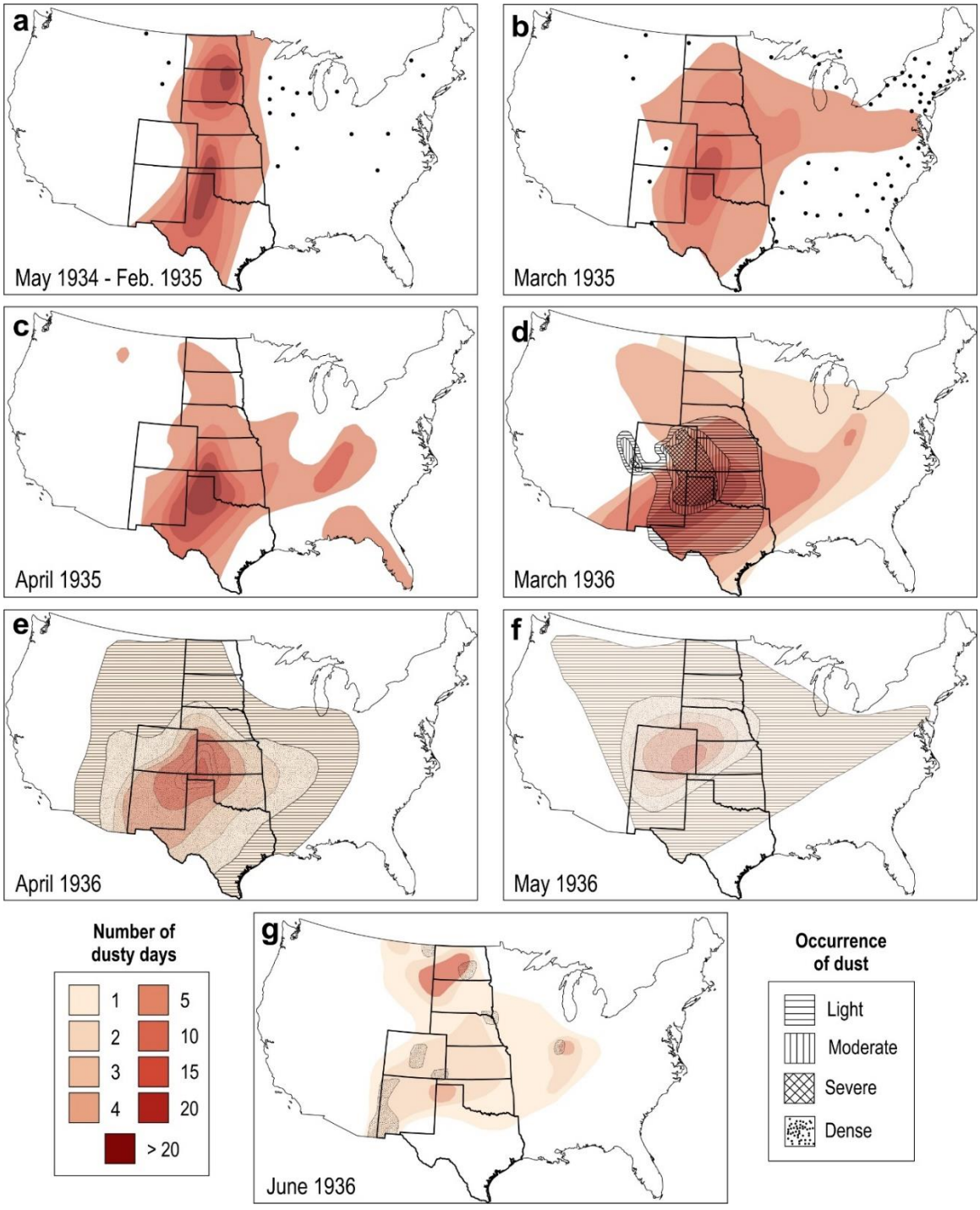

Figure 3.4 Spatial distribution of dust storms and dust occurrence for designated months in 1934, 1935 and 1936 (from Choun, 1936; Mattice, 1935a, 1935b; Martin, 1936a, 1936b, 1936c).

indicated a concentration of dusty days centered over the Texas and the Oklahoma panhandles, though the loci of dust storms shifted northward into southwest Kansas from March to May in 1936 (Fig. 3.4d-f). Another dust source accentuated in the maps was on the Northern High Plains, with peak dusty conditions over the North and South Dakota border area from May 1934 to February 1935, and again June 1936 (Fig. 3.4a, g). Noteworthy is the westward distribution of dust observed in March 1936 that fell in the southern Basin and Range and Northern Rocky Mountains, with an eastward displacement of an upper level ridge (Fig. 3.4d; Namias, 1982; 1990; Higgins et al., 1997). It appears that broad areas of the USGP were dust sources in the 1930s, which could be re-distributed eastward or westward with changing synoptic conditions, such as a dust storm occurring November 12 to 13, 1933 that produced dustfall across the eastern U.S. (Fig. 3.5). In addition, there may be numerous unrecognized secondary sources for dust emissivity from extensively plowed fields in the Midwest and over-utilized pasture lands west of the Front Range (Handy et al., 1960; Brown, 1968).

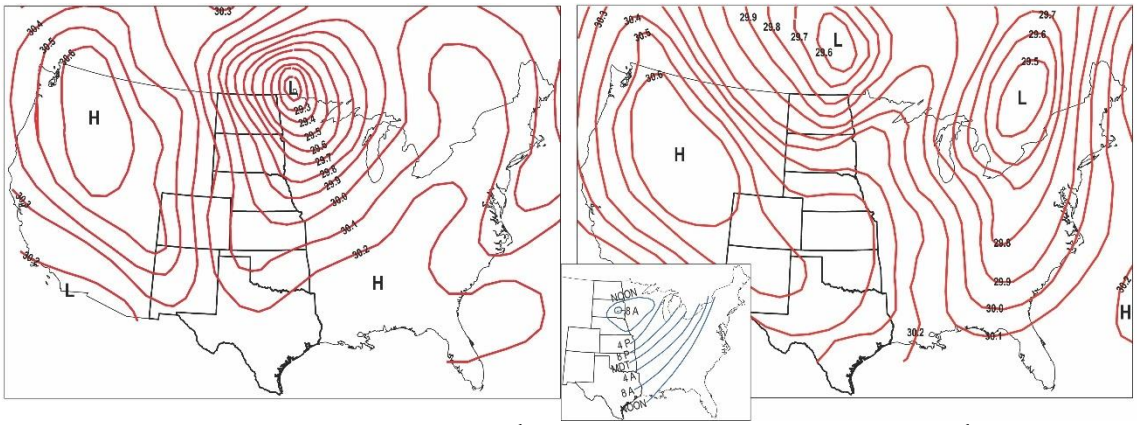

Figure 3.5 Weather map for 8 a.m. November 12th, 1933 (left) and 8 a.m. on November 13th (right), when a dust fall occurred from eastern Ontario, across western New York, the Ohio River Valley, the southern Appalachians and the Gulf States to Texas. Inset map shows isochronal contours for the movement of dust clouds for the same 24-hour period (Miller, 1934).

The spatial extent of SHP severe wind erosion appears to have shifted northward between 1935 and 1938. Whereas, the region of greatest frequency of dust storms remained centered over the Oklahoma panhandle during this same period, a pattern echoed in the dust storms recorded from April 1938 to May 1940 (Fig. 3.6). The SCS experiment sites reported 1,360 storms during these 25 months, lasting a total of ~9,603 hours – nearly 50% of the elapsed time (Table 3.3). Storm activity peaked in the spring, with a maximum in frequency each April (Fig. 3.7a), mirroring records from earlier in the decade (Fig. 3.3). The greatest number of consecutive days with dust storms in this period was documented within this window from Springfield, CO (Fig. 3.6b, site V), where dust blew for 18 days from April 1st to 18th, 1938 for a total of 128 hours (30% of the period), shortly followed by a further nine continuous days of dust storms from April 21st to 29th, for an elapsed time

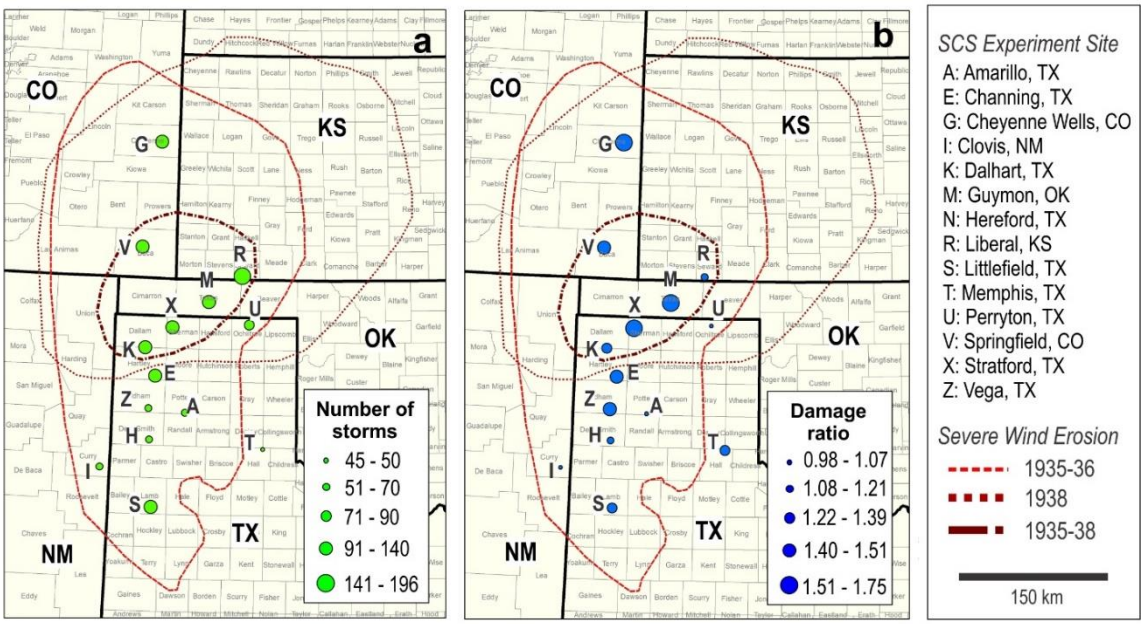

Figure 3.6 (a) The total number of dust storms recorded by location between April 1938 and May 1940, inclusive, and (b) the ratio of the total level of soil damage recorded at each location to the total number of dust storms, relative to the SCS-drawn boundaries of severe wind erosion (map dated March 1954, National Archives, Record Group 114, Entry 5).

of 56 hours. The longest individual storm persisted for 98 hours, also recorded in Springfield, CO, beginning at 8 am on September 11th, 1939 and lasting through 10 am, September 15th. The locations experiencing the greatest ratio of soil damage to storm frequency, i.e. where storms tended to produce more severe damage per occurrence, are Guymon, OK, Springfield, CO, and Stratford, TX (Fig. 3.6, sites M, V, and X). These sites and two others (Dalhart, TX, site K; Liberal, KS, site R) within the area of persistent, severe eolian erosion designated by the SCS were situated in counties with, on average, ~48% of land under cultivation by 1935 and ~25% coverage by eolian deposits.

Table 3.3. Locations of Soil Conservation Service experiment sites recording dust storms used in this study and total number of storms and duration documented from April 1938 to May 1940, inclusive.

Notation	Town	County	State	Storm Count	Duration (hours)	Equivalent Days	% of Study Period
A	AMARILLO	POTTER	TX	56	392.2	16	2.1
E	CHANNING	HARTLEY	TX	128	987.8	41	5.2
G	CHEYENNE WELLS	CHEYENNE	CO	119	858.1	36	4.5
I	CLOVIS	CURRY	NM	62	407.7	17	2.1
K	DALHART	DALLAM	TX	122	678.7	28	3.6
M	GUYMON	TEXAS	OK	107	746.5	31	3.9
N	HEREFORD	DEAF SMITH	TX	53	331.0	14	1.7
R	LIBERAL	SEWARD	KS	196	1607.7	67	8.5
S	LITTLEFIELD	LAMB	TX	91	529.4	22	2.8
T	MEMPHIS	HALL	TX	45	291.7	12	1.5
U	PERRYTON	OCHILTREE	TX	75	488.5	20	2.6
V	SPRINGFIELD	BACA	CO	139	936.6	39	4.9
X	STRATFORD	SHERMAN	TX	123	954.7	40	5.0
Z	VEGA	OLHAM	TX	59	392.6	16	2.1

The characteristic Dust Bowl dust storm, as defined by the median variable value on SHP dust-storm days (Fig. 3.7b), began at 10 am, lasted eight hours, and originated in counties with ~50% area under cultivation and 16% coverage of eolian deposits. The average maximum 2-m windspeed associated with a storm causing slight soil damage was ~9 m s^{-1}, moderate damage occurred with winds an average of 10.9 m s^{-1}, and severe damage with a mean velocity of 13.8 m s^{-1}. The parallel gradient between wind speed and level of soil movement emulates the reported co-occurrence of increasing wind speeds with

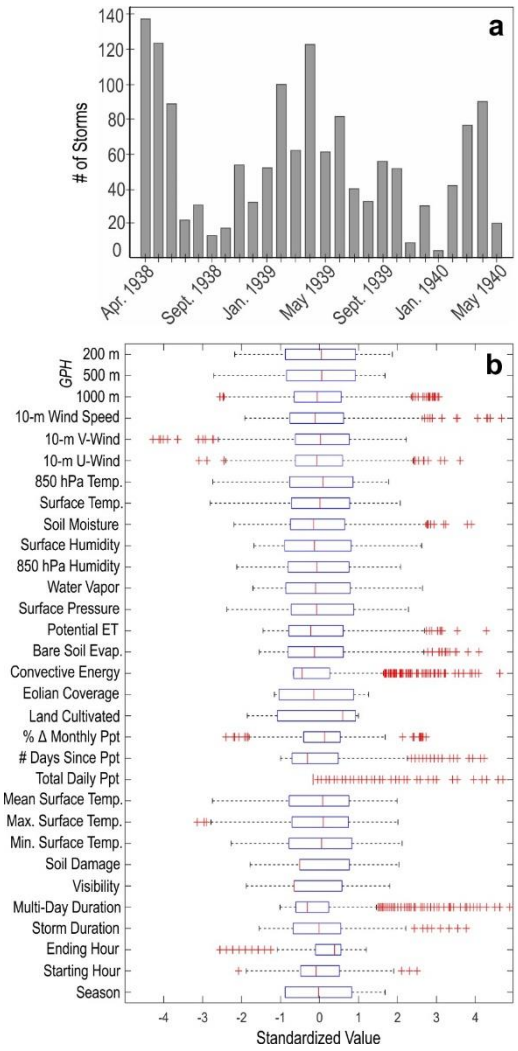

Figure 3.7 (a) The total number of dust storms recorded each month across the 14 experiment sites between April 1938 and May 1940, inclusive. (b) A boxplot of documented storm characteristics and interpolated meteorological and atmospheric conditions on dust-storm days, with the distribution of each variable standardized by mean and standard deviation.

increasing volumes of dust deposition and decreasing visibility (cf. Table 3.2). This is also consistent with observations from the Dalhart experiment station that noted dust storms often occurred with wind speeds > 8.9 m s^{-1} (National Archives, Record Group 114, Entry 112). Daily surface air temperatures on a typical storm day reached a maximum of 19.4°C, with a mean of 11.1°C, and coeval precipitation levels were at a 30% deficit, with the latest rainfall six days prior to the dust storm. Median atmospheric conditions on dust-storm days

exhibited temperatures ~15°C at 850 hPa, with geopotential heights (GPH) ranging from 110 m at 1,000 hPa to 12,133 m at 200 hPa, and potential ET (PET) rates of 295 W m^{-2}. Median storm-day relative humidity was 53%, estimated soil moisture content was 501 kg m^{-2}, atmospheric water vapor content (PWAT) was 19.6 kg m^{-2}, and the energy flux of direct evaporation from bare soil (EVBS) occurred at 32 W m^{-2}. Pairwise correlation analysis indicates that there is significant dependence between climatic conditions on dust-storm days, though few variable pairs received an R_S above the threshold indicative of strong monotonic correspondence. PET trends positively with air temperature at 850 hPa (R_S = 0.865, p-value <0.01). In turn, lower-level atmospheric temperature shares a positive correlation with GPH at 500 and 200 m (R_S = 0.859 and 0.885 respectively, p-value <0.01). Also related to the availability of water, the relationship between specific humidity at the surface is strongly monotonic with PWAT (R_S = 0.905, p-value <0.01). Of note is the strong relation between the surface (2-m) air temperature retrieved from the GHCN and the 2RAP datasets, indicating a highly significant correlation between the observed and interpolated historical temperature data.

Principal Components of Dust-Storm Days on the Southern High Plains, April 1938 to May 1940

Dust storms days can be characterized by 6 PCs that each account for ≥5% of the variance, in total capturing >60% of the variance of all observations (Fig. 3.8a). Seventeen PCs explain 90% of the variance, though the additional 11 PCs contribute individually ≤4% and are of questionable significance for the characterization of DBD dust storms. A triplot of the first three PCs reveals a gradient in dust storms observations and covariances between included variables (Fig. 3.8b). At the landscape level, changes to visibility and

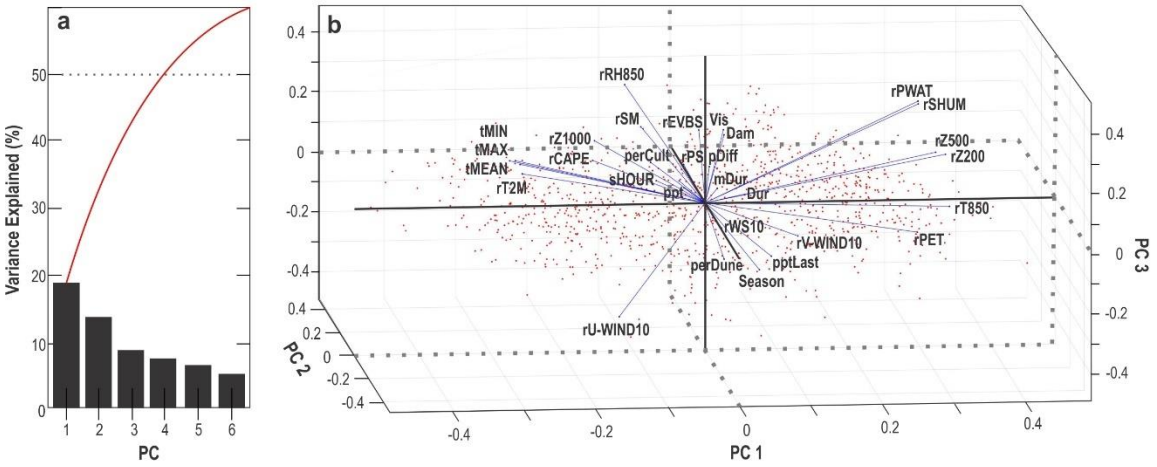

C	Notation	Description	Units	Data Source
	stormID	Recording location and date	--	
	Season	Season of storm occurrence	1: MAM 2: JJA 3: SON 4: DJF	
	sHOUR	Hour of day storm begin		
	eHOUR	Hour of day storm ended		
	Dur	Total daily duration	hours	National Archives, Record Group 114, Entry 112, File: Dust Storm Data Sheets
	mDur	Multi-day duration		
	Vis	Reported change to visibility	L: 6 to 0.75 mi M: 0.75 to 0.5 mi D: <0.5 mi	
	WS	Maximum wind velocity observed during storm	m s^{-1}	
	WD1	Predominant wind direction during storm	°Azimuth	
	Dam	Level of soil damage caused by a storm	1: Slight 2: Moderate 3: Severe	
	tMIN	Daily minimum temperature		
	tMAX	Daily maximum temperature	℃	
	tMEAN	Daily mean temperature		Global Historical Climate Network (Menne et al, 2012)
	Ppt	Daily rainfall	mm	
	pptLast	Number of days since last rainfall		
	pDiff	% difference in total monthly rainfall from "normal", 1895-1930	%	PRISM Historical Data Series (PRISM, 2017)
	perCult	% of county cultivated at maximum extent in 1935		Agricultural Census of 1935 (Gutmann, 2005)
	perDune	% of county mapped as eolian deposits		Muhs & Holliday, 2001
	rCAPE	Convective available potential energy	J kg^{-1}	
	rEVBS	Direct evaporation from bare soil	W m^{-2}	
	rPET	Potential evaporation rate at the surface		
	rPS	Surface air pressure	Pascal	
	rPWAT	Atmospheric water vapor content	kg m^{-2}	
	rRH850	Relative humidity at 850 hPa	%	
	rSHUM	Specific humidity at 2m	kg kg^{-1}	
	rSM	Soil moisture content	kg m^{-2}	
	rT2M	Daily mean air temperature at 2m	°K	20th Century Global Reanalysis Project (Compo et al, 2011)
	rT850	Daily mean air temperature at 850 hPa		
	rUWIND10	u-wind at 0.995 times the surface pressure		
	rVWIND10	v-wind at 0.995 times the surface pressure	m s^{-1}	
	rWS10	Wind speed at 10m		
	rZ1000	Geopotential height at 1000 hPa		
	rZ500	Geopotential height at 500 hPa	m	
	rZ200	Geopotential height at 200 hPa		

Figure 3.8. Results of the principal component analysis of 1,018 dust storms documented on the Southern High Plains between April 1938 and May 1940, inclusive: (a) Screeplot of the first six principal components (PCs), where each individual PC explains at least 5% of the variance of dust-storm days; (b) Triplot of the first three PCs with variable eigenvectors and dust storm observations rotated to component space; (c) Notation and descriptions of the 31 variables included, with original unit of measurement and data source.

extent of soil damage appear to covary with the percentage the of county of dust storm origin under cultivation. Dust storm seasonal occurrence covaries with the coverage (%) of eolian deposits and number of days since the most recent precipitation. The first PC explains 18.5% of the variance and is positively correlated to air temperature at 850 hPa, which covaries with GPH at 200 and 500 hPa, and PET; conversely, the second PC is positively correlated with observed mean surface air temperature on dust-storm days and explains 13.4% of the variance. The third PC captures 8.2% of variance and is predominantly associated with relative humidity at 850 hPa. This atmospheric moisture metric covaries with soil moisture levels and PWAT, and occurrence of northerly or southerly winds. The fourth PC explains 7.2% of the variance, stemming from the duration of dust storms, which is correlated to EVBS and the hour of day a dust storm began. A gradation in dust storm intensity is reflected by the fifth PC, elucidating 6% of variability and associated with the occurrence of multi-day storms, increasing levels of soil damage, and decreasing visibility. Finally, 5.2% of the variance is correlated with the sixth PC, related to the percent coverage of eolian deposits in the county of storm origin, covarying with higher wind speeds, lower soil moisture, and near-surface GPH at 1000 hPa.

Linkages Between Dust Storm Events and Covariance with Meteorological Conditions

Hierarchical clustering analysis yields categorization of dust storms into four broad clusters based on the distance between observations in component space (Fig. 3.9). Euclidean distance and cosine distance measures return the strongest cophenetic correlations of 0.689 and 0.556, respectively. Though clustering analysis using Euclidean distance measures a stronger cluster tree, this linkage differentiates only twelve dust storms from other observations: ten storms that occurred with cooler air temperatures than other

SHP dust storms (Fig. 3.9b, cluster 4), and the two storms most positively correlated with PC 1 (Fig. 3.9b, cluster 3) and PC 2 (Fig. 3.9b, cluster 1). Cosine distance, however, distinguishes storm clusters based on the relative contribution of the first three PCs, corresponding to air temperature at 850 hPa and surface levels, and relative humidity at 850 hPa (Fig. 3.9d).

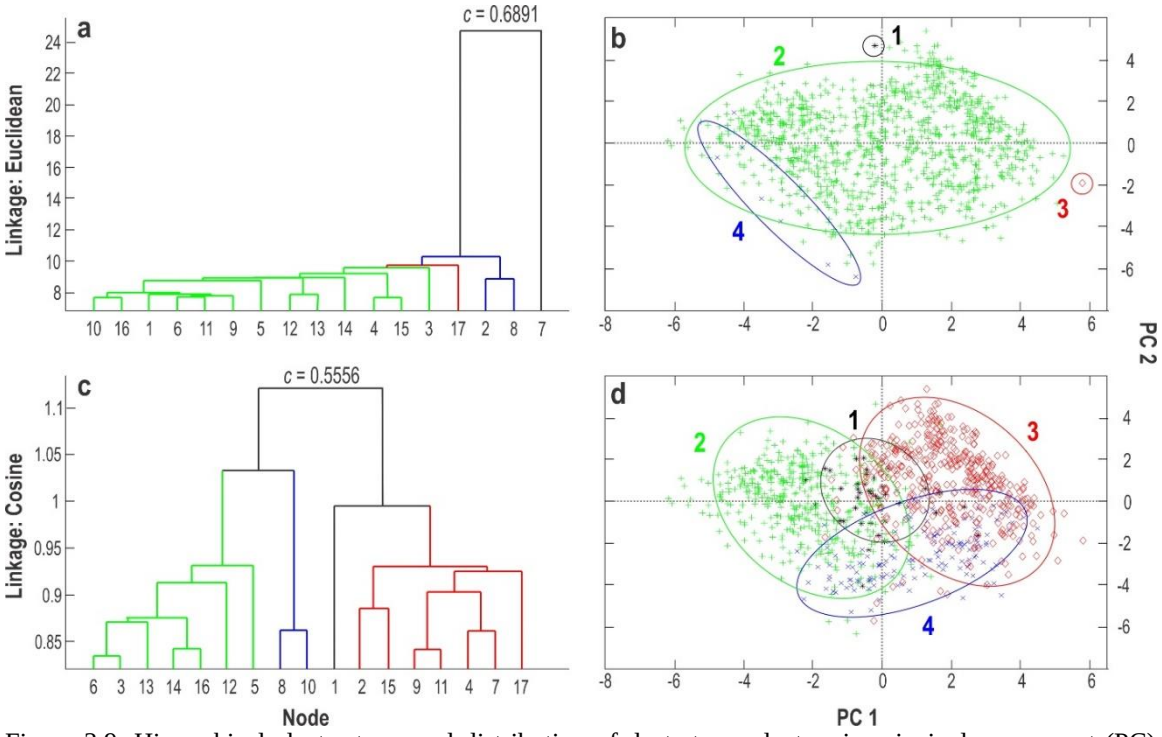

Figure 3.9. Hierarchical cluster trees and distribution of dust storm clusters in principal component (PC) space: (a, b) Euclidean distance, and (c, d) Cosine distance, with cophenetic correlation coefficient (*c*).

The smallest cosine-distance cluster (1, Fig. 3.9d) consists of 40 storms occurring irrespective of season, when surface air temperatures were virtually equal to temperatures at 850 hPa. These storms were most often documented in the Texas panhandle near the cities of Amarillo (A), Stratford (X), and Vega (Z), typically coeval with the highest soil moisture levels and EVBS rates of all dust-storm days, occurring ≤5 days since rainfall, with the lowest surface pressures and GPH at 1000 hPa. Clusters 2 and 3 apparently

discriminate between early and late "blowing season" dust storms. The hundreds (420) of dust storms within cluster 3 often occur in March and early April, when temperatures at 850 hPa are ~10°C warmer than at the surface and relative humidity is ~45%. These early spring storms are associated with greater surficial PET, PWAT, and specific humidity. Cluster 2 dust storms (411) occur in the late spring and early summer (AMJ), concordant with the hottest surface air temperatures at least 10°C higher than temperatures at 850 hPa and maxima in convective potential energy. Relative humidity at 850 hPa reached nearly 80% on these dust-storm days, but median levels of PET and PWAT were lower than in any other dust storm cluster. Finally, cluster 4 contains 147 observations associated with winter storms (DJF). These dust storms are correlated with wetter-than-average months and lower mean surface temperatures than other seasons, but typically occur after extended dry periods (up to 13 days), with warmer temperatures at 850 hPa than the surface.

Particulate Matter Flux from Southern High Plains Soils

The range of soil textures on the SHP, from silt-loam to sand, exhibit extensive heterogeneity in particle (PM_{10}) emissivity (Table 3.4). The dust emissivity estimated from PI-SWERL tests of varying soil surfaces usually increases exponentially above a threshold wind speed (8-10 m s^{-1}), dependent on the presence of surface crust and/or soil clods (Fig. 3.10). This aligns with reported threshold wind speeds between 6 and 14 m s^{-1} during dust storms in Goodwell, OK in 1937 and 1938 (Table 3.2) and for dust storms inventoried in this study. Disturbed silt-loam and disturbed loam soils, and undisturbed, loose loamy-sand soils emit PM_{10} at a mean rate in the upper quartile of all measured soil emissivity. In contrast, crusted silt loam soils with clods, crusted loam soils, and crusted sandy loam soils exhibit PM_{10} flux rates in the lower quartile of potential emissivity.

Table 3.4. Descriptive statistics of particulate matter (PM_{10}) flux values measured by the PI-SWERL for each surface soil condition and selected regression to predict PM_{10} flux, with root mean squared error (RMSE) and for linear models the adjusted R^2, where the given wind speed (x) is first normalized to the mean (μ) and standard deviation (σ) of the range of tested wind velocities.

Plot	Soil Condition	Sample Density	PM_{10} Flux (mg m^{-2} s^{-1})				Function	RMSE (mg m^{-2} s^{-1})	Adj. R^2	Wind Speed (m s^{-1})	
			Minimum	*Maximum*	*Average*	*STD*				μ	σ
a	Disturbed Silt Loam	54	0.002	23.941	4.955	5.832	$f(x) = 0.511x^2 + 3.455x + 3.797$	3.683	0.601	21.12	6.392
	Crusted Silt Loam	69	0.003	17.363	1.515	3.348	$f(x) = 0.108^{2.397x}$	0.609	—	14.41	4.091
b	Disturbed Silt Loam w/ Clods	26	0.002	3.223	0.575	1.006	$f(x) = 0.086^{0.886x}$	0.359	—	21.9	7.76
	Crusted Silt Loam w/ Clods	19	0.007	1.900	0.368	0.474	$f(x) = 0.19^{0.627x}$	0.205	—	18.93	6.385
c	Disturbed Loam	22	0.014	13.816	3.657	4.416	$f(x) = 1.169x^2 + 3.563x + 2.598$	2.149	0.763	17.4	6.001
	Crusted Loam	20	0.007	2.214	0.384	0.674	$f(x) = 0.2864^{0.894x}$	0.585	—	14.68	4.299
d	Disturbed Sandy Loam	42	0.011	13.816	2.026	2.596	$f(x) = 0.815x^2 + 1.882x + 1.267$	0.8276	0.898	17.51	5.495
	Crusted Sandy Loam	16	0.002	0.573	0.095	0.161	$f(x) = 0.025^{1.346x}$	0.024	—	15.18	4.63
	Crusted Sandy Loam Mantled w/ Windblown Sand	90	0.006	13.202	1.922	2.141	$f(x) = 1.247^{0.732x}$	1.05	—	17.51	5.495
e	Loose Loamy Sand	53	0.007	19.722	2.117	2.810	$f(x) = -0.166x^2 + 1.06x + 1.745$	0.893	0.566	16.84	5.031
f	Loose Sand	63	0.002	6.157	1.237	1.296	$f(x) = 0.009x^2 + 0.098x + 0.121$	0.4792	0.863	16.98	4.66
	Loose Sand w/ Gravel	11	0.004	2.772	0.736	1.007	$f(x) = 0.13^{2.237x}$	0.161	—	23.24	6.947

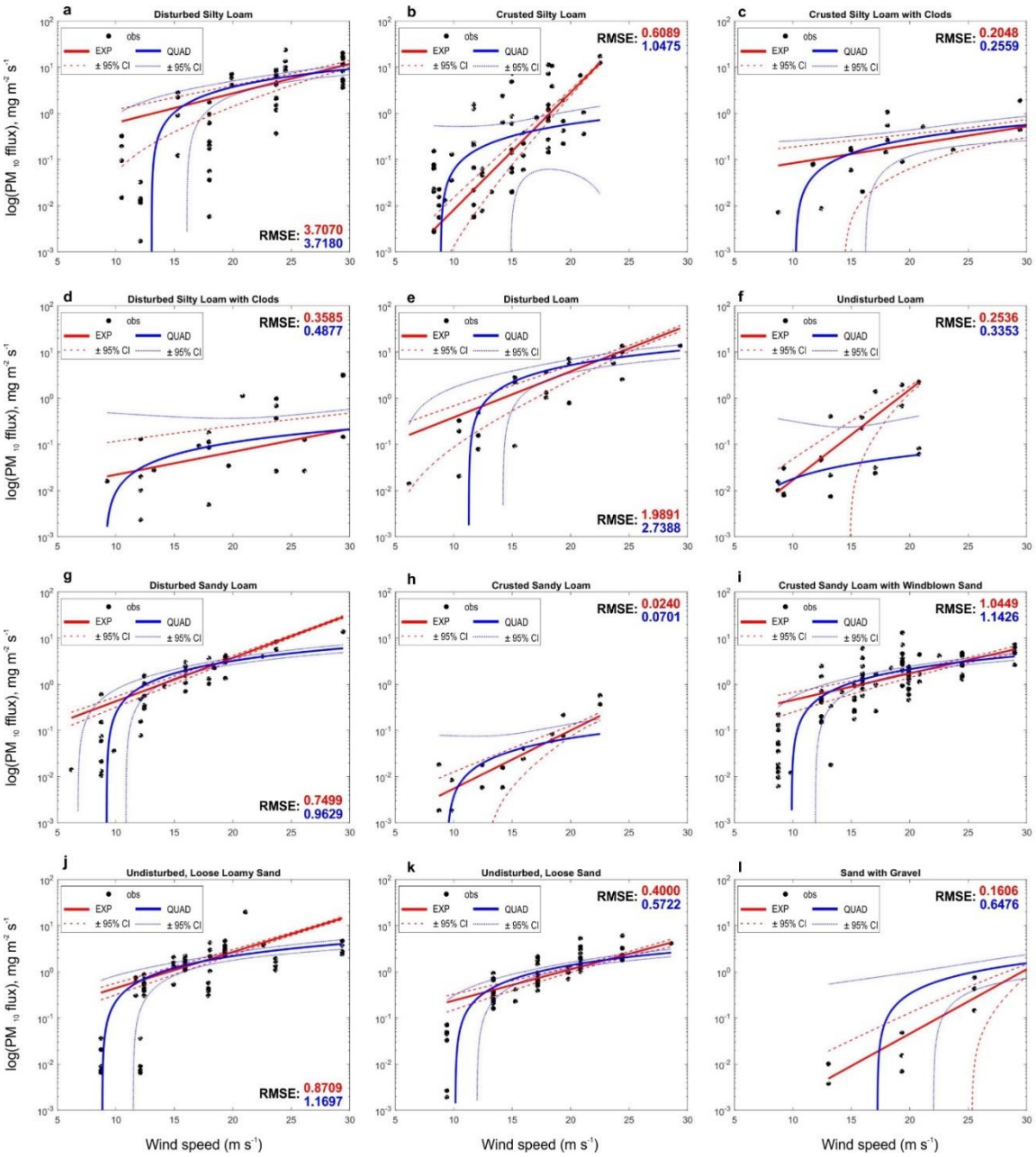

Figure 3.10. Comparison of exponential (EXP) and quadratic polynomial (QUAD) models for PI-SWERL particle flux concentration measurements as a function of windspeed, binned by soil texture and surface treatment.

The PM_{10} emission rates for a range of wind speeds from disturbed surfaces is significantly fit by a quadratic polynomial function (Fig. 3.10a, d, e, g), as are rates for loose, sandy soils (Fig. 3.10i-k). Alternatively, crusted surfaces and those with enhanced surface roughness, such as fluvial sands with gravel or large soil clods, respond to increasing wind speeds as an exponential function (Fig. 3.10b, c, h, l). Disturbed silt-loam soils initiate dust emissions at a magnitude-higher flux rate than other disturbed soil textures post-exposure to the threshold wind velocity, but nearly all disturbed surfaces emit at magnitude higher rates than crusted surfaces (0.01 versus 0.001 mg m^{-2} s^{-1}; Fig. 3.11).

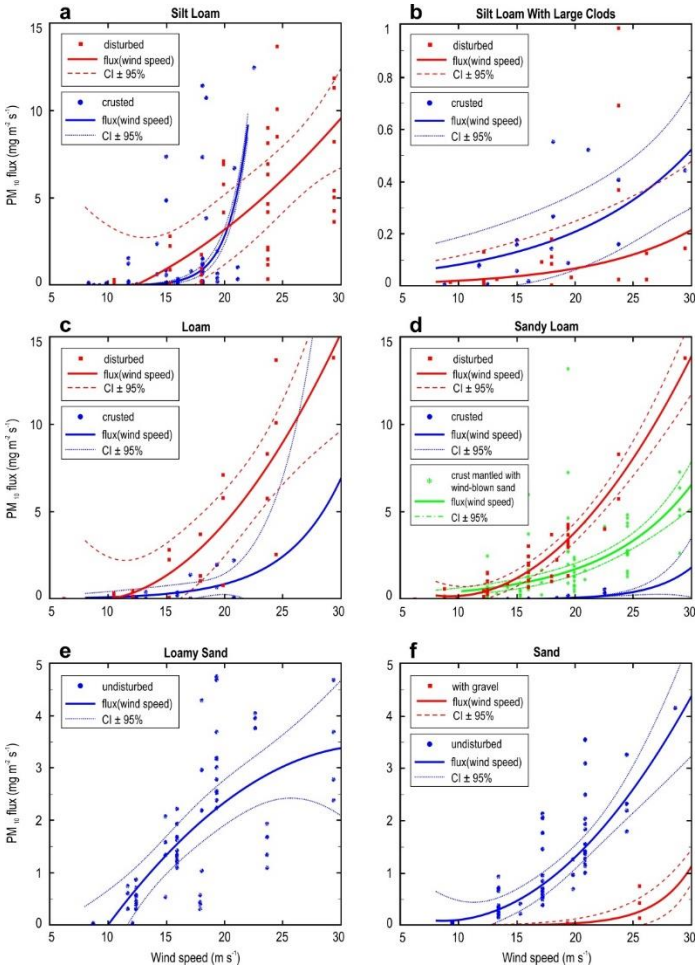

Figure 3.11. Selected regressions for each soil texture contrasting response from disturbed, undisturbed, and crusted surfaces, where particulate matter (PM_{10}) flux is calculated as a function of normalized wind speeds. Refer to Table 4 for curve formulas and associated goodness-of-fit parameters.

The maximum flux rate measured of ~24 ± 6 mg m^{-2} s^{-1} is also associated with disturbed silt-loam soils, though disturbed loam and disturbed sandy loam soils initiate PM_{10} emissivity at a higher level than other surfaces (Table 3.4). However, the surface roughness introduced by cultivation of silt loam with large clods significantly reduces the potential emissions (Fig. 3.11b). Interestingly, particle flux from loose, uncrusted sandy soils formed on dune sands or sandsheet deposits is of the same magnitude as disturbed surfaces with appreciable silt content under equivalent wind speeds (e.g. Fig. 3.11d-f).

Discussion

Controls on Dust Storm Variability at the Heart of the Dust Bowl

The number of dust storms during the DBD was equivalent to or greater than events in dry land areas in present-day northern China (Qian et al., 2004), Mongolia (Natsagdorj et al., 2003), North Africa (Mallone et al., 2011; Gkikas et al., 2013; Stafoggia et al., 2016) and the desert U.S. Southwest (e.g. Flagg et al., 2014; Eagar et al., 2017). In the DBD core area of the Oklahoma and Texas panhandles, and adjacent areas in Kansas and Colorado, up to 140 dust storms yr^{-1} were recorded between 1936 and 1940. The PCA analysis highlights the impact of elevated temperatures and spring precipitation deficits in propagating dust storm activity in the 1930s (Donat et al., 2016; Cowan et al., 2017; Hegerl et al., 2018). The covariance between temperature at 850 hPa and GPH at 500 and 200 m is consistent with documented extraordinary summer heat that likely exacerbated land-surface feedbacks associated with springtime aridity (Donat et al., 2016; Cowan et al., 2017), and would enhance atmospheric subsidence, warming the lower troposphere and increasing near-surface wind speeds (Cowan et al., 2017; Pu and Ginoux, 2018). Extreme temperatures further contributed to reduction in vegetation cover, making previously-

stabilized surfaces susceptible to eolian erosion (Albertson and Weaver, 1944) and increasing surface albedo (Schlesinger et al., 1990). The influence of temperature and relative humidity on the strength of DBD dust storms is consistent with inferred processes in fine dust generation for the western U.S., which find that atmospheric dust concentrations depend on temperature-related feedbacks to synoptic transport (Tai et al., 2012; Achakulwisut et al., 2017). The PCA also demonstrates the elevated temperatures intensified EVBS, depleting soil moisture reserves in late spring and summer (Lee and Gill, 2015), which has been shown to auto-correlate with precipitation anomalies in the subsequent spring (Nandintsetseg and Shinoda, 2015).

The ubiquity of DBD dust storms is often attributed to the over-plowing of agricultural fields (cf. Bennett and Fowler, 1936; Johnson, 1947; Worster, 1979; Hurt, 1981; Hansen and Libecap, 2004). However, PCA analysis indicates that only 2.6% of variance of observed dust storms is attributed to the extent of land under cultivation by 1935. Likewise, the most damaging storms in 1938 and 1939 originated in counties where eolian deposits cover >10% surface area. This analysis indicates that the severity of SHP dust storms related to land use was not exclusively related to poor agricultural stewardship but influenced by the extent of sandy lands left as range, which accounts for >5% of the variance of dust-storm days. Indeed, sand dunes are developed on many areas throughout the SHP, particularly between the Arkansas and Canadian rivers within the specified area of severe wind erosion (Fig. 3.6; Whitfield, 1938; Forman et al., 2001; 2008).

Four Dominant Modes of Dust Bowl Dust Storms

The inferred clusters of dust storms yield insights on the different synoptic conditions conducive for surface erosion and mesoscale dust transport. The first mode of

SHP dust storms is connected to enhanced atmospheric stability. Specifically, an increase in GPHs and concomitant thermal inversion at 850 hPa results in consistent entrainment and lofting of particles. The presence of an anomalous high-pressure outflow in the middle-to-upper troposphere is associated with a strong negative feedback between soil moisture and precipitation and would suppress convection and generate strong winds (Cook et al., 2011; Su et al., 2014). The second mode of dust storms occurs with a peak in surface temperatures (>35°C) relative to temperatures at 850 hPa in the late spring to early summer. This cluster is typically associated with low PET, PWAT, and specific humidity, possibly reinforcing drought conditions through increasing surface latent-heat flux related to decreasing soil moisture (Hong and Kalnay, 2000; Xu et al., 2004) and through diminished net primary productivity (Hong and Kalnay, 2000; Nandintsetseg and Shinoda, 2015). These dust storms often occur with southerly winds and generate extensive soil erosion, associated with peak surface wind speeds (>10 m s^{-1}), and TSP of >10^5 µg m^{-3} (Table 3.2). During this season, the Great Plains Lower Level Jet (GPLLJ) builds in strength diurnally, with the nocturnal mode characterized by a strong, near-surface southerly wind, and flux of moist, warm air from the Gulf of Mexico (Higgins et al., 1997; Kumjian et al., 2006; Pu and Ginoux, 2018). This could elucidate the correlation between air temperature, southerly winds at 10 m, and increasing relative humidity at 850 hPa associated with this storm mode. The next storm mode is associated with winter thermal inversion. Positive precipitation anomalies often occur in winter, though dust storms frequently develop approximately after two weeks without rainfall. At this time of year, convection-related downdrafts generate cold pool outflows and strong winds sufficient to entrain dust particles (Pantillon et al., 2015), contributing to the secondary peak in dust storm frequency (Fig. 3.3b, 7a).

The final dust storm mode discriminates haboobs forming irrespective of season, dominantly occurring over the Texas panhandle when surface and 850 hPa air temperatures are nearly equal. When these dust storms occur, there are low levels of PWAT, but soil moisture content and EVBS rates are 25 to 70% higher than during other storm modes. The low GPH at 1000 hPa and deep convection indicated by the increased rates of EVBS suggest the presence of a steep, low-pressure front (Sidwell, 1938; Smith et al., 1970; Idso et al., 1972; Chen and Fryrear, 2002; Novlan et al., 2007), and correlate with events that began earlier in the day, persisted for ≥24 hours, and with visibility <10 m. The concentration of haboobs over panhandle counties suggests greatly diminished primary productivity to enable such increases in EVBS year-round. However, areas associated with this dust-storm mode were neither heavily cultivated, nor with appreciable coverage by eolian deposits, yielding uncertainty on the land use or geomorphology contributing to haboob generation (Vivoni et al., 2009). Dust storms propagated by MCCs often transport dense concentrations of suspended particles (Table 3.2; >1 g m^{-3}) and can be associated with a magnitude increase in electrostatic charge from saltating sand, which is an underappreciated natural hazard (Williams et al., 2007; Sow et al., 2011; Yair, et al., 2016). A number of dust storms during the DBD and earlier droughts were associated with substantial free-electrical discharges that charred telephone poles, stranded cars, and disrupted power service (e.g. Hovde, 1934; Choun, 1936). Saltation of particles induces formation of a static electric charge, restricted usually to ~1 km above the surface (Nicoll et al., 2011; Sow et al., 2011; Yair et al., 2016). Thus, the tribocharging of sand grains was a potential factor for intensification of dust storms leading to exceptionally low visibility

(<10 m) during the DBD, like conditions on the infamous Black Sunday, on April 14, 1935 (Fig. 3.2c; Stallings, 2001).

Short-Term Potency versus Long-Term Cumulative Particle Emission from Southern High Plains Soils

A broader assessment of the still and aerial photographic record and primary documentation from Soil Conservation Service (SCS) experiment stations reveal a range of land surface conditions from fully vegetated to eolian-eroded, denuded surfaces during the DBD. This complex landscape mosaic is consistent with concepts of heterogeneous ecosystem response to extreme drying or precipitation variability (cf. Schlesinger et al., 1990; Peters et al., 2015; Gheradi and Sala, 2015). Twenty-first century dust storms in the southern U.S. exhibit similar characteristics and are often point-sourced to cropland or rangeland on the SHP (e.g. Lee et al., 2009). PI-SWERL tests reveal that disturbed soils on the SHP begin to emit at a magnitude-higher rate than undisturbed surfaces when the threshold velocity (8 to 10 m s-1) is met, and this rate increases linearly with windspeed. Conversely crusted, undisturbed surfaces do not begin to reach the same flux rate until much higher wind speeds, at which point the crusts are broken and emissivity rates increase rapidly, similar to disturbed surfaces. Significantly, the particle emissivity of undisturbed, loose sandy soils mirrors that of disturbed surfaces in relation to windspeed and potential magnitude of dust emitted. This suggests that the sandier, uncultivated soils of the SHP could be equal to or greater dust sources than cultivated fields. Cultivated surfaces are seasonally unavailable dust sources either via crop cover or soil crust formation between agricultural treatments. Whereas, dunes and sandsheets could persist as available dust sources year-round with the inhibited development of biological surface crusts stemming

from extensive vegetation loss (Veste et al., 2001). Furthermore, the higher relief of eolian landforms, combined with the decreased shear velocity from reduced plant cover, increases sand mobility under higher windspeeds (Lancaster, 1985; Wiggs et al., 1994; Veste et al., 2001). These sand grains, if blown into fields from surrounding denuded areas, could pulverize surface crusts similar to the process of particles pitting and frosting automobile windshields during dust storms (Disterdick, 1933; Martin, 1938).

Conclusion

The DBD of the 1930s was an iconic event of environmental degradation across the USGP with crop failure, denudation of uncultivated and cultivated lands, and with numerous loci for the generation of fugitive dust. This study accessed primary historical archives, the Global Historical Climate Network, the 20th Century Reanalysis Project, field surveys and measurements with a Portable *In-Situ* Wind Erosion Laboratory, to assess the controls and character of dust storm variability and soil surface emissivity across the SHP from April 1938 to May 1940. Multivariate statistical analyses of dust storm variance yielded 6 principal components independently capturing ≥5% of the variance of all dust-storm days, related to lower-level atmospheric (18.5%) and surface (13.4%) air temperatures, lower-level relative humidity (8.2%), total storm duration (7.2%) and start time (6%), and the extent of eolian deposits in the county of storm origin (5.2%). Four modes of dust storms were identified related to the season of occurrence and dominant meteorological controls. The first two modes characterize "blowing season" storms from March to June, with early spring dust storms related to an inversion of surface and atmospheric air temperatures, and late spring-to-early summer dust storms associated with intensified surface temperatures and seasonal strength of the GPLLJ. The third mode of

dust storm occurs during the winter approximately two weeks after precipitation, when convection processes generate cold pool outflows with sufficiently strong winds to entrain particles. The final dust-storm mode reflects the passage of vigorous, multi-day haboobs coeval with maxima in direct evaporation from bare soils, and occur preferentially north of Amarillo, TX, over the Texas and Oklahoma panhandles. Assessment of the potential PM_{10} emissivity from common dust sources across the SHP indicates that anthropogenic disturbance of surface crusts can increase the magnitude of particle emissions (0.001 to 0.01 mg m^{-2} s^{-1}) from siltier soils. Moreover, emissions from loose, uncultivated sandy soils can emit similarly potent levels of dust as disturbed cultivated surfaces, suggesting a more complex narrative than previously recognized for landscape degradation in the 1930s DBD.

Associated Press journalist Robert Geiger, credited with coining the term "Dust Bowl," wrote of the dust as he travelled through Guymon, OK: "It gets into your clothes, literally in your hair, and sometimes it seems in your very soul. Certainly it gets under the skin" (Geiger, 1935). The anomalously elevated temperatures during the 1930s (Donat et al., 2016; Cowan et al., 2017) account for one-third of the variability in Dust Bowl dust storm activity, which carries significant implications for a warming world (e.g. Cook et al., 2015). Dust sources on the SHP abound with predominately sandy soils and are often associated with antecedent dunes and cover sands. Climate models forecast significant aridity and decade-long droughts on the SHP for later in the 21st century coincident with extreme, elevated summer temperatures: ideal conditions for vegetation mortality and formation of haboobs, the quintessential characteristics of the DBD. Such continental-scale dust storms would increase PM loads >20 μg m^{-3} d^{-1}, would be detrimental for public health

in nearby urban centers (Tong et al., 2017), and potentially across North America, dependent on synoptic conditions. Short grasslands in the driest areas of the USGP may shift in ecosystem function with an increase in surficial heterogeneity, like those of the desert grasslands in the SW (Schlesinger et al., 1990; Mangan et al., 2007; Collins et al., 2014; Moran et al., 2014; Svejcar et al., 2015) and similar to landscape response in the 1930s (Bolles and Forman, 2018), potentially precipitating a magnitude increase in mineral dust aerosol emissions from the SHP.

Acknowledgments

This research is supported by the National Geographic Society (#9990-16), the National Science Foundation (Award GSS-1660230), and the Glasscock Endowed Fund for Excellence in Environmental Science (032MBCU31). We are grateful to Dirk Burgdorf of AAA Research for assistance with archival research. Our gratitude is extended to Carol Bolles for digitizing the dust storm data sheets from archived records for use in this study. Thank you to Zequn Wu for providing comprehensive Quaternary geomorphology maps to guide field surveys. Thanks is also given to Connor Mayhack for performing the particle size analyses.

CHAPTER FOUR

Eolian Processes and Heterogeneous Dust Emissivity During the 1930s Dust Bowl Drought and Implications for Projected 21st Century Megadroughts

This chapter is published as: Bolles, K.C., Forman, S.L. & Sweeney, M.S. (2017) Eolian Processes and Heterogeneous Dust Emissivity During the 1930s Dust Bowl Drought and Implications for Projected 21st Century Megadroughts. *The Holocene* 10: 1578-1588.

Abstract

The 1930s Dust Bowl Drought on the U.S. Great Plains was an environmental crisis with failure of agricultural systems, landscape denudation, and elevated atmospheric dust loads. Poor agricultural practices were implicated for triggering widespread eolian erosion and heightened dust emissions, but this assumption is called into question. This study classified land-surface changes in southwest Kansas from aerial images taken in 1936 and in 1939 to infer surficial processes, dust sources, and associated emissivity. Seven distinctive surface classes were identified from an ArcGIS analysis of spectral reflectance values connected to surface vegetation cover and eolian activity, demonstrating a strikingly heterogeneous landscape response to the drought. Stratigraphic studies indicate accumulation of up to 4 m of eolian sand in places with erosion of a subjacent silty pre-1930s soil surface. Potential dust emissivity estimates for particulate matter were derived from the distribution of classified land surfaces and from empirical relations on analogous dust emissive surfaces in the western USA. Over 60% of total suspended particles in 1939 were inferred to be derived from uncultivated sandy surfaces and eolian landforms within the study area, with the remainder from human-modified surfaces. The $PM_{2.5}$ and PM_{10} emissivity estimates for a single dust event with winds over 6 m s^{-1} in the study area were

510-4,514 μg m^{-3} d^{-1} and 4,700-41,607 μg m^{-3} d^{-1} respectively, similar in magnitude to current dust storm events from North Africa and East Asia. Drought frequency is forecast to increase in late 21st century, potentially with greater severity than the Dust Bowl, and may be associated with magnitude increase in atmospheric dust loads.

Introduction

The 1930s Dust Bowl Drought (DBD) on the Great Plains, USA was an environmental crisis with agricultural and economic collapse, poor air quality, heightened respiratory illness and the ultimate out migration of more than 350,000 people (Hurt, 1981; Gregory, 2004; Egan, 2006). There were hundreds of continent-wide dust storms during the 1930s with scores of individual storms that deposited soil-derived dust as far as Washington D.C. (Hand, 1934), on ships 800 km off shore (Hurt, 1981), and increased tropospheric dust loads across the Northern Hemisphere, with likely dust deposition onto the Greenland ice cap (Donarummo, 2003). Recent climate modeling underscores the vulnerability of the Great Plains in the 21st century to extreme droughts, with drying forecasted to exceed historic conditions and with severity similar to decadal-scale megadroughts during the Medieval Climate Anomaly (Dai, 2013; Cook et al., 2015) when many dune systems reactivated on the Great Plains (e.g. Miao et al., 2007; Forman et al., 2008; Hanson et al., 2010; Halfen and Johnson, 2013).

The DBD was most severe between 1934 and 1936 with an average annual Palmer Drought Severity Index (PDSI) of -4 (Burnette and Stahle, 2013; Cook et al., 2014) which encompassed the panhandle areas of Texas and Oklahoma, and adjacent lands in eastern Colorado and western Kansas. Climate modelling of the DBD indicated that higher dust loads resulted in stability of the boundary layer, suppressed warm season precipitation and

thus, expanded the footprint and magnitude of drying (Cook et al., 2008; 2009; 2013). Furthermore, summer temperatures across Kansas were the hottest in the past 180 years with daily maxima exceeding 41°C (Burnette et al., 2010). A long standing assumption is that the dusty conditions during this drought were a direct response to large-scale crop failure of a succession of small farms, which left fields barren and exposed sandy soils to eolian erosion (Bennett and Fowler, 1936; Johnson, 1947; Worster, 1979; Hansen and Libecap, 2004; Schubert et al., 2004; Peters et al., 2007; Cook et al., 2008; 2009; 2013; Lee and Gill, 2015), and these denuded soil surfaces were sources for atmospheric dust loading. Particularly severe dust storms, referred to as "black blizzards", formed during passage of cyclones, darkened the sky, and persisted for up to two days (Mattice, 1935; Martin, 1939; Egan, 2006, p. 198-221). One such dust storm on 11 May 1934 was well-documented which originated on the southern Great Plains and moved eastward across the continent (Hand, 1934; Hurt, 1981, p. 35). A 2-km-high dust cloud descended over Washington, D.C. which resulted in 75% attenuation of solar radiation at the surface (Hand, 1934). An inferred $PM_{2.5}$ concentration for this dust storm was 330 to 840 $\mu g\ m^{-3}$ which is similar in magnitude to dust storms over southern Europe sourced from North Africa (Konare et al., 2008).

There are a variety of estimates on the loss of top soil from the 1930s DBD area from limited field surveys (e.g. Joel, 1937). In 1935, an estimated 771 million metric tons of topsoil was eroded from 1.76 million hectares of the Southern High Plains; a rate of 4.39 x 10^4 g m^{-2} (Joel, 1937; Hansen and Libecap, 2004). The Soil Conservation Service (SCS) reported by 1938 that top soil losses were even greater at 1.1 x10^5 g m^{-2} for Great Plains (Hansen and Libecap, 2004). Other soil erosion estimates for the Dust Bowl area infer that

four million hectares lost the upper ~12.5 cm of soil and an additional 5.5 million hectares lost over 6 cm of top soil (Hansen and Libecap, 2004) to a total of eroded topsoil of almost 14 billion metric tons, yielding soil loss of 2.9×10^4 g m^{-2} yr^{-1} between 1932 and 1939. This level of denudation would result in the potential release of 414 million to 5.5 billion metric tons of dust aerosols (Hansen and Libecap, 2004). If this topsoil loss was exclusive to agricultural areas, as assumed, then at least 7 million hectares of cultivated fields across the Great Plains would have to be stripped uniformly by at least 13 cm of topsoil over the course of the drought, which exceeds observations of the SCS. Therefore, an alternate emission source is necessary to explain dust loads observed during the DBD.

Historical analyses demonstrate just a third of Great Plains land was cultivated by 1935 with the highest concentrations of farming in counties along the eastern fringe (Fig. 4.1a), and in any year ~40% of this cultivated land reaping crops, the remainder either non-productive or fallow (Cunfer, 2005; Sylvester and Rupley, 2012). Landscape disturbance by cattle grazing in the Dust Bowl area was improbable with low and declining livestock usage, at the most 0.19 head of cattle per hectare throughout the 1930s; a two to tenfold decrease compared to the grazing intensities later in 20th century (Cunfer, 2005). Field studies document significant eolian activity in western Kansas during the DBD, with meters of eolian sand burying a pre-1930s land surface (Forman et al., 2008; Cordova and Porter, 2015). Furthermore, observations indicate that dust storms are common occurrences during multi-year droughts on the Great Plains throughout the Holocene (Miao et al., 2007; Forman et al., 2008; Hanson et al., 2010), during the 19th and early 20th centuries prior to European cultivation (Muhs and Holliday, 1995), and during the subsequent 1950s drought, even with wide-spread irrigation (Warn, 1952; Davidson, 1960; Nace and

Pluhowski, 1965). Thus, human agency is questioned as the dominant causative factor for landscape denudation and atmospheric dust loading during the DBD (Cunfer, 2005; Sylvester and Rupley, 2012). Low annual precipitation and anomalously high temperatures associated with such megadroughts lead to eolian activity that often initiates on drier, uncultivated, antecedent dune landforms, traveling across the landscape as a sand sheet (Peters et al., 2007). Therefore, uncultivated dune surfaces and adjacent eolian cover may have been significant sources for dust particles in the 1930s, and possibly for forecasted megadroughts in the 21st century (Cook et al., 2015).

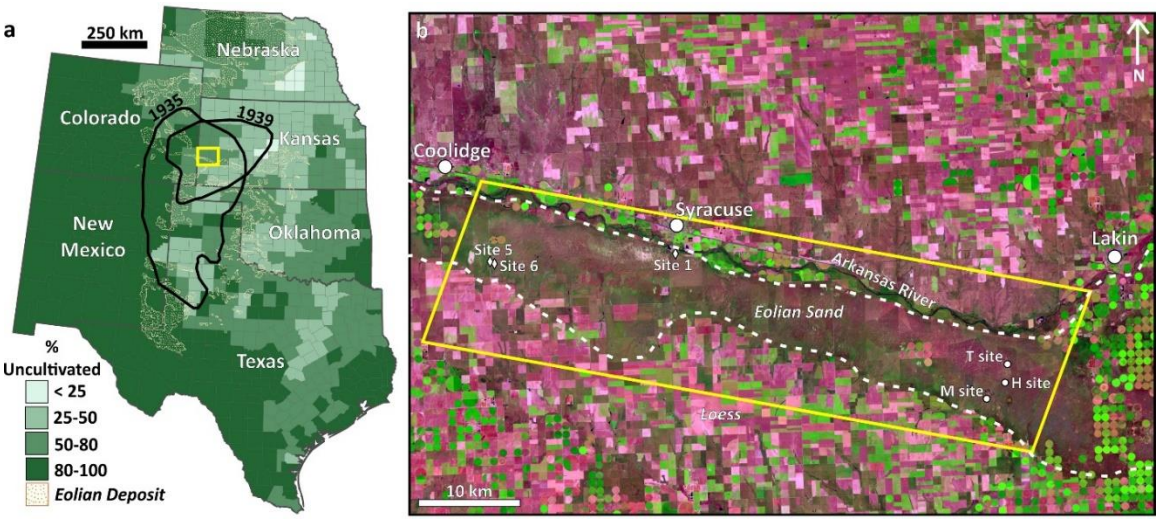

Figure 4.1 Study site location: (a) County-level map of proportion of land uncultivated per the Agricultural Census of 1935 (Gutmann, 2005) with the distribution of mapped eolian deposits (Muhs and Holliday, 1995) and area of strongest meteorological anomaly for 1935 and 1939 outlined in black (Cunfer, 2005), yellow box indicates counties investigated in this study; and (b) LANDSAT 8 image composite of bands 6, 5, and 2 for the Kansas study area with stratigraphic sites from this study denoted with circles and those by diamonds from Forman et al. (2008), yellow box designates coverage of historical aerial imagery.

Fundamental uncertainties remain for earth system models on the magnitude, source, and size of dust particles transported and deposited during the 1930s and other megadroughts (cf. Cook, et al., 2008; 2009; 2014). This study evaluates eolian processes, potential sources and flux of dust for surfaces across an antecedent eolian landscape with

riparian, natural eolian landforms and human-modified areas in southwestern Kansas, at the heart of 1930s DBD (Fig. 4.1). The uncultivated areas host barchanoid-ridge forms, parabolic dunes and sand sheet deposits with meters of relief and were common on terraces and upland surfaces adjacent to the Arkansas River, and also other river systems on the Great Plains (cf. Forman et al., 2001; 2008). This area was at the loci for dust storm generation generally coincident with counties with >40% sandy soils, the highest deficits of precipitation, and anomalously hot summer temperatures (Hovde, 1934; Martin, 1937a, 1937b; Cunfer, 2002; 2005).

Our analyses focused on the first generation of black and white aerial photography taken in 1936 and 1939 at the heart of the DBD in western Kansas to classify land-surface conditions related to vegetation cover and eolian processes. This research will address whether landscape denudation of small farms in western Kansas was the dominant source of suspend particles (Hansen and Libecap 2004; Lee and Gill, 2015) or were dust sources distributed widely across DBD landscape, including non-cultivated surfaces. Geomorphic and stratigraphic field studies of surfaces that reactivated in the 1930s provide insight regarding granulometry, thickness, and lateral continuity of particulate sources. A range of emissivity estimates for total suspended particles (TSP), $PM_{2.5}$ and PM_{10} for this area were derived for the first time from recorded wind speeds for western Kansas, the distribution of classified land surfaces and from empirical relations on dust emissivity for analogous eolian surfaces in the western USA (cf. Goossens and Buck, 2011a, b; Sweeney et al. 2011).

Methods

Eolian Stratigraphic Assessment

The dominant (>90%) surficial geologic deposits in the study area and the wider DBD area are eolian sands and silts, particularly for landforms on terraces above drainage systems (e.g. Busacca et al., 2003; Forman et al., 2008). The study area is covered by 15% stabilized dunes, another 40% of the area by vegetated sandsheet deposits, and much of the remaining surfaces expose loess deposits; all viable sources for dust (Goossens and Buck, 2011a, b; Sweeney et al, 2011; Lee et al., 2012; Flagg et al, 2014). We present stratigraphic, sedimentologic, and pedologic observations for 3 sections at sites in the Arkansas River paleodune field (Fig. 4.2) that complement a previous chronostratigraphic assessment (Forman et al., 2008). Sections were studied with attention to sedimentologic and pedogenic details. The attitude of beds was recorded to assess paleowind directions or

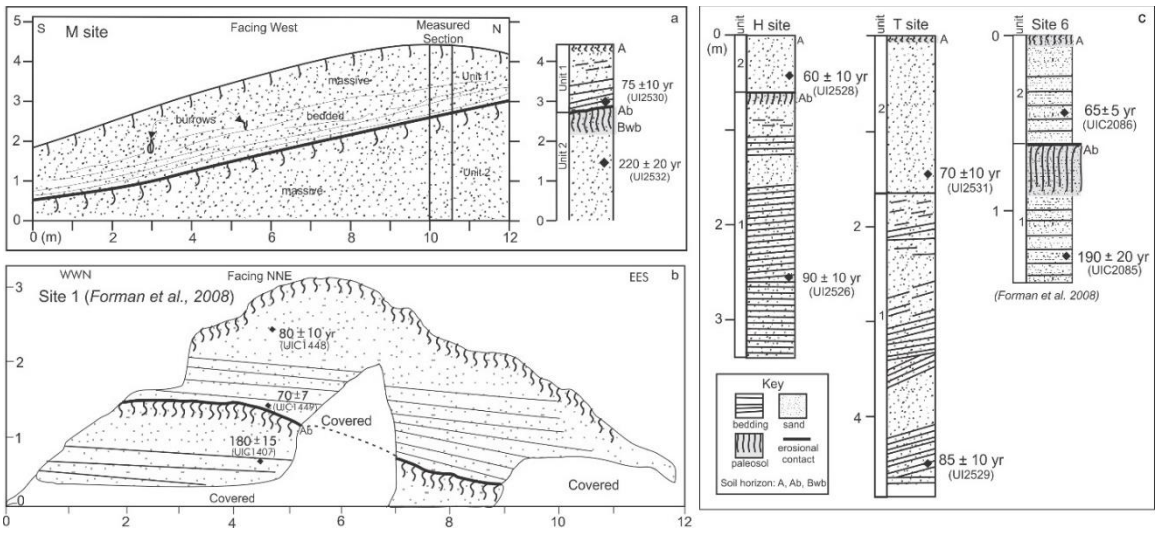

Figure 4.2 Stratigraphic profiles and OSL chronologies of sites M (a), H and T (c) from the Arkansas River paleo-dunefield in southwest Kansas (this study) and sites 1 (b) and 6 (c) from a previous study (Forman et al., 2008; Fig. 4.1).

a sedimentary facies, like a sand sheet. We also recorded changes in bed thickness, variability in bed thickness and granulometry. Attention was focused on bedding planes and unit contacts to assess if there were hiatuses in deposition, sometimes indicated by the presence of a buried soil or localized bioturbation. The recognition and lateral tracing of a buried soil is pivotal because this stratigraphic marker reflects probable landscape stability, associated with relatively mesic conditions. We used well-vetted soil stratigraphic and geomorphic approaches (e.g. Birkeland, 1999). All Munsell soil colors were assessed in the dry state. Age control is provided by optically stimulated luminescence (OSL) dating of quartz grains which is a well-vetted method for dating young (< 1,000 yr old) eolian sediments (e.g. Forman et al., 2008; Madsen and Murray, 2009). Ages presented herein are listed in years before present (yr BP), where "present" refers to AD 2010.

Image Processing and Spatial Analysis

Thousands of images from continent-wide aerial photographic surveys in the 1930s remain an untapped archive of land-surface changes during the DBD. This study used 175 printed photographs from negatives covering ~250 km^2, retrieved from the National Archives in College Park, MD with acquisition dates between 17 and 25 August 1936 and on 22 March 1939. Analyses focused on aerial photography taken of the DBD in Hamilton and Kearny counties, KS because this area exhibits proportionally 70% uncultivated to 30% cultivated land surface. This area is also representative of the mix of land use at the county level, and broadly for the Great Plains in the 1930s (Cunfer, 2005; Gutmann, 2005), and was at the center of the meteorological anomalies associated with the drought (Fig. 4.1a). We acknowledge that the aerial photographs capture surface conditions for an instant during the DBD. However, the inferred eolian processes from geomorphic and stratigraphic

analyses indicate a persistence of processes at least on a yearly timescale, which is consistent with agricultural census data (Gutmann, 2005). Aerial photographs were scanned at 1200 DPI and initially mosaicked and georeferenced (± 1-2 m error) within a GIS exploiting Kansas state road systems and AD 1898 USGS topographic maps for ground control points. Subsequently, these photomosaics were corrected radiometrically within AutoPano Giga against designated reference images. Gamma scaling was balanced across survey days to maximize grayscale range. Spatial analyses focused on the 1939 photomosaic because of greater tonal range than in often over-exposed 1936 images.

An unsupervised classification was developed within ArcGIS for 1939 land surfaces based on differences in spectral reflectance associated with relative vegetation cover and varying amounts of eolian processes across the landscape (Fig. 4.3a, 3b). Selecting the number of tonal classes was an iterative process based on the range and resolution of grayscale values in the normalized photomosaic. This scheme is similar to other approaches for mapping eolian landscapes to identify a range of dust emissive surfaces (cf. Bullard et al., 2011; Hugenholtz et al., 2012; Lee et al., 2012; Parajuli et al., 2014). Criteria for identifying each surface class was assessed by stereoscopic analyses of aerial photographs with an Abrams Stereoscope (model CB-1), pre- and post-1930 topographic data, and stratigraphic studies at 21st century sites where eolian activity was identified on the 1939 images. The aerial images showed important details under stereoscopic magnification, like groups of bushes and trees, blowouts, landform asymmetry and deep-plowing practices, such as listing, which aided spectral interpretations. This analysis was able to distinguish between shadows from steep slopes,

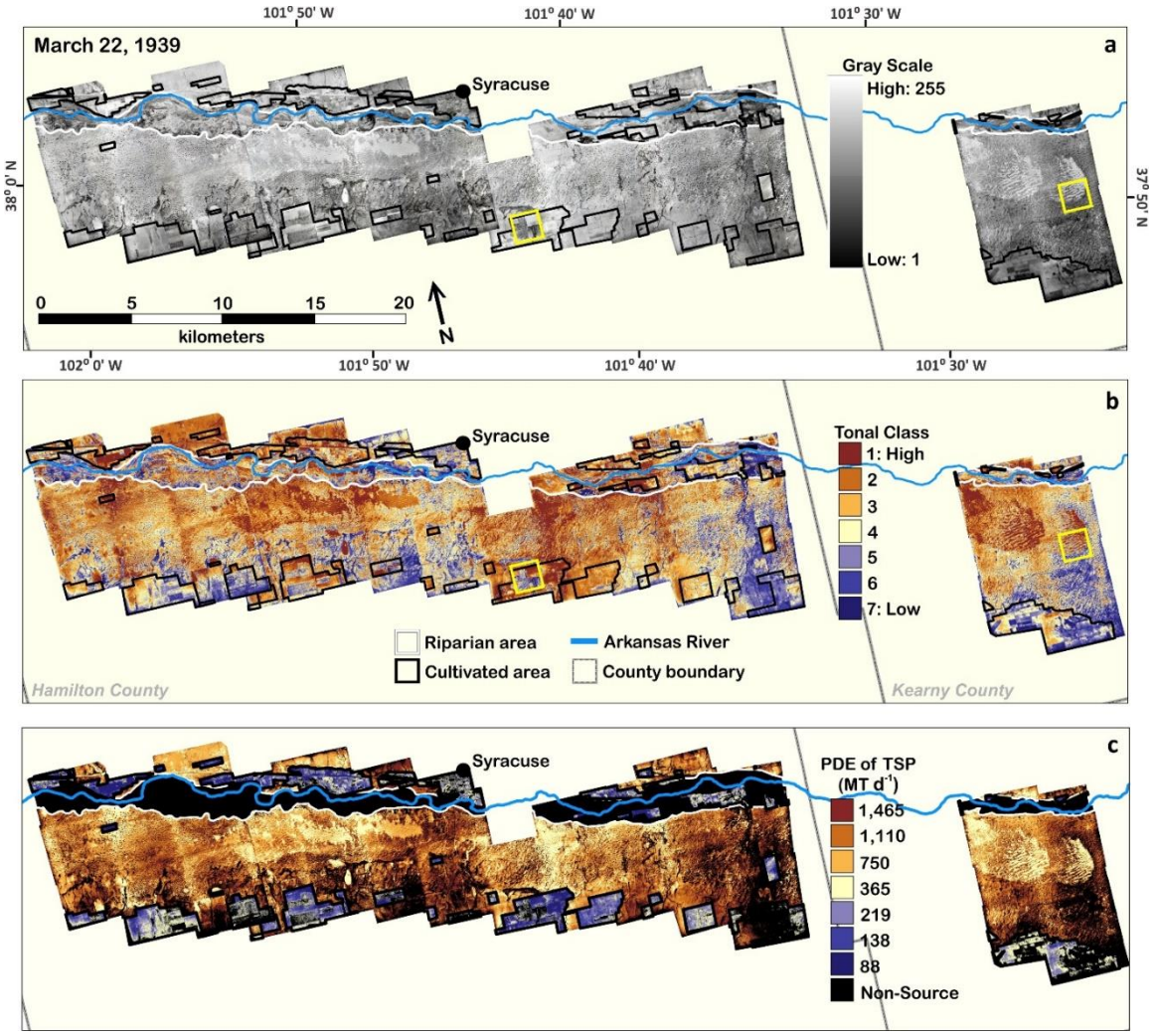

Figure 4.3. (a) Mosaicked, gamma-balanced, and geo-referenced aerial photographs of Hamilton and Kearny counties, Kansas; (b) Unsupervised classification of normalized gray-scale spectral reflectance values; and (c) Estimated potential dust emission (PDE) of total suspended particles (TSP; in MT) for a dust event 22 March 1939. Yellow boxes correspond to areas shown Figure 4.4.

densely vegetated, or wet areas with the former a smaller population of classified pixels (<2%) corrected through majority and boundary enhancing filters.

Estimate of Potential Dust Emission for Hamilton County, Kansas

The mean, minimum, and maximum estimates of potential dust emissivity (PDE) were calculated for these classified surfaces by equation 1 (US EPA, 2001; Penfold et al., 2005):

$$PDE = c \cdot k \cdot s^{0.6} \cdot a \cdot w \; or \; p \qquad (1)$$

where $\boldsymbol{c}$ is the emissivity rate of the land surface type (in mg m^{-2} s^{-1}), $\boldsymbol{k}$ is a dimensionless aerodynamic particle size multiplier (PSM), $\boldsymbol{s}$ is the percent silt content of the top 20 cm of soil, $\boldsymbol{a}$ is the spatial extent of each surface class (m^2), and $\boldsymbol{w}$ describes dust emissions as a function of wind speeds (Sullivan and Ajwa, 2011) with p, the number of agricultural operations performed on a given surface in a given season (Table 4.1). These calculations assumed minimum particle aggregation because of the dominance of Entisols and Inceptisols with >80% well-sorted fine to medium sand. Initial wind erosion is also effective in disaggregating soil particles (Lee and Gill, 2015).

The particle size multipliers (k) are based on standards from the U.S. Environmental Protection Agency (EPA) AP-42 (1995) for open and agricultural fugitive dust sources. Silt content (s) is based on data accessed from the Digital General Soil Map of the United States (Soil Survey Staff, 2016) for Dust Bowl counties, and reflects the mean percentage of silt in the upper 20 cm of soils across eolian and non-eolian landscapes. The relative proportion of dust and non-dust emissive surfaces classified for southwestern Kansas was used to determine likely source areas (a). Wind speed data for each day of year in 1939 was gleaned from Monthly Meteorological Summaries from the USDA Weather Bureau

for Dodge City, KS, and wind duration was extrapolated from Garden City, KS regional airport meteorological station based on decadal means of the predominant wind regime. These data are used to derive a daily wind factor (w), modified from an empirical formula from Sullivan and Ajwa (2011):

$$w = A(u - u_{th})^B \qquad (2)$$

where u is the daily average of fastest 1-minute wind speed, u_{th} is the threshold velocity wind speed (6 m s^{-1}), A is the duration (in seconds) of the fastest 1-minute wind speed, B is a magnitude scaler based on speed over the threshold velocity. Days with recorded precipitation and the following 24-hour period were removed as potential days for dust emission reflecting the impact of increased soil moisture (Sullivan and Ajwa, 2011).

Table 4.1. Sources and values defined for potential dust emission equation parameters.

Surface Type	**Emissivity Rate (*c*; mg m^{-2} s^{-1})**			**PSM (*k*)**	**Silt ($s^{0.6}$)**	**Area (*a*; m^2)**	**Operation (*p*)**
	Mean	***CI Min***	***CI Max***				
Uncultivated							
Class 1	0.1443	0.0485	0.4295	TSP: 1	1.8548	19,695,324	
Class 2	0.0866	0.0291	0.2577	PM_{10}: 0.5	3.4284	36,890,641	
Class 3	0.0797	0.0268	0.2371	$PM_{2.5}$: 0.05	5.0019	40,633,714	
Class 4	0.0765	0.0257	0.2276		8.1491	34,340,644	
Cultivated							
Year-round (Failed & Idle)							
Class 1	0.1443	0.0485	0.4295	TSP: 1	1.8548	4,808,095	
Class 2	0.0866	0.0291	0.2577	PM_{10}: 0.21	3.4284	6,777,378	
Class 3	0.0797	0.0268	0.2371	$PM_{2.5}$: 0.042	5.0019	8,015,365	
Class 4	0.0765	0.0257	0.2276		8.1491	8,650,530	
Seasonally (All; mg m^{-2}-tilled)							
Class 1	537.95	432.09	643.81	TSP: 1	1.8548	4,808,095	AMJ: 1
Class 2				PM_{10}: 0.21	3.4284	6,777,378	JA: 2
Class 3				$PM_{2.5}$: 0.042	5.0019	8,015,365	SON: 4
Class 4					8.1491	8,650,530	
Class 5					8.1491	7,980,828	
Class 6					8.1491	4,874,428	
Class 7					8.1491	2,458,699	
Source(s)							
Uncultivated	Goossens and Buck, 2011a, b; Sweeney et al, 2011; 2016; Flagg et al, 2014			Cowherd et al., 2006; Ono et al., 2003	NRCS STATSGO Database	Image Analysis (this study)	
Cultivated	Holmen et al, 2001; Cassel et al, 2003; Wang et al., 2010; Penfold et al., 2011			Penfold et al., 2005; U.S. EPA AP-42 (1995)			Cole and Mathews, 1938; Hambidge, 1938

Tillage practices in the 1930s were complex, with re-plowing (listing) of bare agricultural fields intended to retain soil moisture, which instead augmented dust emissivity from these surfaces (cf. Hambidge, 1938; Cook, et al, 2008; 2009; Lee and Gill, 2015). To determine an operation parameter (*p*), cultivation practices were inferred from documented preferences of the decade (Cole and Mathews, 1938), constrained by a planting and harvesting schedule for Kansas (USDA National Agricultural Statistics Service, 2010). Our study area was dominantly planted in winter wheat, per the Agricultural Census of 1940 (Gutmann, 2005). Based on the typic planting schedule for this crop in Kansas, we assume *p* would be minimum 4 during fall planting, 1 during the spring harvest, and 2 during summer fallow work. A generalized mean emission rate of ~538 mg m^{-2}-tilled was used for all agricultural surfaces during seasonal cultivation, as this standard is broadly representative of various operations and crop types (Penfold et al., 2005; Wang et al., 2010). Minimum and maximum confidence intervals of this rate were derived from the mean standard deviation of emission rates reported in studies of modern tillage operations (cf. Holmén et al., 2001; Cassel et al, 2003; Wang et al., 2010). In addition to particulates released during cultivation, failed and idle fields were assumed to emit dust at similar rates to uncultivated surfaces year-round, as these surfaces display similar sedimentological properties, were largely unvegetated, and therefore susceptible to frequent dust emission. Mean eolian emission rates of 2.26 g m^{-2} d^{-1} to over 40 g m^{-2} d^{-1} were derived from *in situ* measurement of dust flux from active dunes and sand sheet areas in the western U.S. (Goossens and Buck, 2011a; Sweeney et al., 2011). The geometrical mean of this emission rate was calculated for two sigma limits (Sweeney et al., 2011) to provide bounding dust flux rates by land surface type for dune surfaces. Studies of

analogous sandy surfaces demonstrate emissivity rates decrease with decreasing sand content (Goossens and Buck, 2011a, b), so the mean eolian emission rate was decreased proportionally with soil texture to infer emissivity of non-dune uncultivated surfaces. Eolian transport is severely limited on surfaces with vegetation cover of >30% and thus, visibly vegetated surfaces were assumed to be non-dust emissive (Kuriyama et al., 2005).

Whereas the U.S. EPA has assessed the accuracy of various emissions factors such as those in equation 1 (cf. Cowherd et al 2006; US EPA, 2007), uncertainty persists in quantifying highly variable dust emission by landform. Currently topographic effects are not included as emission factors, but would be expected to increase dust fluxes for dune fields given the increased surface area and concentration of airflow over these surfaces (Sullivan and Ajwa, 2011). Furthermore, we assumed a threshold wind velocity of 6 m s^{-1} at 10 m height, which is the estimated saltation threshold for fine sand grains. A lower threshold velocity is possible and would increase the saltation rate and associated dust loads. Therefore, these calculations provide a minimum potential estimate of daily dust emissions for TSP, $PM_{2.5}$ and PM_{10}, reflecting conservative estimates on dust sources and associated emissivity.

Results

Stratigraphic Record of 1930s Eolian Deposition

A previous study documented geomorphic, stratigraphic and geochronologic evidence for eolian activity in the ca. 1930s (Sites 1, 5, and 6; Forman et al, 2008). A 1.5 m thick eolian sand was identified that yielded OSL ages of 65 ± 5 yr BP (UIC2086), 80 ± 10 yr BP (UIC1448) and 70 ± 7 yr BP (UIC1407) that bury a soil, with underlying eolian sand that returned ages of 180 ± 15 yr BP (UIC1407) and 190 ± 20 yr BP (UIC2085).

These stratigraphic sequences indicate sand sheet deposition AD 1790 ± 20 yr BP with an intervening period of pedogenesis until ca. AD 1935, when this soil was buried by another sand sheet associated with the DBD. Subsequent stratigraphic studies (Fig. 4.2) further document the record of eolian deposition in the 1930s for study areas in southwestern Kansas. Stratigraphic sections reveal an appreciable lightening of the 1930s buried soil from an A horizon that is a dark yellowish-brown (10YR 3/4) to a brownish-yellow C horizon (10YR6/6), which would be reflected in gray tones of the photomosaics on eroded surfaces.

H site (37º 49.923'N; 101º 23.259'W).

This site is located in a barrow pit for a gas/oil pad that bisects an apparent barchanoid-ridge type dune within the Arkansas River Dune Field (Fig. 4.1b). The lowest most eolian unit (1) is a brownish yellow (10YR 6/6) well-sorted medium to fine sand with discontinuous cm-scale sub-horizontal bedding (Fig. 4.2b). These strata reflect ripple-bed migration with accretion by winds from the north to northwest. The upper 5 cm in unit 1 contains a weak yellowish brown (10YR5/4) Ab-horizon. The uppermost unit (2) is a yellowish brown (10YR 5/6) massive, well sorted medium to fine sand and contains the modern soil (weak A/C horizon) within the upper 5 centimeters. Bed remnants in the lower portion of unit 2 are traced laterally for 20 to 40 cm and down dip 5º-10º toward N70ºW. Quartz grains isolated from units 1 and 2 sands returned optical ages of 60 ± 10 yr BP (UIC2525) and 90 ± 10 yr BP (UIC2526), respectively.

T site (*37º 50.906'N; 101º 23.049'W).*

This site is a prominent blow-out of an east-west trending barchanoid-ridge dune (Fig. 4.1b). The basal eolian unit (1) is a very well sorted, brownish yellow (10YR 6/6) fine to medium sand with variable bedding (Fig. 4.2**c**). There are distinct 20 cm thick intervals with millimeter-scale low to moderate angle cross-bedding and intervals that are massive or contain 10-20 cm long bed remnants. Maximum measured bed inclination is 15° to 24° with an azimuth of S70E to S80E, indicating paleo-winds from the WNW. The overlying unit 2 is mostly massive very well sorted medium to fine sand; strata near the basal boundary dip downward 10° toward S75W, reflecting winds from NNE. Quartz grains isolated from unit 1 yield optical ages of 85 ± 10 yr BP (UI2529) and 70 ± 10 yr BP (UI2531) from unit 2.

M site (37º 49.101'N, 101º 24.544'W).

This site is located in a blowout within an area of complex dune types dominated by blowout forms south of the barchanoid dunes (Fig 1b). The basal unit (**2**) is a massive, brownish yellow (10YR 6/6) very well-sorted medium to fine sand (Fig. 4.2**a**). **The** overlying unit **1** is a brownish yellow (10YR 5/6), well-sorted medium sand, with 20-40 cm long bed remnants. A paleosol is developed in the upper 20 cm of unit 2. This paleosol exhibits clear A-horizon and is dark yellowish-brown (10YR 3/4) with a subjacent cambic horizon with weak subangular blocky structure. The upper unit (1) is a massive to discontinuously bedded medium to fine sand with a weak surface soil, indicated by an A-horizon. Quartz grains extracted from units 1 and 2 gave corresponding optical ages of 75 ± 10 yr BP (UI2530) and 220 ± 20 yr BP (UI2532).

GIS Classification of 1939 Land Surfaces

The three major land surface types, uncultivated, cultivated and riparian areas, were identified from analysis of the 1939 photomosaic (Fig. 4.3a). The uncultivated areas were mostly grass-covered, antecedent eolian surfaces with meters-scale relief, undivided by fencing, and with no visible roads or cattle trails. In contrast, cultivated areas were identified by outlines of rectangular fields with variable gray tones, fence line vegetation, nearby buildings, access roads, and some showed plowed furrows. Riparian areas covered < 10% of classified surfaces and were confined to zones adjacent to the Arkansas River. The range of gray-tone values for the mosaicked photographs outside of riparian areas reflect the relative presence or lack of vegetation and the depth of erosion into the pre-existing soil (Table 4.2).

Table 4.2. Results of spectral proxy classification by total area and land surface type with tonal class interpretations.

Tonal Class	Interpretation	Photogrammetric Description	Total Area		Land Surface (%)		
			(km^2)	*(%)*	*Cult.*	*Uncult.*	*Fluvial*
1	Active eolian	Higher, drier topographic areas of exposed sand, including apparent dune forms	27.7	11	11	11	10
2	Bare sand	Bare earth areas associated with eolian activity and/or fallow cropland	48.1	19	16	21	14
3	Exposed soil with sand deposition	Areas where sand is being removed and/or deposited on exposed soil through eolian processes	53.8	21	18	23	16
4	Disturbed A-horizon	Surfaces where soil is exposed, frequently associated with anthropogenically-altered surfaces	48.5	19	20	20	17
5	Moister soil and/or sparse vegetation	Lower topographic areas with wetter soil conditions and/or nascent vegetation colonization	36.5	15	18	13	18
6	Dense vegetation	Areas of continuous vegetation including cropland and natural grassland	23.7	9	11	8	16
7	Densest vegetation	Tree stands, shrubs and thickly vegetation deflation basins; densely planted cropland and heavy vegetation at fence lines	12	5	6	4	9

Tonal classes 1, 2, and 3 with the greatest spectral reflectance account for 51% of the land surface in 1939 and occur preferentially in uncultivated areas (56%) over cultivated areas (45%; Fig. 4.3b). Vegetation of any discernable height was rarely viewed in these areas. Class 1 surfaces showed evidence for active eolian transport palimpsest

with preexisting stoss and lee dune forms and associated with pervasive, accretionary sand-sheet deposits and fallow fields with moving sand (Fig. 4.4a, 4b). In places, this transported sand buries vegetation and the pre-existing soil, which is consistent with stratigraphic observations at sites 1 and 6 (Fig. 4.2b, 2c; Forman et al., 2008). Eolian sand associated with Class 1 can exceed 3 m in thickness as shown by exposed strata at H and T sites (Fig. 4.2c). Class 2 is associated commonly with Class 1 and under stereo pairs appears as loose sand on slopes, bare areas within the sand sheet and/or at the edges of bare fields. Class 3 includes exposed soil areas with variable sand deposition, and conversely, where there is less sand remaining after eolian erosion. The M stratigraphic site (Fig. 4.2a) occurred on Class 3 area and was characterized by a sand sheet deposit 0.5 to 2 m thick that draped an underlying, eroded buried soil that merges in places with the surface soil. Under stereoscopy these areas were of low relief and adjacent to surfaces with active erosion of the soil, associated with Classes 1 and 2.

Classes 4, 5, 6 and 7 have had the least spectral reflectance and were associated with variable vegetation cover or tonal qualities of recently exposed soils. Class 4 was observed typically where there was a disturbed A-horizon that lacks major sand deposits or vegetation cover and was frequently indicative of an anthropogenically-altered surface, such as the soil between planted crops, listed fields and along roads (Fig. 4.4c, 4d). Class 5 was observed consistently across the study site commonly adjacent to lower spectral reflectance areas. This class includes areas of nascent vegetation colonization and/or possibly more soil moisture, with limited eolian erosion into the surface soil. Classes 6 and 7 were areas predominantly (>60%) covered by vegetation such as grasses in uncultivated areas or planted fields. Class 7 accounted for only 5% of the total area and increased in

frequency towards the east and occurs more frequently in cultivated fields. Stereo pairs revealed that classes 6 and 7 generally include tree crowns, heavily vegetated depressions and fluvial terraces**,** water remaining in the river and stream network, and densely planted cropland and concentrated vegetation at fence-lines.

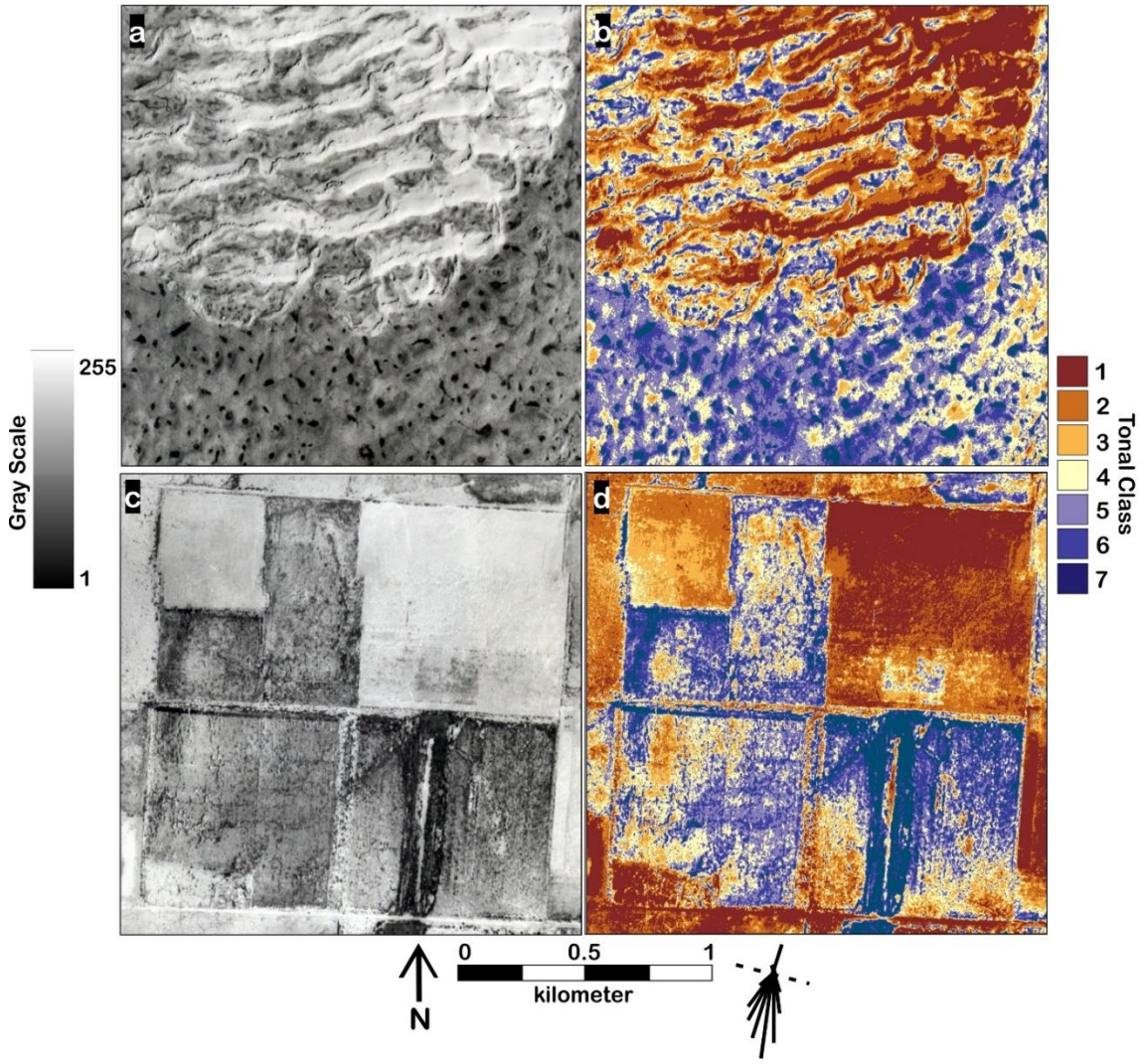

Figure 4.4. Ratio 1:12,000 scale view of typic uncultivated (a, b) and cultivated (c, d) areas. Sand rose (bottom) of modern (1973-2007) summer (JJA) resultant drift direction (RDD) for Dodge City, Elkhart, Garden City, and Liberal, KS (Schmeisser et al., 2010). For location refer to yellow boxes on Figure 4.3.

Potential Dust Emissivity from Southwest Kansas in 1939

We inferred a range of dust fluxes for 1939 on a daily basis from emissivity estimates for the classified surfaces and the wind speed record. The values for dust emissivity are minimum estimates because only surface classes 1 to 4 were considered dust sources and only within the boundaries of the study area, though other areas on the Great Plains were also dust sources (Brown et al., 1935; Blue, 1938; Chepil et al., 1963; Lee and Tchakerian, 1995). The basis of estimated emissions of TSP is the potential source area identified in the image classification, which for this area revealed 70% coverage of dust-emissive surfaces (Table 4.2). This is roughly consistent with limited field observations of Hamilton County made in 1937 that indicate ~78% of acreage was damaged by wind erosion (Joel, 1937). The potential TSP from the study area in 1939 was between 0.78 and 6.88 million metric tons, at a rate of 3,100 to 27,500 g m^{-2} yr^{-1}, which is consistent with estimates from the SCS that approximate an annual topsoil loss of ~29,000 g m^{-2} yr^{-1} by the end of the 1930s (Joel, 1937; Hansen and Libecap, 2004). The inferred potential TSP, PM_{10} and $PM_{2.5}$ emissions in the study area for an individual dust storm with a threshold wind speed of 6 m s^{-1} was 10,509-92,976 μg m^{-3}, 4,700-41,607 μg m^{-3} and 510-4,514 μg m^{-3} respectively; the latter estimate is magnitudes higher than the current EPA air quality standard of $PM_{2.5}$ 12 to 15 μg m^{-3} d^{-1} (NAAQS, 2016). The majority of particles (>65% of TSP) appear to be derived from uncultivated areas, particularly Class 3 and 4 surfaces, with the remainder from cultivated, human-modified surfaces (Fig. 4.3c). These emission estimates are consistent for dust storms in western Kansas in April 1935, with measured concentrations of 19,580 to 68,200 μg m^{-3} (Brown et al., 1935).

Discussion

The distribution of the seven surface classes from aerial photographic analysis indicated a heterogeneous landscape response within this Dust Bowl region with the loss of grass cover, erosion of soil particulates, the spread of sandsheets, and in places the dominance of shrubs with a deep root systems (Schlesinger et al., 1990; Mangan et al., 2004). This analysis of land surface processes during the 1930s showed the preferential loss of vegetation in uncultivated areas, coeval with less denudation in cultivated zones. The majority of the uncultivated area was coincident with antecedent eolian landforms, with 15% of the surface covered by dune forms and an additional area of ~44% covered by sandsheet deposits (Fig. 4.1**b**; Fig. 4.3). Stratigraphic studies with OSL ages indicate up to 4 m of eolian sand accumulated during the 1930s drought with erosion of a subjacent silt-rich pre-1930s soil. Reactivation of these landforms, with saltation, would introduce a productive and a consistent dust source (Miao et al., 2007; Cook et al., 2009; Goossens and Buck, 2011a, b; Sweeney et al., 2011; Flagg et al., 2014) that could initiate a cascading effect of eolian activity across the landscape (Peters et al., 2007).

Dune systems may be a sustained source for regional dust loads (Bullard et al., 2004; 2007; 2008; Bullard and White, 2005; Crouvi et al., 2008; 2012). Dunes and sand sheet deposits can contain up to 5% silt (< 63 μm) incorporated with landform stabilization via dust-trapping by vegetation and soil formation (cf. Forman et al., 2014). These fines can be liberated as dust when dunes are reactivated. The saltation and ballistic impacts of sand grains can yield added dust emissions either as fractured grains of coarse silt, removal of grain coatings, or suspension of silt grains from subjacent eroding soils, often at lower-than-average friction velocities (Bullard et al., 2004; Crouvi et al., 2008; Goossens and

Buck, 2011a, b; Sweeney et al., 2011). Dunes appear to be a consistent source of emitted dust under sustained, high wind velocities (>15 m s^{-1}), compared to peaked emissions from supply-limited areas (Sweeney et al., 2011; 2016a; 2016b; Bhattachan et al., 2013). Holocene loess deposits in southern Nebraska are hypothesized to be derived primarily from saltation within the Nebraska Sand Hills (Miao et al., 2007). Thus, preferential aridification of uncultivated, antecedent eolian sand deposits is implicated as a prime source for suspended particulates during the DBD, rather than exclusively from agricultural fields, which was the implicit assumption for the past 80 years as the cause of this environmental crisis (Bennett and Fowler, 1936; Johnson, 1947; Worster, 1979; Hansen and Libecap, 2004; Schubert et al., 2004; Peters et al., 2007; Cook et al., 2008; 2009; 2013; Lee and Gill, 2015). This analysis is consistent with historical documentation that demonstrates just 30% of the Dust Bowl area was ever cultivated (Cunfer, 2005; Sylvester and Rupley, 2012), but deviates significantly from climate model assumptions that limited dust sources exclusively from denuded cropland (cf. Cook, et al., 2008; 2009).

Conclusion

The Dust Bowl emissivity ranges are on par to the few measurements of particulate depositional rates with the passage of dust storms in southwestern Kansas (Brown et al., 1935), and eastern Oklahoma (Blue, 1938); and with particulate fluxes along the eastern seaboard (Hand, 1934). Dust concentrations of this magnitude, e.g. $PM_{2.5}$ 10^2 to 10^3 μg m^{-3} d^{-1} have been measured in the 21st century during extreme dust storms on the Southern Great Plains (Lee and Tchakerian, 1995). The inferred dust emissivity for 1939 is similar in magnitude to satellite observations of modern dust events that originated from North Africa and eastern Asia where PM_{10} concentrations are 5,000 to 14,000 μg $m^{-3}d^{-1}$ (WHO,

2003; Chen et al., 2004; Kim et al., 2010; Marticorena et al., 2010). Health-based studies of populations in western Kansas during the DBD indicate increased morbidity and mortality from acute respiratory ailments with dust storms, even though mortality decreased in the broader American population in the 1930s (Cutler et al., 2007; Granados and Roux, 2009).

Currently, over 40 million people live on the Plains and like during the DBD are at risk from projected megadroughts on the Great Plains in the 21st century with higher frequency of hot (>40°C) temperatures (Cook et al., 2014). Prolonged, severe droughts, like during the DBD, may initiate partial reactivation of pervasive eolian systems on Great Plains, which are potent sources for magnitude increase in $PM_{2.5-10}$ emissivity. This enhanced dust load in the lower troposphere may lead to increased boundary layer stability, expanding the extent and severity of droughts (Cook et al., 2009). A greater frequency of drought conditions may be associated with substantial increases in atmospheric dust loads for adjacent urban areas and globally, which may cause heightened risks to premature mortality and morbidity from respiratory, cardiovascular and dust-borne viral diseases (Griffin, 2007; Anenberg et al., 2010; Park et al., 2010).

Acknowledgments

We thank National Archives in College Park, MD for access to 1930s aerial photographic record. The assistance is appreciated of J. Pierson, J. Mazzocco, and L. Marin. The comments are appreciated of S. Driese, D. Peppe, D. Wright, J. Hoggarth, and M. Waters.

CHAPTER FIVE

Conclusion

The 1930s DBD was an environmental crisis with agricultural and economic collapse, poor air quality, heightened respiratory illness and the ultimate out migration of more than 350,000 people (Egan, 2006; Gregory, 2004; Hurt, 1981). Dust storms during the 1930s were continental in scale and deposited soil-derived dust as far as Washington D.C. (Hand, 1934; Hovde, 1934; Mattice, 1935; Martin, 1937), on ships 800 km off shore (Hurt, 1981, p. 34), and increased broadly tropospheric dust loads across the Northern Hemisphere, with likely dust deposition onto the Greenland ice cap (Donarummo et al., 2003). Recent climate modeling underscores the vulnerability of the Great Plains in the 21st century to extreme droughts, with drying forecasted to exceed historic conditions and with severity similar to decadal-scale megadroughts during the MCA (Dai, 2011; 2013; Cook, et al., 2015) when many dune systems reactivated on the USGP (e.g. Miao et al., 2007; Forman et al., 2008; Hanson et al., 2010; Schwalb et al., 2010; Halfen and Johnson, 2013).

An inherent historical assumption is that the dust storms during the DBD were a direct response to large-scale crop failure of a succession of small farms, which left fields barren and exposed sandy soils to eolian erosion (e.g. Bennett and Fowler, 1936; Worster, 1979; Hurt, 1981; Schubert et al., 2004; Egan, 2006). This project scrutinized this hypothesis via examination of historical aerial photographs acquired between 1936 and 1941 with emerging semi-automated image analysis methods, field assessments of eolian deposition and dust flux from dominant soil textures on the SHP, and statistical re-

evaluation of archived primary documentation from the SCS in context with coeval meteorological conditions derived from atmospheric reanalyses (Compo et al, 2011; Menne et al, 2012). At the regional scale, the USGP demonstrated heterogenous denudation and resistance or resilience to the DBD (Bolles and Forman, 2018). The dominant sources of degradation found for sites east of the 100th meridian were cultivated fields and fluvial deposits, associated with woody vegetation response to water availability in uncultivated areas. For sites to the west, denuded surfaces were predominantly eolian sandsheets and dunes, correlated with intensity of drought conditions and reduced plant diversity. Discrete spatial signatures of the drought were observed not only within the classically recognized southern Dust Bowl area, but also in the northern and central plains. Multivariate statistical analyses of site variability suggest landscape response to the DBD is most strongly influenced by the arid–humid divide and severity of precipitation and temperature anomalies.

The SHP is recognized in historical documentation as the area of most severe wind erosion. Evaluation of the inventory of dust storms recorded at SCS experiment sites across the SHP demonstrated that the commonly recognized boundaries of eolian degradation generally agree with the available historical documentation, though field assessment of SHP land surfaces elucidated the variability in surficial processes contributing to available areal extent and potency of surficial dust sources (Bolles, Sweeney and Forman, *Submitted*). Disturbed soils on the SHP begin to emit at a magnitude-higher rate than undisturbed surfaces as soon as the threshold velocity (8 to 10 m s^{-1}) is reached, and this rate increases linearly with wind speed. Conversely crusted, undisturbed surfaces do not begin to reach the same flux rate until much higher wind speeds, at which point the crusts

are broken and emissivity rates increase rapidly, with similar flux to disturbed surfaces. Significantly, the particle emissivity of undisturbed, loose sandy soils mirrors that of disturbed surfaces in relation to wind speed and potential magnitude of dust emitted. This suggests that the sandier, uncultivated soils of the SHP could be equal to or greater dust sources than cultivated fields, which were unavailable for part of the blowing season either via crop cover or crust formation between agricultural treatments.

A sub-meter scale classification of land surface changes in southwest Kansas, located within the SHP region of most persistent severe erosion, revealed a strikingly heterogeneous landscape response to the drought (Bolles, Forman and Sweeney, 2017). Stratigraphic studies indicated accumulation of up to 4 m of eolian sand in places with erosion of a subjacent silty pre-1930s soil surface. Potential dust emissivity estimates for particulate matter were derived from the distribution of classified land surfaces and from empirical relations on analogous dust emissive surfaces in the western USA. Over 60% of total suspended particles in 1939 were inferred to be derived from uncultivated sandy surfaces and eolian landforms within the study area, with the remainder from human-modified surfaces. The $PM_{2.5}$ and PM_{10} emissivity estimates for a single dust event with winds over 6 m s^{-1} in the study area were 510-4,514 μg m^{-3} d^{-1} and 4,700-41,607 μg m^{-3} d^{-1} respectively, similar in magnitude to current dust storm events from North Africa and East Asia.

Associated Press journalist Robert Geiger, credited with coining the term “Dust Bowl,” wrote of the dust as he travelled through Guymon, OK: “It gets into your clothes, literally in your hair, and sometimes it seems in your very soul. Certainly it gets under the skin” (Geiger, 1935). Local publications decried the extra cleaning burden on housewives,

unable to keep the dust out of homes (e.g. *Wichita Beacon*, nd.). During dust storms, the peak of daytime could appear more like "a moonlight night, yellow with a tinge of red", with the air so dense with soil it seemed like mud (*Chicago Tribune*, 1933). Such dramatic decreases in near-surface visibility often necessitated street lamps to be turned on and caused collisions, both pedestrian and vehicular (Disterdick, 1933). Automobiles were often abandoned when charged particles disabled ignition systems, and sustained extensive damage from blowing sand stripping paint, pitting windshields, and impeding carburetors (Disterdick, 1933; Martin 1938).

Public health decreased with the passage of dust storms, with increases in cardiovascular morbidity and mortality and dust-borne diseases (cf. Brown et al., 1935; Blue, 1938; Hagen and Woodruff, 1973; Griffin, 2007; Anenberg et al., 2010; Park et al, 2010; Esmaeil et al., 2014; Giannadaki et al., 2014; Tong et al., 2017). A study from the Kansas Board of Health found that in the first six months of 1935 a measles epidemic was two-times as widespread as the previous high point of occurrence in 1917, killing 145 persons in the first four months (Brown et al, 1935). Acute respiratory infections were observed in "unusually" high numbers throughout the state, with a 50-100% increase in pneumonia cases compared to the same months of 1934 (Brown et al, 1935). Red Cross officials referred to the aggravation of respiratory illness in the Great Plains as "dust pneumonia" and attributed the deaths of many area residents to particle exposure (*Chicago Tribune*, 1935a). Respiratory infections were coupled with a marked increase in complications, such as sinusitis, laryngitis, pharyngitis, bronchitis, and numerous cases of corneal ulcers and eye infections (Brown et al, 1935). One newspaper article reports five deaths in one week related to the dust storms in Kansas during March 1935, three of which

were children: a 2-month old baby, a 2-year-old boy and a 13-year-old girl (*Chicago Tribune*, 1935a). By April 30th of the same year, local private hospitals were at capacity with pneumonia victims and a fourth emergency field hospital was opened in the "dust belt", where nine pneumonia deaths were reported within one week (*Chicago Tribune*, 1935b). Dust storms in eastern Colorado and western Kansas in 1936 were ranked as the most severe and prolonged for the decade with visibility at times reduced to zero, associated with mortality of livestock, infants suffocating in cribs, and respiratory distress of 100s of people (Choun, 1936; Martin, 1936a). Current residents of the SHP may face similarly increased health risks with climate change.

With a projected increase 21st century aridity, eolian processes cascading across western grasslands, like during the Dust Bowl, may significantly impact future dust particle emission and land and carbon storage management. Such continental-scale dust storms would increase $PM_{2.5}$ loads >20 $\mu g\ m^{-3}\ d^{-1}$, would be detrimental for public health in nearby urban centers, and potentially across the eastern and the western U.S., dependent on synoptic conditions. For the USGP, grasslands are expected to experience a shift in ecosystem functioning and increasing patches of bare soil surfaces, like those of the desert grasslands in the SW (Collins et al, 2014; Moran et al, 2014; Svejcar et al, 2015) and similar to the 1930s (Bolles and Forman, 2018), potentially precipitating a magnitude increase in mineral dust aerosol emissions from the SHP. More work is needed to understand patterns in historical vital statistics correlated with mineral dust aerosol exposure during the DBD and to project future "hotspots" of dust-related changes to air quality and associated diseases on the USGP, particularly in the now identified "Northern Dust Bowl", centered on the Dakotas.

BIBLIOGRAPHY

Achakulwisut, P., Shen, L., & Mickley, L. J. (2017) What Controls Springtime Fine Dust Variability in the Western United States? Investigating the 2002-2015 Increase in Fine Dust in the U.S. Southwest: Controlling factors of western U.S. dust. Journal of Geophysical Research: Atmospheres, 122(22), 12,449-12,467. https://doi.org/10.1002/2017JD027208

Aguilera, P. A., Fernández, A., Fernández, R., Rumí, R., & Salmerón, A. (2011) Bayesian networks in environmental modelling. Environmental Modelling & Software, 26(12), 1376–1388. http://doi.org/10.1016/j.envsoft.2011.06.004

Albertson, F. W., & Weaver, J. E. (1944) Effects of drought, dust, and intensity of grazing on cover and yield of short-grass pastures. Ecological Monographs, 14(1), 1–29.

Albertson, F. W., & Weaver, J. E. (1944) Nature and degree of recovery of grassland from the great drought of 1933 to 1940. Ecological Monographs 14(4): 393–479.

Anderson JJ, Cobb NS (2004) Tree cover discrimination in panchromatic aerial imagery of pinyon–juniper woodlands. Photogrammetric Engineering & Remote Sensing 70(9): 1063–1068.

Anenberg SC, Horowitz LW, Tong DQ, et al. (2010) An Estimate of the Global Burden of Anthropogenic Ozone and Fine Particulate Matter on Premature Human Mortality Using Atmospheric Modeling. Environmental Health Perspectives 118(9): 1189–1195.

Baas, A. C. W. (2007) Complex systems in aeolian geomorphology. Geomorphology, 91(3-4), 311–331. http://doi.org/10.1016/j.geomorph.2007.04.012

Bacon, S. N., E. V. McDonald, R. Amit, Y. Enzel, and O. Crouvi (2011), Total suspended particulate matter emissions at high friction velocities from desert landforms, J. Geophys. Res., 116, F03019, doi:10.1029/2011JF001965.

Baddock, M. C., Ginoux, P., Bullard, J. E., & Gill, T. E. (2016) Do MODIS-defined dust sources have a geomorphological signature?. Geophysical Research Letters, 43(6), 2606–2613. https://doi.org/10.1002/2015GL067327

Bakker, M, Lane, SN (2017) Archival photogrammetric analysis of river–floodplain systems using Structure from Motion (SfM) methods. Earth Surface Processes and Landforms 42(8): 1274–1286

Ball GH, Hall DJ (1967) A clustering technique for summarizing multivariate data. Behavioral science, 12(2), 153–155.

Barandiaran, D., Wang, S.-Y., & Hilburn, K. (2013) Observed trends in the Great Plains low-level jet and associated precipitation changes in relation to recent droughts: TRENDS IN GREAT PLAINS LOW-LEVEL JET. Geophysical Research Letters, 40(23), 6247–6251. http://doi.org/10.1002/2013GL058296

Barchyn, T. E., & Hugenholtz, C. H. (2012) Aeolian dune field geomorphology modulates the stabilization rate imposed by climate. Journal of Geophysical Research, 117(F2) http://doi.org/10.1029/2011JF002274

Basara, J. B., Maybourn, J. N., Peirano, C. M., Tate, J. E., Brown, P. J., Hoey, J. D., & Smith, B. R. (2013) Drought and Associated Impacts in the Great Plains of the United States—A Review. International Journal of Geosciences, 04(06), 72–81. http://doi.org/10.4236/ijg.2013.46A2009

Bastin GN, Ludwig JA, Eager RW, Chewings, VH, Liedloff AC (2002) Indicators of landscape function: comparing patchiness metrics using remotely–sensed data from rangelands. Ecological Indicators 1(4): 247–260.

Bel, G., & Ashkenazy, Y. (2014) The effects of psammophilous plants on sand dune dynamics. Journal of Geophysical Research: Earth Surface, 119(7), 1636-1650.

Belnap, J., Munson, S. M., & Field, J. P. (2011) Aeolian and fluvial processes in dryland regions: the need for integrated studies. Ecohydrology, 4(5), 615–622. http://doi.org/10.1002/eco.258

Ben–Dor E (2002) Quantitative remote sensing of soil properties. Advances in Agronomy 75: 173–244.

Bennett, H. H., & Fowler, F. H. (1936) Report of the Great Plains Drought Area Committee. Government Printing Office, Washington, DC.

Bestelmeyer BT, Ward JP, Havstad KM (2011) Analysis of abrupt transitions in ecological systems. Ecosphere 2(12): Article 129.

Bhattachan A, D'Odorico P, Okin GS, Dintwe K (2013) Potential dust emissions from the southern Kalahari's dunelands. Journal of Geophysical Research-Earth Surface 118(1): 307-314.

Birkeland, P. (2001), SOILS AND GEOMORPHOLOGY edited by Peter W. Birkeland, Oxford University Press, New York, 1999. No. of pages: 430

Blaschke T, Hay GJ, Kelly M, Lang S, Hofmann P, Addink E, Tiede D (2014) Geographic object–based image analysis–towards a new paradigm. ISPRS Journal of Photogrammetry and Remote Sensing 87: 180–191

Blue JA (1938) Dust—its effect on man from a medical standpoint with special reference to the Dust Bowl. Southern Med. J. 31:1101–1106.

Bochert, J.R., (1971) The Dust Bowl in the 1970s. Ann. Assoc. Am. Geogr. 61, 1-22.

Bolles K. C., Forman S.L., Sweeney M (2017) Eolian processes and heterogeneous dust emissivity during the 1930s Dust Bowl Drought and implications for projected 21st–century megadroughts. The Holocene 27(10): 1578–1588.

Bolles, K. C., & Forman, S. L. (2018) Evaluating Landscape Degradation Along Climatic Gradients During the 1930s Dust Bowl Drought From Panchromatic Historical Aerial Photographs, United States Great Plains. Frontiers in Earth Science, 6. https://doi.org/10.3389/feart.2018.00153

Bolles, Kasey, 2018a, "KS_HAMILTON_1939", doi:10.18738/T8/X91MGH, Texas Data Repository Dataverse, V1

Bolles, Kasey, 2018b, "ND_WARD_1938", doi:10.18738/T8/JQ1PBY, Texas Data Repository Dataverse, V1

Bolles, Kasey, 2018c, "NE_McPHERSON_1939", doi:10.18738/T8/GNNZMS, Texas Data Repository Dataverse, V1

Bolles, Kasey, 2018d, "NM_QUAY_1936", doi:10.18738/T8/BXLC1P, Texas Data Repository Dataverse, V1

Bolles, Kasey, 2018e, "OK_TILLMAN_1937", doi:10.18738/T8/VYX0JB, Texas Data Repository Dataverse, V1

Bolles, Kasey, 2018f, "TX_LAMAR_1940", doi:10.18738/T8/KKA6E1, Texas Data Repository Dataverse, V1

Bolles, Kasey, 2018g, "TX_REDRIVER_1940", doi:10.18738/T8/XTIURO, Texas Data Repository Dataverse, V1

Bolles, Kasey, 2018h, "TX_WICHITA_1937", doi:10.18738/T8/SVAGLL, Texas Data Repository Dataverse, V1

Bolles, Kasey, 2018i, "TX_WILBARGER_1937", doi:10.18738/T8/YCNHIO, Texas Data Repository Dataverse, V1

Borradaile G (2003) “Correlation and Comparison of Variables.” In Statistics of Earth Science Data (pp. 157–185) Springer, Berlin, Heidelberg

Boucher, O., Randall, D., Artaxo, P., Bretherton, C., Feingold, G., Forster, P., … others. (2013) Clouds and aerosols. In Climate change 2013: the physical science basis. Contribution of Working Group I to the Fifth Assessment Report of the Intergovernmental Panel on Climate Change (pp. 571–657) Cambridge University Press.

Boulter, C., Bateman, M. D., & Frederick, C. D. (2010) Understanding geomorphic responses to environmental change: a 19 000-year case study from semi-arid central Texas, USA. Journal of Quaternary Science, 25(6), 889–902. http://doi.org/10.1002/jqs.1365

Breshears DD, Barnes FJ (1999) Interrelationships between plant functional types and soil moisture heterogeneity for semiarid landscapes within the grassland/forest continuum: a unified conceptual model. Landscape Ecology 14(5): 465–478.

Brönnimann, S., Stickler, A., Griesser, T., Ewen, T., Grant, A. N., Fischer, A. M., … Ross, T. (2009) Exceptional atmospheric circulation during the "Dust Bowl." Geophysical Research Letters, 36(8) http://doi.org/10.1029/2009GL037612

Brown E. G., Gottlieb S., Laybourn R.L., (1935) Dust storms and their possible effect on health. Public Health Rep. 50, 1369–1383.

Brown, M. J., Krauss, R.K., Smith, R.M., (1968) Dust deposition and weather. Weatherwise 21, 66-70.

Browning DM, Archer SR, Byrne AT (2009) Field validation of 1930s aerial photography: What are we missing? Journal of Arid Environments 73(9): 844–853.

Bryant, R. G. (2013) Recent advances in our understanding of dust source emission processes. Progress in Physical Geography, 37(3), 397–421. http://doi.org/10.1177/0309133313479391

Bullard J, Baddock M, McTainsh G, Leys J (2008) Sub-basin scale dust source geomorphology detected using MODIS. Geophysical Research Letters 35(15) doi:10.1029/2008GL033928.

Bullard J.E., McTainsh GH, Pudmenzky C (2004) Aeolian abrasion and modes of fine particle production from natural red dune sands: An experimental study. Sedimentology 51(5):1103-1125.

Bullard J.E., Mctainsh GH, Pudmenzky C (2007) Factors affecting the nature and rate of dust production from natural dune sands. Sedimentology 54(1):169–182.

Bullard, J. E., & Livingstone, I. (2002) Interactions between aeolian and fluvial systems in dryland environments. Area, 34(1), 8–16.

Bullard, J. E., & White, K. (2005) Dust production and the release of iron oxides resulting from the aeolian abrasion of natural dune sands. Earth Surface Processes and Landforms, 30(1), 95–106. https://doi.org/10.1002/esp.1148

Bullard, J. E., Harrison, S. P., Baddock, M. C., Drake, N., Gill, T. E., McTainsh, G., & Sun, Y. (2011) Preferential dust sources: A geomorphological classification designed for use in global dust-cycle models. Journal of Geophysical Research, 116(F4) http://doi.org/10.1029/2011JF002061

Burnette, D. J., Stahle, D. W., (2013) Historical perspective on the dust bowl drought in the central United States. Clim. Change 116, 479-494.

Burnette, D. J., Stahle, D. W., Mock, C. J., (2010) Daily-Mean Temperature Reconstructed for Kansas from Early Instrumental and Modern Observations. J. Climate 23, 1308-1333.

Busacca AJ, Begét JE, Markewich HW, et al. (2003) Eolian sediments. In: Developments in Quaternary Sciences, Elsevier, pp. 275–309.

Byrne KM, Adler PB, Lauenroth WK (2017) Contrasting effects of precipitation manipulations in two Great Plains plant communities. Journal of Vegetation Science 28(2): 238–249.

Camino, C., Cuevas, E., Basart, S., Alonso-Perez, S., Baldasano, J. M., Terradellas, E., Marticorena, B., Rodriguez, S., Berjon, A., (2015) An empirical equation to estimate mineral dust concentrations from visibility observations in Northern Africa. Aeol. Research 16, 55-68.

Carmel Y, Kadmon R (1998) Computerized classification of Mediterranean vegetation using panchromatic aerial photographs. Journal of Vegetation Science 9(3): 445–454

Cassel T, Trzepla-Nabaglo K and Flocchini R (2003) PM10 emission factors for harvest and tillage of row crops. In: 12th International Emission Inventory Conference, San Diego, CA.

Caylor J (2000) Aerial photography in the next decade. Journal of Forestry 98(6): 17–19.

Chen Y-S, Sheen P-C, Chen E-R, et al. (2004) Effects of Asian dust storm events on daily mortality in Taipei, Taiwan. Environmental Research 95(2): 151–155.

Chen, W., Fryrear, D. W., (2002) Sedimentary characteristics of a haboob dust storm. Atmo. Res. 61, 75-85.

Chepil, W. S., Siddoway, F. H., & Armbrust, D. (1963) Climatic index of wind erosion conditions in the Great Plains. Soil Science Society of America Journal, 27(4), 449–452.

Chepli, W. S., (1957) Dust Bowl: Causes and Effects. J. Soil Water Conserv. 12, 108-111.

Choun, H. F., (1936) Duststorms in the southwestern plains area. Mon. Weather Rev. 64,195.

Cole JS, Mathews OR (1938) Tillage. In G Hambidge (Ed.), Soils and Men: Yearbook of Agriculture (pp. 321-328) Washington, DC: US Department of Agriculture.

Collins, S. L., Belnap, J., Grimm, N. B., Rudgers, J. A., Dahm, C. N., D'Odorico, P., … Wolf, B. O. (2014) A Multiscale, Hierarchical Model of Pulse Dynamics in Arid-Land Ecosystems. Annual Review of Ecology, Evolution, and Systematics, 45(1), 397–419. https://doi.org/10.1146/annurev-ecolsys-120213-091650

Collins, S. L., Knapp, A. K., Briggs, J. M., Blair, J. M., & Steinauer, E. M. (1998) Modulation of diversity by grazing and mowing in native tallgrass prairie. Science, 280(5364), 745-747.

Compo, G.P., J.S. Whitaker, P.D. Sardeshmukh, N. Matsui, R.J. Allan, X. Yin, B.E. Gleason, R.S. Vose, G. Rutledge, P. Bessemoulin, S. Brönnimann, M. Brunet, R.I. Crouthamel, A.N. Grant, P.Y. Groisman, P.D. Jones, M. Kruk, A.C. Kruger, G.J. Marshall, M. Maugeri, H.Y. Mok, Ø. Nordli, T.F. Ross, R.M. Trigo, X.L. Wang, S.D. Woodruff, and S.J. Worley, (2011): The Twentieth Century Reanalysis Project. Quarterly J. Roy. Meteorol. Soc., 137, 1-28. http://dx.doi.org/10.1002/qj.776

Cook, B. I., Ault, T. R., & Smerdon, J. E. (2015) Unprecedented 21st century drought risk in the American Southwest and Central Plains. Science Advances, 1(1), e1400082–e1400082. https://doi.org/10.1126/sciadv.1400082

Cook, B. I., Miller, R. L., & Seager, R. (2008) Dust and sea surface temperature forcing of the 1930s "Dust Bowl" drought. Geophysical Research Letters, 35(8) http://doi.org/10.1029/2008GL033486

Cook, B. I., Miller, R. L., & Seager, R. (2009) Amplification of the North American "Dust Bowl" drought through human-induced land degradation. Proceedings of the National Academy of Sciences, 106(13), 4997–5001. http://doi.org/10.1073/pnas.0810200106

Cook, B. I., Seager, R., & Miller, R. L. (2011) Atmospheric circulation anomalies during two persistent North American droughts: 1932-1939 and 1948-1957. Climate Dynamics, 36, 2339–2355.

Cook, B. I., Seager, R., & Miller, R. L. (2011) The impact of devegetated dune fields on North American climate during the late Medieval Climate Anomaly: DUNES AND MEDIEVAL CLIMATE. Geophysical Research Letters, 38(14), n/a–n/a. http://doi.org/10.1029/2011GL047566

Cook, B. I., Seager, R., & Smerdon, J. E. (2014) The worst North American drought year of the last millennium: 1934. Geophysical Research Letters, 41(20), 7298–7305. https://doi.org/10.1002/2014GL061661

Cook, B. I., Seager, R., Miller, R. L., & Mason, J. A. (2013) Intensification of North American Megadroughts through Surface and Dust Aerosol Forcing*. Journal of Climate, 26(13), 4414–4430. https://doi.org/10.1175/JCLI-D-12-00022.1

Cook, B. I., Smerdon, J. E., Seager, R., & Coats, S. (2014) Global warming and 21st century drying. Climate Dynamics, 43(9-10), 2607–2627. http://doi.org/10.1007/s00382-014-2075-y

Cook, B. I., Smerdon, J. E., Seager, R., & Cook, E. R. (2014) Pan-Continental Droughts in North America over the Last Millennium*. Journal of Climate, 27(1), 383–397. http://doi.org/10.1175/JCLI-D-13-00100.1

Cook, E. R., Seager, R., Cane, M. A., & Stahle, D. W. (2007) North American drought: Reconstructions, causes, and consequences. Earth-Science Reviews, 81(1–2), 93–134. https://doi.org/10.1016/j.earscirev.2006.12.002

Cook, E. R., Seager, R., Heim, R. R., Vose, R. S., Herweijer, C., & Woodhouse, C. (2010) Megadroughts in North America: placing IPCC projections of hydroclimatic change in a long-term palaeoclimate context. Journal of Quaternary Science, 25(1), 48–61. http://doi.org/10.1002/jqs.1303

Cordova C. E., Porter, JC (2015) The 1930s Dust Bowl: Geoarchaeological lessons from a 20th century environmental crisis. The Holocene, 25(10):1707-1720.

Cordova, C. E., Johnson, W. C., Mandel, R. D., & Palmer, M. W. (2011) Late Quaternary environmental change inferred from phytoliths and other soil-related proxies: Case studies from the central and southern Great Plains, USA. CATENA, 85(2), 87–108. http://doi.org/10.1016/j.catena.2010.08.015

Cordova, C. E., Porter, J., Lepper, K., Kalchgruber, R., & Scott, G. (2005) Preliminary assessment of sand dune stability along a bioclimatic gradient, North Central and Northwestern Oklahoma. Great Plains Research: A Journal of Natural and Social Sciences, Paper 783.

Cowan, T., Hegerl, G. C., Colfescu, I., Bollasina, M., Purich, A., & Boschat, G. (2017) Factors Contributing to Record-Breaking Heat Waves over the Great Plains during the 1930s Dust Bowl. Journal of Climate, 30(7), 2437–2461. https://doi.org/10.1175/JCLI-D-16-0436.1

Cowherd C, Donaldson J, Hegarty R, Ono D (2006) Proposed revisions to fine fraction ratios used for AP-42 fugitive dust emission factors, US EPA 15th Annual Emission Inventory Conference, New Orleans, 2006.

Cronin, F. D., Beers, H. W., (1937) Areas of intense drought distress 1930-1936. Washington, D.C.: Works Progress Administration, Division of Social Research, 54 pp.

Crouvi O, Amit R, Enzel Y, Porat N, Sandler A (2008) Sand dunes as a major proximal dust source for late Pleistocene loess in the Negev Desert, Israel. Quaternary Research 70(2): 275-282.

Crouvi, O., Schepanski, K., Amit, R., Gillespie, A. R., Enzel, Y., (2012) Multiple dust sources in the Sahara Desert: The importance of sand dunes. Geophys. Res. Lett.39, L13401.

Cunfer G (2005) On the Great Plains: Agriculture and Environment (No. 20) College Station: Texas A&M University Press.

Cunfer, G. (2002) Causes of the Dust Bowl. In Past Time, Past Place: GIS for History (pp. 95–103) Redlands, CA: ESRI Press.

Cutler DM, Miller G, Norton DM (2007) Evidence on early-life income and late-life health from America's Dust Bowl era. Proceedings of the National Academy of Sciences 104(33): 13244-13249.

Dai, A. (2012) Increasing drought under global warming in observations and models. Nature Climate Change, 3(1), 52–58. http://doi.org/10.1038/nclimate1633

Dai, A. (2013) The influence of the inter-decadal Pacific oscillation on US precipitation during 1923–2010. Climate Dynamics, 41(3-4), 633–646. http://doi.org/10.1007/s00382-012-1446-5

Davidson, DT (1960) Geologic and engineering properties of Pleistocene materials in Iowa (No. 20) Iowa State University of Sciences and Technology.

Dean WE (1997) Rates, timing, and cyclicity of Holocene eolian activity in north–central United States: Evidence from varved lake sediments. Geology 25(4): 331.

Derickson, D., Kocurek, G., Ewing, R. C., & Bristow, C. (2008) Origin of a complex and spatially diverse dune-field pattern, Algodones, southeastern California. Geomorphology, 99(1-4), 186–204. http://doi.org/10.1016/j.geomorph.2007.10.016

Derner JD, Boutton TW, Briske DD (2006) Grazing and ecosystem carbon storage in the North American Great Plains. Plant and Soil 280(1–2): 77–90.

Diaz, H. F., Trigo, R., Hughes, M. K., Mann, M. E., Xoplaki, E., & Barriopedro, D. (2011) Spatial and temporal characteristics of climate in medieval times revisited. Bulletin of the American Meteorological Society, 92(11), 1487-1500.

Dirmeyer, P. A., & Brubaker, K. L. (1999) Contrasting evaporative moisture sources during the drought of 1988 and the flood of 1993. Journal of geophysical research, 104(19), 383-19.

Disterdick, F. L., (1933) Severe sand storm in eastern Wyoming, January 18, 1933. Mon. Weather Rev. 61, 16-17.

Donarummo, J. (2003) Possible deposit of soil dust from the 1930's U.S. dust bowl identified in Greenland ice. Geophysical Research Letters, 30(6) https://doi.org/10.1029/2002GL016641

Donat, M. G., King, A. D., Overpeck, J. T., Alexander, L. V., Durre, I., & Karoly, D. J. (2016) Extraordinary heat during the 1930s US Dust Bowl and associated large-scale conditions. Climate Dynamics, 46(1–2), 413–426. https://doi.org/10.1007/s00382-015-2590-5

Doneus M, Wieser M, Verhoeven G, Karel W, Fera M, Pfeifer N (2016) Automated Archiving of Archaeological Aerial Images. Remote Sensing 8(3): 209.

Duncan, D., Burns, K., (2012) The Dust Bowl: An Illustrated History. Chronicle Books, San Francisco, CA, 232 pp.

Eagar, J. D., Herckes, P., & Hartnett, H. E. (2017) The characterization of haboobs and the deposition of dust in Tempe, AZ from 2005 to 2014. Aeolian Research, 24, 81–91. https://doi.org/10.1016/j.aeolia.2016.11.004

Egan, T., (2006) The Worst Hard Time: The untold story of those who survived the great American dust bowl. Houghton Mifflin Harcourt, New York, 340 pp.

Engelstaedter, S., Tegen, I., & Washington, R. (2006) North African dust emissions and transport. Earth-Science Reviews, 79(1–2), 73–100. https://doi.org/10.1016/j.earscirev.2006.06.004

Escadafal R, Huete AR (1992) Soil optical properties and environmental applications of remote sensing. Technical Commission VII: Interpreation of Photoaphic and Remote Sensing Data (Washington, D.C.), pp 709–715.

Etyemezian, V., Gillies, J. A., Shinoda, M., Nikolich, G., King, J., & Bardis, A. R. (2014) Accounting for surface roughness on measurements conducted with PI-SWERL: Evaluation of a subjective visual approach and a photogrammetric technique. Aeolian Research, 13, 35-50.

Etyemezian, V., Nikolich, G., Ahonen, S., Pitchford, M., Sweeney, M., Purcell, R., .. & Kuhns, H. (2007) The Portable In Situ Wind Erosion Laboratory (PI-SWERL): A new method to measure PM10 windblown dust properties and potential for emissions. Atmospheric Environment, 41(18), 3789-3796.

Evans SE, Byrne KM, Lauenroth WK, Burke IC (2011) Defining the limit to resistance in a drought–tolerant grassland: long–term severe drought significantly reduces the dominant species and increases ruderals. Journal of Ecology 99(6): 1500–1507.

Ewing, R. C., & Kocurek, G. (2010) Aeolian dune-field pattern boundary conditions. Geomorphology, 114(3), 175–187. http://doi.org/10.1016/j.geomorph.2009.06.015

Ewing, R. C., Kocurek, G., & Lake, L. W. (2006) Pattern analysis of dune-field parameters. Earth Surface Processes and Landforms, 31(9), 1176–1191. http://doi.org/10.1002/esp.1312

Feng, S., Hu, Q., & Oglesby, R. J. (2011) Influence of Atlantic sea surface temperatures on persistent drought in North America. Climate Dynamics, 37(3-4), 569–586. http://doi.org/10.1007/s00382-010-0835-x

Feng, S., Oglesby, R. J., Rowe, C. M., Loope, D. B., & Hu, Q. (2008) Atlantic and Pacific SST influences on Medieval drought in North America simulated by the Community Atmospheric Model. Journal of Geophysical Research, 113(D11) http://doi.org/10.1029/2007JD009347

Ferguson, I. M., & Maxwell, R. M. (2010) GROUNDWATER—LAND SURFACE—ATMOSPHERE FEEDBACKS: IMPACTS OF GROUNDWATER PUMPING AND IRRIGATION ON LAND-ATMOSPHERE INTERACTIONS. W00F02, DOI, 10.

Field, J. P., Breshears, D. D., & Whicker, J. J. (2009) Toward a more holistic perspective of soil erosion: Why aeolian research needs to explicitly consider fluvial processes and interactions. Aeolian Research, 1(1-2), 9–17. http://doi.org/10.1016/j.aeolia.2009.04.002

Flagg, C. B., Neff, J. C., Reynolds, R. L., & Belnap, J. (2014) Spatial and temporal patterns of dust emissions (2004–2012) in semi-arid landscapes, southeastern Utah, USA. Aeolian Research, 15, 31–43. https://doi.org/10.1016/j.aeolia.2013.10.002

Forman SL, Tripaldi, A Ciccioli, PL (2014) Sand sheet deposition in the San Luis paleodune field, western Argentina as an indicator of a semi-arid environment through the Holocene. Paleogeography, Paleoclimatology, Paleoecology 411: 122-135.

Forman, S. L. (2015) Episodic eolian sand deposition in the past 4000 years in Cape Cod National Seashore, Massachusetts, USA in response to possible hurricane/storm and anthropogenic disturbances. Frontiers in Earth Science, 3, 3.

Forman, S. L., Marín, L., Gomez, J., & Pierson, J. (2008) Late Quaternary eolian sand depositional record for southwestern Kansas: Landscape sensitivity to droughts. Palaeogeography, Palaeoclimatology, Palaeoecology, 265(1-2), 107–120. http://doi.org/10.1016/j.palaeo.2008.04.028

Forman, S. L., Marín, L., Pierson, J., Gómez, J., Miller, G. H., & Webb, R. S. (2005) Aeolian sand depositional records from western Nebraska: landscape response to droughts in the past 1500 years. The Holocene, 15(7), 973–981. http://doi.org/10.1191/0959683605hl871ra

Forman, S. L., Oglesby, R., & Webb, R. S. (2001) Temporal and spatial patterns of Holocene dune activity on the Great Plains of North America: megadroughts and climate links. Global and Planetary Change, 29, 1–29.

Fye, F. K., Stahle, D. W., Cook, E. R., & Cleaveland, M. K. (2006) NAO influence on sub-decadal moisture variability over central North America. Geophysical Research Letters, 33(15) http://doi.org/10.1029/2006GL026656

Geiger, R., (1935) Oklahoma Battles Another Severe Dust Storm, The Evening Star. W.D. Wallach & Hope, Washington, D.C., June 15, 1935, p. A-2.

Gennaretti F, Ripa MN, Gobattoni F, Boccia L, Pelorosso R (2011) A methodology proposal for land cover change analysis using historical aerial photos. Journal of Geography and Regional Planning 4(9): 542–556.

Gherardi, L. A., Sala, O. E., (2015) Enhanced precipitation variability decreases grass- and increases shrub-productivity. Proc. Natl. Acad. Sci. U.S.A. 112, 12735-12740.

Gillette, D. A., Adams, J., Endo, A., Smith, D., & Kihl, R. (1980) Threshold velocities for input of soil particles into the air by desert soils. Journal of Geophysical Research: Oceans, 85(C10), 5621-5630.

Gillette, D. A., Adams, J., Muhs, D., & Kihl, R. (1982) Threshold friction velocities and rupture moduli for crusted desert soils for the input of soil particles into the air. Journal of Geophysical Research: Oceans, 87(C11), 9003-9015.

Gillette, DA, (1988) Threshold friction velocities for dust production for agricultural soils. J Geophysical Research Atmospheres 93, D10, 12645-12662.

Ginoux, P., Prospero, J. M., Gill, T. E., Hsu, N. C., & Zhao, M. (2012) Global-scale attribution of anthropogenic and natural dust sources and their emission rates based on MODIS Deep Blue aerosol products. Reviews of Geophysics, 50(3) http://doi.org/10.1029/2012RG000388

Giordano S, Le Bris A, Mallet C (2017) Fully automatic analysis of archival aerial images current status and challenges. Urban Remote Sensing Event (JURSE), 2017 Joint (IEEE): 1–4.

Gkikas A., Hatzianastassiou N., Mihalopoulos N., Katsoulis V., Kazadzis S., Pey J., (2013) The regime of desert dust episodes in the Mediterranean based on contemporary satellite observations and ground measurements. Atmos. Chem. Phys. 13, 12135–12154.

Goble, R.J., Mason, J.A., Loope, D.B., and Swinehart, J.B. 2004. Optical and radiocarbon ages of stacked paleosols and dune sands in the Nebraska Sand Hills, USA, Quaternary Science Reviews, 23: 1173–1182.

Gomez C (2012) Historical 3D topographic reconstruction of the Iwaki volcano using structure from motion from uncalibrated aerial photographs. https: //hal.archives-ouvertes.fr/hal-00765723

Gonçalves JA (2016) Automatic orientation and mosaicking of archived aerial photography using structure from motion. ISPRS – International Archives of the Photogrammetry, Remote Sensing and Spatial Information Sciences XL–3/W4: 123–126.

Goossens, D., & Buck, B. (2009) Dust emission by off-road driving: Experiments on 17 arid soil types, Nevada, USA. Geomorphology, 107(3-4), 118-138.

Goossens, D., & Buck, B. (2011a) Gross erosion, net erosion and gross deposition of dust by wind: field data from 17 desert surfaces. Earth Surface Processes and Landforms, 36(5), 610–623. https://doi.org/10.1002/esp.2080

Goossens, D., & Buck, B. (2011b) Emission and deposition of dust by wind in the Nellis Dunes Recreation Area.

Gosselin DC, Sridhar V, Harvey FE, Goeke JW (2006) Hydrological effects and groundwater fluctuations in interdunal environments in the Nebraska Sand Hills. Great Plains Research 16(1): 12.

Goudie, A. S., (1983) Dust Storms in Space and Time. Progress in Physical Geography 7, 502-530.

Goudie, A. S., (1994) Deserts in a Warmer World. Environmental Change in Drylands: Biogeographical and Geomorphological Perspectives, 1-24.

Goudie, A. S., (2009) Dust storms: Recent developments. J. Environ. Manage. 90, 89-94.

Goudie, A. S., (2014) Desert dust and human health disorders. Env. Internat. 63, 101-113.

Goudie, A. S., Middleton, N. J., (1992) The Changing Frequency of Dust Storms through Time. Clim. Change 20, 197-225.

Goudie, A.S., (2001) The global distribution of dust storms: Patterns and controls. Annals of arid zone 40, 303-315.

Granados JAT, Roux AVD (2009) Life and death during the Great Depression. Proceedings of the National Academy of Sciences,106(41): 17290-17295.

Gregory, JN (2004) The Dust Bowl Migration. Poverty in the United States: An Encyclopedia of History, Politics and Policy. ABC-Clio, Santa Barbara.

Griffin DW (2007) Atmospheric movement of microorganisms in clouds of desert dust and implications for human health. Clinical Microbiology Reviews 20: 459-477.

Gutmann MP (2005) Great Plains Population and Environment Data: Agricultural Data, 1870-1997 [United States]. ICPSR04254-v1. Ann Arbor, MI: Inter-university Consortium for Political and Social Research [distributor], http://doi.org/10.3886/ICPSR04254.v13.

Hahnenberger, M., & Nicoll, K. (2012) Meteorological characteristics of dust storm events in the eastern Great Basin of Utah, U.S.A. Atmospheric Environment, 60, 601–612. https://doi.org/10.1016/j.atmosenv.2012.06.029

Halfen, A. F., & Johnson, W. C. (2013) A review of Great Plains dune field chronologies. Aeolian Research, 10, 135–160. http://doi.org/10.1016/j.aeolia.2013.03.001

Hambidge G (1938) Soils and Men, A Summary. In In G Hambidge (Ed.), Soils and Men: Yearbook of Agriculture (pp. 321-328) Washington, DC: US Department of Agriculture.

Hand, I. F., (1934) The character and magnitude of the dense dust-cloud which passed over Washington, DC, May 11, (1934) Mon. Weather Rev. 62, 156.

Handy, R. L., Lyon, C. A., Davidson, D. T., (1960) Analysis of wind-blown silt, In: Davidson, D.T. (Ed.), in Geologic and Engineering Properties of Pleistocene Materials, Iowa State University Joint Publication Bulletin No. 191, Iowa State University, Iowa City, Iowa, pp. 1-13.

Hansen, Z. K., & Libecap, G. D. (2004) Small farms, externalities, and the Dust Bowl of the 1930s. Journal of Political Economy, 112(5), 665–694.

Hanson, P. R., Arbogast, A. F., Johnson, W. C., Joeckel, R. M., & Young, A. R. (2010) Megadroughts and late Holocene dune activation at the eastern margin of the Great Plains, north-central Kansas, USA. Aeolian Research, 1(3-4), 101–110. http://doi.org/10.1016/j.aeolia.2009.10.002

Hanson, P. R., Joeckel, R. M., Young, A. R., & Horn, J. (2009) Late Holocene dune activity in the Eastern Platte River Valley, Nebraska. Geomorphology, 103(4), 555-561.

Haralick RM, Shanmugam K, Dinstein IH (1973) Textural features for image classification. IEEE Transactions on systems, man, and cybernetics, 3(6), 610–621.

Harvey FE, Swinehart JB, Kurtz TM (2007) Ground Water Sustenance of Nebraska's Unique Sand Hills Peatland Fen Ecosystems. Ground Water 45(2): 218–234.

He Y (2014) The effect of precipitation on vegetation cover over three landscape units in a protected semi–arid grassland: Temporal dynamics and suitable climatic index. Journal of Arid Environments 109: 74–82.

Hegerl, G. C., Brönnimann, S., Schurer, A., & Cowan, T. (2018) The early 20th century warming: Anomalies, causes, and consequences. Wiley Interdisciplinary Reviews: Climate Change, 9(4), e522.

Heil Jr., C. W., King, J. W., Zárate, M. A., & Schultz, P. H. (2010) Climatic interpretation of a 1.9 Ma environmental magnetic record of loess deposition and soil formation in the central eastern Pampas of Buenos Aires, Argentina. Quaternary Science Reviews, 29(19-20), 2705–2718. http://doi.org/10.1016/j.quascirev.2010.06.024

Heipke C (1997) Automation of interior, relative, and absolute orientation. ISPRS journal of photogrammetry and remote sensing 52(1): 1–19.

Higgins, R. W., Yao, Y., & Wang, X. L. (1997) Influence of the North American monsoon system on the US summer precipitation regime. Journal of Climate, 10(10), 2600–2622.

Hodell, D. A., Brenner, M., & Curtis, J. H. (2007) Climate and cultural history of the northeastern Yucatan Peninsula, Quintana Roo, Mexico. Climatic Change, 83(1), 215-240.

Holliday, V. T. (2001) Stratigraphy and geochronology of upper Quaternary eolian sand on the Southern High Plains of Texas and New Mexico, United States. Geological Society of America Bulletin, 113(1), 88–108.

Holmén BA, James TA, Ashbaugh LL, et al. (2001) Lidar-assisted measurement of PM 10 emissions from agricultural tilling in California's San Joaquin Valley–Part II: emission factors. Atmospheric Environment 35(19): 3265–3277.

Hong, S.-Y., & Kalnay, E. (2000) Role of sea surface temperature and soil-moisture feedback in the 1998 Oklahoma–Texas drought. Nature, 408(6814), 842–844.

Hong, S.-Y., & Kalnay, E. (2002) The 1998 Oklahoma-Texas drought: Mechanistic experiments with NCEP global and regional models. Journal of Climate, 15(9), 945–963.

Hornbeck, R. (2012) The Enduring Impact of the American Dust Bowl: Short- and Long-Run Adjustments to Environmental Catastrophe. American Economic Review, 102(4), 1477–1507. https://doi.org/10.1257/aer.102.4.1477

Houser, C., Bishop, M. P., & Barrineau, P. (2015) Characterizing instability of aeolian environments using analytical reasoning: ANALYTICAL REASONING OF AEOLIAN INSTABILITY. Earth Surface Processes and Landforms, 40(5), 696–705. http://doi.org/10.1002/esp.3679

Hovde, M. R., (1934) The Great Dust storm of November 12, 1933. Mon. Weather Rev. 62, 12-13.

Hu, Q., Torres-Alavez, J. A., & Van Den Broeke, M. S. (2018) Land-Cover Change and the "Dust Bowl" Drought in the US Great Plains. Journal of Climate, 31(12), 4657-4667.

Hugenholtz CH, Levin N, Barchyn TE, Baddock MC (2012) Remote sensing and spatial analysis of aeolian sand dunes: A review and outlook. Earth-Science Reviews 111(3-4): 319–334.

Hugenholtz CH, Wolfe SA (2006) Morphodynamics and climate controls of two aeolian blowouts on the northern Great Plains, Canada. Earth Surface Processes and Landforms 31(12): 1540–1557.

Hugenholtz, C. H., & Barchyn, T. E. (2010) Spatial analysis of sand dunes with a new global topographic dataset: new approaches and opportunities. Earth Surface Processes and Landforms, 35(8), 986–992. http://doi.org/10.1002/esp.2013

Hugenholtz, C. H., & Wolfe, S. A. (2005) Biogeomorphic model of dunefield activation and stabilization on the northern Great Plains. Geomorphology, 70(1-2), 53–70. http://doi.org/10.1016/j.geomorph.2005.03.011

Hugenholtz, C. H., Wolfe, S. A., Walker, I. J., & Moorman, B. J. (2009) Spatial and temporal patterns of aeolian sediment transport on an inland parabolic dune, Bigstick Sand Hills, Saskatchewan, Canada. Geomorphology, 105(1), 158-170.

Hunt GR, Salisbury JW (1970) Visible and near infrared spectra of minerals and rocks: I: Silicate minerals. Modern Geology 1: 283–300.

Hurrell, J. W. (1995) Decadal trends in the North Atlantic Oscillation: Regional temperatures and precipitation. Science, 269(5224), 676–679.

Hurt, R. D., (1981) The Dust Bowl: An Agricultural and Social History. Taylor Trade Publications, Chicago, 214 pp.

Hurtt, G. C., Frolking, S., Fearon, M. G., Moore, B., Shevliakova, E., Malyshev, S., ... & Houghton, R. A. (2006) The underpinnings of land-use history: Three centuries of global gridded land-use transitions, wood-harvest activity, and resulting secondary lands. Global Change Biology, 12(7), 1208-1229.

Idso, S. B., Ingram, R. S. and Pritchard, J. M. (1972) ‘An American Haboob’ B. Am. Meteorol. Soc. 53, 930-955.

Jickells, T. D. (2005) Global Iron Connections Between Desert Dust, Ocean Biogeochemistry, and Climate. Science, 308(5718), 67–71. http://doi.org/10.1126/science.1105959

Joel, A. H. (1937) Soil conservation reconnaissance survey of the Souther Great Plains wind-erosion area (Technical Bulletin No. 556) Washington, D.C.: U.S. Department of Agriculture.

Johnson, V., (1947) Heaven's Tableland, Da Capo Press, New York, 288 pp.

Jones SK, Collins SL, Blair JM, Smith MD, Knapp AK (2016) Altered rainfall patterns increase forb abundance and richness in native tallgrass prairie. Scientific Reports 6.

Jurena PN, Archer S (2003) Woody plant establishment and spatial heterogeneity in grasslands. Ecology 84(4): 907–919.

Kadmon R, Harari–Kremer R (1999) Studying long–term vegetation dynamics using digital processing of historical aerial photographs. Remote Sensing of Environment 68: 164–176.

Kim SW, Yoon SC, Kim J, Kang JY, Sugimoto N. (2010) Asian dust event observed in Seoul, Korea, during 29–31 May 2008: analysis of transport and vertical distribution of dust particles from lidar and surface measurements. Science of the Total Environment 408(7):1707-1718.

King, J., Etyemezian, V., Sweeney, M., Buck, B. J., & Nikolich, G. (2011) Dust emission variability at the Salton Sea, California, USA. Aeolian Research, 3(1), 67–79. https://doi.org/10.1016/j.aeolia.2011.03.005

Knippertz, P. (2014) Meteorological aspects of dust storms. In Mineral Dust (pp. 121-147) Springer, Dordrecht.

Koerner SE, Collins SL (2014) Interactive effects of grazing, drought, and fire on grassland plant communities in North America and South Africa. Ecology 95(1): 98–109.

Konare A, Zakey AS, Solmon F, et al. (2008) A regional climate modeling study of the effect of desert dust on the West African monsoon. Journal of Geophysical Research 113(D12) Available from: http://doi.wiley.com/10.1029/2007JD009322 (accessed 2 March 2016)

Konings AG, Williams AP, Gentine P (2017) Sensitivity of grassland productivity to aridity controlled by stomatal and xylem regulation. Nature Geoscience 10: 284–288.

Koster, R. D., Dirmeyer, P. A., Guo, Z., Bonan, G., Chan, E., Cox, P., ... & Yamada, T. (2004) Regions of strong coupling between soil moisture and precipitation. Science, 305(5687), 1138-1140.

Krishnamurthy, L., Vecchi, G. A., Msadek, R., Wittenberg, A., Delworth, T. L., & Zeng, F. (2015) The Seasonality of the Great Plains Low-Level Jet and ENSO Relationship. Journal of Climate, 28(11), 4525–4544. http://doi.org/10.1175/JCLI-D-14-00590.1

Kumjian, M., Evans, J., & Guyer, J. (2006) The relationship of the Great Plains low level jet to nocturnal MCS development. In Preprints, 23rd Conf. on Severe Local Storms, St. Louis, MO, Amer. Meteor. Soc. P (Vol. 1)

Kunkel, K., Stevens, L., Stevens, S., & Sun, L. (2013) Part 4. Climate of the US Great Plains (NOAA Technical Report No. NESDIS 142-4)

Kuriyama Y, Mochizuki N, Nakashima T (2005) Influence of vegetation on aeolian sand transport rate from a backshore to a foredune at Hasaki, Japan. Sedimentology 52(5):1123-1132.

Kuss, A. J. M., & Gurdak, J. J. (2014) Groundwater level response in U.S. principal aquifers to ENSO, NAO, PDO, and AMO. Journal of Hydrology, 519, 1939–1952. http://doi.org/10.1016/j.jhydrol.2014.09.069

Laird KR, Fritz SC, Cumming BF (1998) A diatom–based reconstruction of drought intensity duration and frequency from Moon Lake North Dakota: a sub–decadal record of the last 2300 years. Journal of Paleolimnology 19(2): 161–179.

Laliberte AS, Rango A, Havstad KM, Paris JF, Beck RF, McNeely R, et al. (2004) Object–oriented image analysis for mapping shrub encroachment from 1937 to 2003 in southern New Mexico. Remote Sensing of Environment 93(1–2): 198–210.

Lancaster, N. (1985) Variations in wind velocity and sand transport on the windward flanks of desert sand dunes. Sedimentology, 32(4), 581-593.

Lancaster, N. (2004) Relations between aerodynamic and surface roughness in a hyper-arid cold desert: McMurdo Dry Valleys, Antarctica. Earth Surface Processes and Landforms: The Journal of the British Geomorphological Research Group, 29(7), 853-867.

Lange, D., (1981) Dorothea Lange: Farm Security Administration Photographs, 1935-1939 (Dorothea Lange), Volume II. Tech-Fiche Press, 236 pp.

Langham, W. H., Foster, R. L., Daniel, H. A., (1938) The amount of dust in the air at plant height during wind storms at Goodwell, Oklahoma in 1936-1937. J. Am. Soc. Agron. 30, 139-144.

Lee, J. A., & Gill, T. E. (2015) Multiple causes of wind erosion in the Dust Bowl. Aeolian Research, 19, 15–36. http://doi.org/10.1016/j.aeolia.2015.09.002

Lee, J. A., & Tchakerian, V. P. (1995) Magnitude and frequency of blowing dust on the Southern High Plains of the United States, 1947-1989. Annals of the Association of American Geographers, 85(4), 684–693.

Lee, J. A., Baddock, M. C., Mbuh, M. J., & Gill, T. E. (2012) Geomorphic and land cover characteristics of aeolian dust sources in West Texas and eastern New Mexico, USA. Aeolian Research, 3(4), 459–466.

Lee, J. A., Gill, T. E., Mulligan, K. R., Dominguez Acosta, M., & Perez, A. E. (2009) Land use/land cover and point sources of the 15 December 2003 dust storm in southwestern North America. Geomorphology, 105(1–2), 18–27. https://doi.org/10.1016/j.geomorph.2007.12.016

Leedy DL (1948) Aerial Photographs, Their Interpretation and Suggested Uses in Wildlife Management. The Journal of Wildlife Management 12(2): 191.

Lei T, Pang Z, Wang X, Li L, Fu J, Kan G, et al. (2016) Drought and Carbon Cycling of Grassland Ecosystems under Global Change: A Review. Water 8(10)

Lei, H., & Wang, J. X. L. (2014) Observed characteristics of dust storm events over the western United States using meteorological, satellite, and air quality measurements. Atmospheric Chemistry and Physics, 14(15), 7847–7857. https://doi.org/10.5194/acp-14-7847-2014

Lepper, K., & Scott, G. F. (2005) Late Holocene aeolian activity in the Cimarron River valley of west–central Oklahoma. Geomorphology, 70(1-2), 42–52. http://doi.org/10.1016/j.geomorph.2005.03.010

Li H, Reynolds J F (1995) On definition and quantification of heterogeneity. Oikos 73(2): 280–284.

Lindquist, A. K., Feinberg, J. M., & Waters, M. R. (2011) Rock magnetic properties of a soil developed on an alluvial deposit at Buttermilk Creek, Texas, USA: MAGNETISM OF AN ALLUVIAL SOIL. Geochemistry, Geophysics, Geosystems, 12(12), n/a–n/a. http://doi.org/10.1029/2011GC003848

Lishawa SC, Treering DJ, Vail LM, McKenna O, Grimm EC, Tuchman, NC (2013) Reconstructing plant invasions using historical aerial imagery and pollen core analysis: Typha in the Laurentian Great Lakes. Diversity and Distributions 19(1): 14–28.

Liu B., Coulthard T. J. (2017) Modelling the interaction of aeolian and fluvial processes with a combined cellular model of sand dunes and river systems. Computers & Geosciences 106: 1–9.

Liu JG, Mason PJ (2016) “Image processing and GIS for remote sensing: Techniques and applications.” John Wiley & Sons.

Liu, B., & Coulthard, T. J. (2015) Mapping the interactions between rivers and sand dunes: Implications for fluvial and aeolian geomorphology. Geomorphology, 231, 246–257. http://doi.org/10.1016/j.geomorph.2014.12.011

Lockeretz, W., (1978) Lessons of the Dust Bowl. Am. Sci. 66, 560-569.

Lookingbill, B. D., (2001)Dust Bowl, USA: Depression America and the ecological imagination, 1929-1941. Ohio University Press, Athens, OH, 190 pp.

Maddox, R. A. (1983) Large-scale meteorological conditions associated with midlatitude, mesoscale convective complexes. Monthly Weather Review, 111(7), 1475-1493.

Madsen, A. T., & Murray, A. S. (2009) Optically stimulated luminescence dating of young sediments: a review. Geomorphology, 109(1), 3-16.

Maestre FT, Cortina J, Bautista S, Bellot J, Vallejo R (2003) Small–scale Environmental Heterogeneity and Spatiotemporal Dynamics of Seedling Establishment in a Semiarid Degraded Ecosystem. Ecosystems 6(7): 630–643.

Mahowald, N., Albani, S., Kok, J. F., Engelstaeder, S., Scanza, R., Ward, D. S., Flanner, M. G., (2014) The size distribution of desert dust aerosols and its impact on the Earth system. Aeol. Research 15, 53-71.

Mallone, S., Stafoggia, M., Faustini, A., Gobbi, G. P., Marconi, A., & Forastiere, F. (2011) Saharan Dust and Associations between Particulate Matter and Daily Mortality in Rome, Italy. Environmental Health Perspectives, 119(10), 1409–1414. https://doi.org/10.1289/ehp.1003026

Mangan JM, Overpeck JT, Webb RS, Wessman C, Goetz AF (2004) Response of Nebraska Sand Hills natural vegetation to drought, fire, grazing, and plant functional type shifts as simulated by the century model. Climatic Change 63(1-2): 49-90.

Mantua, N., & Hare, S. (2002) The Pacific Decadal Oscillation. Journal of Oceanography, 58, 35–44.

Marticorena B, et al. (2010) Temporal variability of mineral dust concentrations over West Africa: analyses of a pluriannual monitoring from the AMMA Sahelian Dust Transect. Atmospheric Chemistry and Physics 10(18): 8899–8915.

Martin, R. J. (1939) Duststorms of 1938 in the United States. Monthly Weather Review 67(1): 12-15.

Martin, R. J., (1936a) Dust Storms in the United States, April 1936. Mon. Weather Rev. 64, 137.

Martin, R. J., (1936b) Dust Storms of May 1936 in the United States. Mon. Weather Rev. 64, 176.

Martin, R. J., (1936c) Dust Storms of July 1936 in the United States. Mon. Weather Rev. 64, 239.

Martin, R. J., (1938) Dust Storms of May-December 1937 in the United States. Mon. Weather Rev. 66, 9.

Mason, J. A., Swinehart, J. B., Goble, R. J., & Loope, D. B. (2004) Late-Holocene dune activity linked to hydrological drought, Nebraska Sand Hills, USA. The Holocene, 14(2), 209–217. http://doi.org/10.1191/0959683604hl677rp

Mather PM, Koch M (2011) “Computer processing of remotely–sensed images: an introduction.” Wiley–Blackwell, Chichester, West Sussex, UK; Hoboken, NJ. 4th ed.

Mattice, W. A., 1935a. Dust Storms, November 1933 to May 1934. Mon. Weather Rev. 63, 53-55.

Mattice, W. A., 1935b. Dust Storms. Mon Weather Rev, 63, 113-115.

Meng, L., & Quiring, S. M. (2010) Observational relationship of sea surface temperatures and precedent soil moisture with summer precipitation in the US Great Plains. International Journal of Climatology, 30(6), 884-893.

Menne, M.J., I. Durre, R.S. Vose, B.E. Gleason, and T.G. Houston, (2012): An overview of the Global Historical Climatology Network-Daily Database. Journal of Atmospheric and Oceanic Technology, 29, 897-910, doi.10.1175/JTECH-D-11-00103.1

Mertes JR, Gulley JD, Benn DI, Thompson SS, Nicholson LI (2017) Using structure–from–motion to create glacier DEMs and orthoimagery from historical terrestrial and oblique aerial imagery: SfM on Differing Historical Glacier Imagery Sets. Earth Surface Processes and Landforms. doi: 10.1002/esp.4188.

Meyers, T. P. (2001) A comparison of summertime water and CO 2 fluxes over rangeland for well watered and drought conditions. Agricultural and Forest Meteorology, 106(3), 205–214.

Miao XD, Mason JA, Johnson WC, Wang H (2007) High-resolution proxy record of Holocene climate from a loess section in Southwestern Nebraska, USA. Palaeogeography Palaeoclimatology Palaeoecology 245(3-4): 368-381.

Miao, X., Mason, J. A., Swinehart, J. B., Loope, D. B., Hanson, P. R., Goble, R. J., & Liu, X. (2007) A 10,000 year record of dune activity, dust storms, and severe drought in the central Great Plains. Geology, 35(2), 119–122.

Miller, E. R., (1934) The dustfall of November 12-13, 1933. Mon. Weather Rev. 62, 14-15.

Mo, K. C. (2003) Influence of sea surface temperature anomalies in the Gulf of California on North American monsoon rainfall. Journal of Geophysical Research, 108(D3) http://doi.org/10.1029/2002JD002403

Mo, K. C., Paegle, J. N., Higgins, R. W., (1997) Atmospheric processes associated with summer floods and droughts in the central United States. J. Climate 10, 3028-3046.

Mölg N, Bolch T (2017) Structure–from–Motion Using Historical Aerial Images to Analyse Changes in Glacier Surface Elevation. Remote Sensing 9(10): 1021.

Moran, M. S., Ponce-campos, G. E., Huete, A. R., & McClaran, M. P. (2014) Functional response of U.S. grasslands to the early 21st-century drought. Ecology, 95(8), 2121–2133.

Morgan JL, Gergel SE (2010) Quantifying historic landscape heterogeneity from aerial photographs using object–based analysis. Landscape Ecology 25(7): 985–998.

Morgan JL, Gergel SE (2013) Automated analysis of aerial photographs and potential for historic forest mapping. Canadian Journal of Forest Research 43(8): 699–710.

Morgan JL, Gergel SE, Coops NC (2010) Aerial Photography: A Rapidly Evolving Tool for Ecological Management. BioScience 60(1): 47–59.

Morman, S. A., & Plumlee, G. S. (2013) The role of airborne mineral dusts in human disease. Aeolian Research, 9, 203–212. https://doi.org/10.1016/j.aeolia.2012.12.001

Muhs DR, Holliday VT (1995) Evidence of active dune sand on the Great Plains in the 19th century from accounts of early explorers. Quaternary Research 43: 198–208.

Muhs, D. R., & Holliday, V. T. (2001) Origin of late Quaternary dune fields on the Southern High Plains of TX and NM. Geological Society of America Bulletin, 113(1), 75–87.

Murray DB, White JD, Swint P (2013) Woody Vegetation Persistence and Disturbance in Central Texas Grasslands Inferred From Multidecadal Historical Aerial Photographs. Rangeland Ecology & Management 66(3): 297–304.

Nace RL, Pluhowski EJ (1965) Drought of the 1950's with special reference to the Mid-continent: Water Supply Paper 1804. US Government Printing Office [http://pubs.er.usgs.gov/publication/wsp1804ER]

Nagarajan S, Schenk T (2016) Feature–based registration of historical aerial images by Area Minimization. ISPRS Journal of Photogrammetry and Remote Sensing 116: 15–23.

Namias, J., (1982) Anatomy of Great Plains protracted heat waves especially in the 1980 U.S. summer drought. Mon. Weather Rev. 110, 824-838.

Namias, J., (1990) Spring and summer 1988 drought over the contiguous United States-causes and prediction. J. Climate 4, 54-65.

Nandintsetseg, B., & Shinoda, M. (2015) Land surface memory effects on dust emission in a Mongolian temperate grassland: Land surface memory effects on dust. Journal of Geophysical Research: Biogeosciences, 120(3), 414–427. https://doi.org/10.1002/2014JG002708

National Ambient Air Quality Standards (NAAQS) http://www3.epa.gov/ttn/naaqs/criteria.html [Accessed February 9, 2016]

National Archives and Record Administration [NARA] (2017, June 26) "Aerial Photographs" in Cartographic and Architectural Records General Information Leaflet, Number 26. https: //www.archives.gov/publications/general–info–leaflets/26–cartographic.html#aerial1

National Archives and Records Administration [NARA], Records of the Natural Resources Conservation Service, Record Group 114.

Natsagdorj, L., Jugder, D., & Chung, Y. S. (2003) Analysis of dust storms observed in Mongolia during 1937–1999. Atmospheric Environment, 37(9-10), 1401-1411.

Nebiker S, Lack N, Deuber M (2014) Building Change Detection from Historical Aerial Photographs Using Dense Image Matching and Object–Based Image Analysis. Remote Sensing 6(9): 8310–8336.

Nicoll, K. A., Harrison, R. G., Ulanowski, Z., (2011) Observations of Saharan dust layer electrification. Environ. Res. Lett. 6, 014001.

Nield, J. M., & Baas, A. C. (2008) The influence of different environmental and climatic conditions on vegetated aeolian dune landscape development and response. Global and Planetary Change, 64(1), 76-92.

Nielsen DC (2018) Influence of Latitude on the US Great Plains East–West Precipitation Gradient. ael 3(1): 0.

Nielsen-Gammon, J. W. (2011) The Changing Climate of Texas. In The Impact of Global Warming on Texas (Second) Texas Climate Initiative.

Nigam, S., Guan, B., & Ruiz-Barradas, A. (2011) Key role of the Atlantic Multidecadal Oscillation in 20th century drought and wet periods over the Great Plains. Geophysical Research Letters, 38(16)

Ninth victim of dust pneumonia dies in Kansas (1935, April 30), Chicago Tribune. Retrieved from: https: //chicagotribune.newspapers.com/

Novlan, D. J., Hardiman, M., Gill, T. E., (2007) A synoptic climatology of blowing dust events in El Paso, Texas from 1932-2005. in 87th AMS Annual Meeting, San Antonio, TX, January,14-18, J3.12.

O'Brien MJ, Beets JL, Warren RE, Hotrabhavananda T, Barney TW, Voigt EE (1982) Digital enhancement and grey–level slicing of aerial photographs: Techniques for archaeological analysis of intrasite variability. World Archaeology 14(2): 173–190.

Oglesby, R., Feng, S., Hu, Q., & Rowe, C. (2012) The role of the Atlantic Multidecadal Oscillation on medieval drought in North America: Synthesizing results from proxy data and climate models. Global and Planetary Change, 84-85, 56–65. http://doi.org/10.1016/j.gloplacha.2011.07.005

Ohm, K. B., (1980) Dorthea Lang and the Documentary Tradition. Louisiana State University Press, Baton Rouge, LA, 277 pp.

Oke, T.R., (1978) Boundary Layer Climates. Methuen & Co Ltd, London, 372 p.

Okeke F, Karnieli A (2006) Methods for fuzzy classification and accuracy assessment of historical aerial photographs for vegetation change analyses. Part I: Algorithm development. International Journal of Remote Sensing 27(1): 153–176.

Ono DM, Weaver S, Richmond K (2003) Quantifying particulate matter emissions from wind blown dust using real-time sand flux measurements, 12th International Emission Inventory Conference, San Diego, 2003. EPA Clearinghouse for Inventories & Emissions Factors.

Orgill, M. M., Sehmel, G. A., (1976) Frequency and Diurnal-Variation of Dust Storms in Contiguous USA. Atmos. Environ. 10, 813-825.

Pacina J, Popelka J (2017) Accuracy of Digital Surface Models derived from archival aerial photographs. Case study for the Czech Republic. Geoinformatics FCE CTU 16(1): 53.

Packer, G., (2011) Photographs of Arthur Rothstein: The Library of Congress. D. Giles Ltd, UK, 154 pp.

Pantillon, F., Knippertz, P., Marsham, J. H., & Birch, C. E. (2015) A parameterization of convective dust storms for models with mass-flux convection schemes. Journal of the Atmospheric Sciences, 72(6), 2545-2561.

Parajuli SP, Zender CS (2017) Connecting geomorphology to dust emission through high–resolution mapping of global land cover and sediment supply. Aeolian Research 27: 47–65.

Parajuli, S. P., Yang, Z.-L., & Kocurek, G. (2014) Mapping erodibility in dust source regions based on geomorphology, meteorology, and remote sensing: Land cover and erodibility mapping. Journal of Geophysical Research: Earth Surface, 119(9), 1977–1994. https://doi.org/10.1002/2014JF003095

Park SK, Auchincloss AH, O'Neill MS, et al. (2010) Particulate Air Pollution, Metabolic Syndrome, and Heart Rate Variability: The Multi-Ethnic Study of Atherosclerosis (MESA) Environmental Health Perspectives 118(10): 1406–1411.

Parton WJ, Gutmann MP, Ojima D (2007) Long–term Trends in Population, Farm Income, and Crop Production in the Great Plains. BioScience 57(9): 737–747.

Patterson, E. M., Gillette, D. A., (1976) Measurements of Visible and Infrared Imagery Index of Refraction and of Size Distribution for Saharan Dust Aerosols over Atlantic. B. Am. Meteorol. Soc. 57, 146-146.

Penfold BM, Sullivan DC, Reid SB, Chinkin LR (2005) Development of Agricultural Dust Emissions Inventories for the Central States Regional Air Planning Association [Accessed January 13, 2016].

Peters, D. P. C., Havstad, K. M., Archer, S. R., Sala, O. E., (2015) Beyond desertification: new paradigms for dryland landscapes. Front. Ecol. Environ.13, 4-12.

Peters, D. P. C., Osvaldo, E. S., Allen, C. D., Covich, A., & Brunson, M. (2007) Cascading events in linked ecological and socioeconomic systems. Frontiers in Ecology and the Environment, 5(4), 221–224.

Peters, D. P., Pielke, R. A., Bestelmeyer, B. T., Allen, C. D., Munson-McGee, S., & Havstad, K. M. (2004) Cross-scale interactions, nonlinearities, and forecasting catastrophic events. Proceedings of the National Academy of Sciences of the United States of America, 101(42), 15130–15135.

Petrie MD, Brunsell NA, Vargas R, Collins SL, Glanagan LB, Hanan NP, et al. (2016) The sensitivity of carbon exchanges in Great Plains grasslands to precipitation variability. Journal of Geophysical Research: Biogeosciences 121(2)

Pewe, T. L., (1981) Desert Dust: An overview, In: Pewe, T.L. (Ed.), Desert Dust: Origin, characteristics and effect on man. Special Paper 186, The Geological Society of America, Boulder, CO, pp. 1-10.

Pickett ST., Cadenasso M. (1995) Landscpae Ecology: Spatial Heterogeneity in Ecological Systems. Science 269(5222): 331–334.

Porter, J., (2012) Lessons from the Dust Bowl: Human-Environment Education on the Great Plains. J. Geog. 111, 127-136.

Porter, J., Finchum, G. A., (2009) Redefining the dust bowl region via popular perception and geotechnology. Great Plains Res. 19, 201-214

Pu, B., & Ginoux, P. (2017) Projection of American dustiness in the late 21st century due to climate change. Scientific Reports, 7(1) https://doi.org/10.1038/s41598-017-05431-9

Pu, B., & Ginoux, P. (2018) Climatic factors contributing to long-term variations in surface fine dust concentration in the United States. Atmospheric Chemistry & Physics, 18(6)

Qian, W. H., Tang, X., Quan, L. S., (2004) Regional characteristics of dust storms in China. Atm. Env. 38, 4895-4907.

Raman, A., Arellano, A. F., & Brost, J. J. (2014) Revisiting haboobs in the southwestern United States: An observational case study of the 5 July 2011 Phoenix dust storm. Atmospheric Environment, 89, 179–188. https://doi.org/10.1016/j.atmosenv.2014.02.026

Rango A, Havstad K, Estell R (2011) The Utilization of Historical Data and Geospatial Technology Advances at the Jornada Experimental Range to Support Western America Ranching Culture. Remote Sensing 3(12): 2089–2109.

Rango A, Laliberte AS, Winters C (2008) Role of aerial photos in compiling a long–term remote sensing data set. Journal of Applied Remote Sensing 2(023541) doi: 10.1117/1.3009225.

Ravi, S., Breshears, D. D., Huxman, T. E., & D'Odorico, P. (2010) Land degradation in drylands: Interactions among hydrologic–aeolian erosion and vegetation dynamics. Geomorphology, 116(3-4), 236–245. http://doi.org/10.1016/j.geomorph.2009.11.023

Redecker AP (2008) Historical aerial photographs and digital photogrammetry for impact analyses on derelict land sites in human settlement areas. Int. Arch. Photogramm. Remote Sens. Spat. Inf. Sci. 37: 5–10.

Redweik P, Roque D, Marques A, Matildes R, Marques F (2009) Recovering Portugal aerial images repository. International Archives of Photogrammetry and Remote Sensing 38: 1–4.

Rich, J., & Stokes, S. (2011) A 200,000-year record of late Quaternary Aeolian sedimentation on the Southern High Plains and nearby Pecos River Valley, USA. Aeolian Research, 2(4), 221–240. http://doi.org/10.1016/j.aeolia.2010.12.003

Riebsame, W. E., (1986) The dust bowl historical image, psychological anchor, and ecological taboo. Great Plains Quart. 6, 127-136.

Rivera Rivera, N. I., Gill, T. E., Bleiweiss, M. P., & Hand, J. L. (2010) Source characteristics of hazardous Chihuahuan Desert dust outbreaks. Atmospheric Environment, 44(20), 2457–2468. https://doi.org/10.1016/j.atmosenv.2010.03.019

Ruiz-Barradas, A., & Nigam, S. (2005) Warm season rainfall variability over the US Great Plains in observations, NCEP and ERA-40 reanalyses, and NCAR and NASA atmospheric model simulations. Journal of Climate, 18(11), 1808-1830.

Ruppert JC, Harmoney K, Henkin Z, Snyman HA, Sternberg M, Willms W, et al. (2015) Quantifying drylands' drought resistance and recovery: the importance of drought intensity, dominant life history and grazing regime. Global Change Biology 21(3): 1258–1270.

Sala, O. E., Parton, W. J., Joyce, L. A., & Lauenroth, W. K. (1988) Primary production of the central grassland region of the United States. Ecology, 69(1), 40-45.

Samson FB, Knopf FL, Ostlie WR (2004) Great Plains ecosystems: past, present, and future. Wildlife Society Bulletin 32(1): 6–15.

Schlesinger, W. H., Reynolds, J. F., Cunningham, G. L., Huenneke, L. F., Jarrell, W. M., Virginia, R. A., & Whitford, W.G. (1990) Biological Feedbacks in Global Desertification. Science, 247(4946), 1043–1048.

Schmeisser RL, Loope DB, Mason JA (2010) Modern and late Holocene wind regimes over the Great Plains (central U.S.A.) Quaternary Science Reviews 29(3-4): 554–566.

Schook, D. M., Rathburn, S. L., Friedman, J. M., & Wolf, J. M. (2017) A 184–year record of river meander migration from tree rings, aerial imagery, and cross sections. Geomorphology, 293, 227–239.

Schowengerdt RA (2012) Techniques for image processing and classifications in remote sensing. Academic Press.

Schubert, S., Gutzler, D., Wang, H., Dai, A., Delworth, T., Deser, C., … Zeng, N. (2009) A U.S. CLIVAR Project to Assess and Compare the Responses of Global Climate Models to Drought-Related SST Forcing Patterns: Overview and Results. Journal of Climate, 22(19), 5251–5272. http://doi.org/10.1175/2009JCLI3060.1

Schubert, S., Suarez, M., Pegion, P., Koster, R., & Bacmeister, J. (2004) On the Cause of the 1930s Dust Bowl. Science, 303(5665), 1855–1859.

Schwartz, D. E. (1978) Sedimentology of the braided-to-meandering transition zone of the Red River, Oklahoma and Texas (Doctor of Philosophy) University of Texas at Dallas, Dallas, TX.

Seager R, Lis N, Feldman J, Ting M, Williams AP, Nakamura J, et al. (2018) Whither the 100th Meridian? The Once and Future Physical and Human Geography of America's Arid–Humid Divide. Part I: The Story So Far. Earth Interactions, 22(5): 1–22.

Seager, R., & Hoerling, M. (2014) Atmosphere and Ocean Origins of North American Droughts*. Journal of Climate, 27(12), 4581–4606. http://doi.org/10.1175/JCLI-D-13-00329.1

Seager, R., Burgman, R., Kushnir, Y., Clement, A., Cook, E., Naik, N., & Miller, J. (2008) Tropical Pacific Forcing of North American Medieval Megadroughts: Testing the Concept with an Atmosphere Model Forced by Coral-Reconstructed SSTs*. Journal of Climate, 21(23), 6175–6190. https://doi.org/10.1175/2008JCLI2170.1

Seager, R., Tzanova, A., & Nakamura, J. (2009) Drought in the Southeastern United States: Causes, Variability over the Last Millennium, and the Potential for Future Hydroclimate Change*. Journal of Climate, 22(19), 5021–5045. http://doi.org/10.1175/2009JCLI2683.1

Seifert, C. L., Cox, R. T., Forman, S. L., Foti, T. L., Wasklewicz, T. A., & McColgan, A. T. (2009) Relict nebkhas (pimple mounds) record prolonged late Holocene drought in the forested region of south-central United States. Quaternary Research, 71(3), 329–339. http://doi.org/10.1016/j.yqres.2009.01.006

Sevara C, Verhoeven G, Doneus M, Draganits E (2017) Surfaces from the Visual Past: Recovering High–Resolution Terrain Data from Historic Aerial Imagery for Multitemporal Landscape Analysis. Journal of Archaeological Method and Theory. doi: 10.1007/s10816–017–9348–9.

Shao, Y., Raupach, M. R., & Findlater, P. A. (1993) Effect of saltation bombardment on the entrainment of dust by wind. Journal of Geophysical Research: Atmospheres, 98(D7), 12719-12726.

Shapley MD, Johnson WC, Engstrom DR, Osterkamp WR (2005) Late–Holocene flooding and drought in the Northern Great Plains, USA, reconstructed from tree rings, lake sediments and ancient shorelines. The Holocene 15(1): 29–41.

Sidwell, R., (1938) Sand and Dust Storms in Vicinity of Lubbock, Texas. Econ. Geog.14, 98-102.

Sims, P. L., & Bradford, J. A. (2001) Carbon dioxide fluxes in a southern plains prairie. Agricultural and Forest Meteorology, 109(2), 117–134.

Skaggs R, Edwards Z, Bestelmeyer BT, Wright JB, Williamson J, Smith P (2011) Vegetation maps at the passage of the Taylor Grazing Act (1934): a baseline to evaluate rangeland change after a regime shift. Rangelands 33(1): 13–19.

Skirvin SM, Kepner WG, March SE, Drake SE, Maingi JK, Edmonds CM, et al. (2004) Assessing the accuracy of satellite–derived land–cover classification using historical aerial photography, digital orthophoto quadrangles, and airborne video data. Remote sensing and GIS accuracy assessment 9: 115–131.

Smith, R. M., Twiss, P. C., Krauss, R. K., Brown, M. J., (1970) Dust Deposition in Relation to Site, Season, and Climatic Variables. The Soil and Water Conservation Research Division, Department of Agronomy Contribution no. 1076, Kansas Agricultural Experimental Station, Manhattan, KS, pp. 112-117.

Soil Survey Staff, Natural Resources Conservation Service, United States Department of Agriculture. Web Soil Survey. Available online at the following link: https: //websoilsurvey.sc.egov.usda.gov/. Accessed October 2017.

Sow, M., Crase, E., Rajot, J. L., Sankaran, R. M., Lacks, D. J., (2011) Electrification of particles in dust storms: field measurements during the monsoon period in Niger. Atm. Res. 102, 343–350.

Sprigg, W. A., Nickovic, S., Galgiani, J. N., Pejanovic, G., Petkovic, S., Vujadinovic, M., … El-Askary, H. (2014) Regional dust storm modeling for health services: The case of valley fever. Aeolian Research, 14, 53–73. https://doi.org/10.1016/j.aeolia.2014.03.001

Stafoggia, M., Zauli-Sajani, S., Pey, J., Samoli, E., Alessandrini, E., Basagana, X., Cernigliaro, …and others, (2016) Desert Dust Outbreaks in Southern Europe: Contribution to Daily PM10 Concentrations and Short-Term Associations with Mortality and Hospital Admissions. Env. Health Perspect. 124, 413-419.

Stahle, D. W., Fye, F. K., Cook, E. R., & Griffin, R. D. (2007) Tree-ring reconstructed megadroughts over North America since a.d. 1300. Climatic Change, 83(1-2), 133–149. http://doi.org/10.1007/s10584-006-9171-x

Stallings, F. L. jr., Black Sunday. The Great Dust Storm of April 14, 1935. Eakin Press, Fort Worth, Texas, 152 pp.

Su, H., Yang, Z.-L., Dickinson, R. E., & Wei, J. (2014) Spring soil moisture-precipitation feedback in the Southern Great Plains: How is it related to large-scale atmospheric conditions?: SU ET AL. Geophysical Research Letters, 41(4), 1283–1289. http://doi.org/10.1002/2013GL058931

Sullivan, D. A., & Ajwa, H. A. (2011) Evaluation of Wind Erosion Emissions Factors for Air Quality Modeling. Soil Science Society of America Journal 75(4): 1285-1294.

Sutton, L.J., (1931) Haboobs. Quarterly Journal of the Royal Meteorological Society 57, 143-161.

Svejcar LN, Bestelmeyer BT, Duniway MC, James DK (2015) Scale–Dependent Feedbacks Between Patch Size and Plant Reproduction in Desert Grassland. Ecosystems 18(1): 146–153.

Sweeney MR, Zlotnik VA, Joeckel RM, Stout JE (2016b) Geomorphic and hydrologic controls of dust emissions during drought from Yellow Lake playa, West Texas, USA. Journal of Arid Environments 133: 37-46. doi:10.1016/j.aridenv.2016.05.007

Sweeney, M. R., & Mason, J. A. (2013) Mechanisms of dust emission from Pleistocene loess deposits, Nebraska, USA. Journal of Geophysical Research: Earth Surface, 118(3), 1460-1471.

Sweeney, M. R., Lu, H., Cui, M., Mason, J. A., Feng, H., Xu, Z., (2016a) Sand dunes as potential sources of dust in northern China. Sci. China Ser. D 59, 760-769.

Sweeney, M. R., McDonald, E. V., & Etyemezian, V. (2011) Quantifying dust emissions from desert landforms, eastern Mojave Desert, USA. Geomorphology, 135(1–2), 21–34. https://doi.org/10.1016/j.geomorph.2011.07.022

Sweeney, M., Etyemezian, V., Macpherson, T., Nickling, W., Gillies, J., Nikolich, G., & McDonald, E. (2008) Comparison of PI-SWERL with dust emission measurements from a straight-line field wind tunnel. Journal of Geophysical Research: Earth Surface, 113(F1)

Sylvester, K. M., & Rupley, E. S. A. (2012) Revising the Dust Bowl: High Above the Kansas Grasslands. Environmental History, 17(3), 603–633. https://doi.org/10.1093/envhis/ems047

Tai, A. P. K., Mickley, L. J., Jacob, D. J., Leibensperger, E. M., Zhang, L., Fisher, J. A., & Pye, H. O. T. (2012) Meteorological modes of variability for fine particulate matter (PM2.5) air quality in the United States: implications for PM2.5 sensitivity to climate change. Atmospheric Chemistry and Physics, 12(6), 3131–3145. https://doi.org/10.5194/acp-12-3131-2012

Takaro, T. K., & Henderson, S. B. (2015) Climate change and the new normal for cardiorespiratory disease. Canadian Respiratory Journal, 22(1), 52–54.

Takaro, T. K., Knowlton, K., & Balmes, J. R. (2013) Climate change and respiratory health: current evidence and knowledge gaps. Expert Review of Respiratory Medicine, 7(4), 349–361. https://doi.org/10.1586/17476348.2013.814367

Tegen, I., Lacis, A. A., & Fung, I. (1996) The influence on climate forcing of mineral aerosols from disturbed soils. Nature, 380(6573), 419–422. http://doi.org/10.1038/380419a0

Tilman, D. and Downing, J. A.1994. Biodiversity and stability in grasslands. – Nature 367: 363-365. Tripaldi, A., & Forman, S. L. (2007) Geomorphology and chronology of Late Quaternary dune fields of western Argentina. Palaeogeography, Palaeoclimatology, Palaeoecology, 251(2), 300-320.

Tong, D. Q., Wang, J. X. L., Gill, T. E., Lei, H., & Wang, B. (2017) Intensified dust storm activity and Valley fever infection in the southwestern United States: Dust and Valley Fever Intensification. Geophysical Research Letters, 44(9), 4304–4312. https://doi.org/10.1002/2017GL073524

Tongway DJ, Ludwig JA (1994) Small–scale resource heterogeneity in semi–arid landscapes. Pacific Conservation Biology 1: 201–208.

Turnbull L, Wainwright J, Brazier RE, Bol R (2010) Biotic and Abiotic Changes in Ecosystem Structure over a Shrub–Encroachment Gradient in the Southwestern USA. Ecosystems 13(8): 1239–1255.

Turner MG (1989) Landscape ecology: the effect of pattern on process. Annual review of ecology and systematics 20(1): 171–197.

US EPA (1995) AP-42, Compilation of Air Pollutant Emission Factors, 5th Edition. Research Triangle Park, NC: Office of Air Quality Planning and Standards. https://www3.epa.gov/ttnchie1/ap42/ [Accessed January 13, 2016]

US EPA (2001) Procedures Document for National Emission Inventory, Criteria Air Pollutants 1985-1999. EPA-454/R-01-006 (pp. 4-276) Research Triangle Park, NC: Office of Air Quality Standards.

US EPA (2007) Emissions Factor Uncertainty Assessment. Research Triangle Park, NC: Office of Air Quality Standards.

USDA National Agricultural Statistics Service (2010) Usual Planting and Harvesting Dates for U.S. Field Crops. In Agricultural Handbook 628 (pp. 39)

Veste, M., Littmann, T., Breckle, S. W., & Yair, A. (2001) The role of biological soil crusts on desert sand dunes in the northwestern Negev, Israel. In Sustainable Land Use in Deserts (pp. 357-367) Springer, Berlin, Heidelberg.

Vivoni, E. R., Tai, K., & Gochis, D. J. (2009) Effects of Initial Soil Moisture on Rainfall Generation and Subsequent Hydrologic Response during the North American Monsoon. Journal of Hydrometeorology, 10(3), 644–664. https://doi.org/10.1175/2008JHM1069.1

Vogels MFA, de Jong SM, Sterk G, Addink EA (2017) Agricultural cropland mapping using black–and–white aerial photography, Object–Based Image Analysis and Random Forests. International Journal of Applied Earth Observation and Geoinformation 54: 114–123.

Volland, A. Aerosols: Tiny particles, big impact. Earth Oberservatory (2010) Accessed Dec. 8, 2014

Wang T, Istanbulluoglu E, Lenters J, Scott D (2009) On the role of groundwater and soil texture in the regional water balance: An investigation of the Nebraska Sand Hills, USA. Water Resources Research 45(10) doi: 10.1029/2009WR007733.

Wang, H., Schubert, S., Suarez, M., & Koster, R. (2010) The Physical Mechanisms by Which the Leading Patterns of SST Variability Impact U.S. Precipitation. Journal of Climate, 23(7), 1815–1836. http://doi.org/10.1175/2009JCLI3188.1

Wang, J., Miller, D.R., Sammis, T.W., Hiscox, A.L., Yang, W., Holmén, B.A., (2010) Local Dust Emission Factors for Agricultural Tilling Operations. Soil Science 175: 194–200. doi:10.1097/SS.0b013e3181dae283

Warn, G.F (1952) Some dust storm conditions of the southern high plains. Bull. Am. Meteorol. Soc. 33.

Waters, M. R., Forman, S. L., Jennings, T. A., Nordt, L. C., Driese, S. G., Feinberg, J. M., ... & Wiederhold, J. E. (2011) The Buttermilk Creek complex and the origins of Clovis at the Debra L. Friedkin site, Texas. Science, 331(6024), 1599-1603.

Weaver, J. E., & Albertson, F. W. (1936) Effects on the Great Drought on the Prairies of Iowa, Nebraska and Kansas. Ecology, 17(4), 567–639.

Weaver, J. E., & Albertson, F. W. (1943) Resurvey of grasses, forbs, and underground plant parts at the end of the great drought. Ecological Monographs 13(1): 63–117.

Weaver, J. E., & Albertson, F. W. (1956) "Grasslands of the Great Plains: Their nature and use." Lincoln, Nebraska: Johnsen Publishing Co.

Werner, C. M., Mason, J. A., & Hanson, P. R. (2011) Non-linear connections between dune activity and climate in the High Plains, Kansas and Oklahoma, USA. Quaternary Research, 75(1), 267–277. http://doi.org/10.1016/j.yqres.2010.08.001

Whitfield, C. J. (1938) Sand dunes of recent origin in southern Great Plains. Journal of Agricultural Research, 56(12), 907–917.

Wiens J A (1989) Spatial scaling in ecology. Functional ecology 3(4): 385–397.

Wigdahl CR, Saros JE, Fritz SC, Stone JR, Engstrom DR (2014) The influence of basin morphometry on the regional coherence of patterns of diatom–inferred salinity in lakes of the northern Great Plains (USA) The Holocene 24(5): 603–613.

Wiggs, G. F. S., Livingstone, I., Thomas, D. S. G., & Bullard, J. E. (1994) Effect of vegetation removal on airflow patterns and dune dynamics in the southwest Kalahari Desert. Land Degradation & Development, 5(1), 13-24.

Wilks DS (2011) "Statistical Methods in the Atmospheric Sciences Third Edition." New York: Academic Press

Williams, E. R., (2007) Comment on "Atmospheric controls on the annual cycle of North African dust" by S. Engelstaedter and R. Washington. J. Geophys. Res.-Atm. 113, D23109.

Williams, E. R., Nathou, N., Hicks, E., Pontikis, C., Russell, B., Miller, M., Bartholomew, M. J., (2009) The electrification of dust-lofting gust fronts ('haboobs') in the Sahel. Atm. Res. 91, 292-298.

Williamson JC, Burkett LM, Bestelmeyer BT, Skaggs R, Havstad KM (2011) Reinterpreting historical data for evidence–based shrubland management. Natural Resources and Environmental Issues 17(1): 18.

Wintle, A. G. (2008) Luminescence dating: where it has been and where it is going. Boreas, 37(4), 471-482.

Wolfe, S. A., & Hugenholtz, C. H. (2009) Barchan dunes stabilized under recent climate warming on the northern Great Plains. Geology, 37(11), 1039-1042.

Wolter, K., & Timlin, M. S. (2011) El Niño/Southern Oscillation behaviour since 1871 as diagnosed in an extended multivariate ENSO index (MEI.ext) International Journal of Climatology, 31(7), 1074–1087. http://doi.org/10.1002/joc.2336

Wong, C. I., Banner, J. L., & Musgrove, M. (2015) Holocene climate variability in Texas, USA: An integration of existing paleoclimate data and modeling with a new, high-resolution speleothem record. Quaternary Science Reviews. http://doi.org/10.1016/j.quascirev.2015.06.023

Woodhouse, C. A., & Overpeck, J. T. (1998) 2000 years of drought variability in the Central United States. Bulletin of the American Meteorological Society, 79(12), 2693–2714.

Woodhouse, C. A., Meko, D. M., MacDonald, G. M., Stahle, D. W., & Cook, E. R. (2010) A 1,200-year perspective of 21st century drought in southwestern North America. Proceedings of the National Academy of Sciences, 107(50), 21283–21288. http://doi.org/10.1073/pnas.0911197107

World Health Organization (2003) Health aspects of air pollution with particulate matter, ozone and nitrogen dioxide: report on a WHO working group, Bonn, Germany 13-15 January 2003. Available at: http://apps.who.int/iris/handle/10665/107478 [Accessed February 10, 2016].

Worster, D., (1979) Dust Bowl: The Southern Plains in the 1930s. Oxford University Press, New York, 290 pp.

Xu, J., Shuttleworth, W. J., Gao, X., Sorooshian, S., & Small, E. E. (2004) Soil moisture–precipitation feedback on the North American monsoon system in the MM5-OSU model. Quarterly Journal of the Royal Meteorological Society, 130(603), 2873–2890. https://doi.org/10.1256/qj.03.192

Yair, Y., Katz, S., Yaniv, R., Ziv, B., Price, C., (2016) An electrified dust storm over the Negev desert, Israel. Atm. Res. 181, 63-71.

Zhang XY, Gong SL, Zhao TL, Arimoto R, Wang YQ, Zhou ZJ (2003) Sources of Asian dust and role of climate change versus desertification in Asian dust emission. Geophysical Research Letters 30(24) doi: 10.1029/2003GL018206.